Scientific Reports

https://doi.org/10.1038/s41598-026-63668-9

Article in Press

Thermodynamic design and energy–exergy analysis of a water-cooled photovoltaic–thermal systems under tropical conditions

Received: 6 February 2026

Accepted: 20 July 2026

Published online: 22 July 2026

Cite this article as: Mundu M.M., Ssempewo J.I., Nnamchi S.N. *et al.* Thermodynamic design and energy–exergy analysis of a water-cooled photovoltaic–thermal systems under tropical conditions. *Sci Rep* (2026). https://doi.org/10.1038/s41598-026-63668-9

M. M. Mundu, J. I. Ssempewo, S. N. Nnamchi & Daniel Ejim Uti

We are providing an unedited version of this manuscript to give early access to its findings. Before final publication, the manuscript will undergo further editing. Please note there may be errors present which affect the content, and all legal disclaimers apply.

If this paper is publishing under a Transparent Peer Review model then Peer Review reports will publish with the final article.

ARTICLE IN PRESS

© The Author(s) 2026. **Open Access** This article is licensed under a Creative Commons Attribution-NonCommercial-NoDerivatives 4.0 International License, which permits any non-commercial use, sharing, distribution and reproduction in any medium or format, as long as you give appropriate credit to the original author(s) and the source, provide a link to the Creative Commons licence, and indicate if you modified the licensed material. You do not have permission under this licence to share adapted material derived from this article or parts of it. The images or other third party material in this article are included in the article's Creative Commons licence, unless indicated otherwise in a credit line to the material. If material is not included in the article's Creative Commons licence and your intended use is not permitted by statutory regulation or exceeds the permitted use, you will need to obtain permission directly from the copyright holder. To view a copy of this licence, visit http://creativecommons.org/licenses/by-nc-nd/4.0/.

ARTICLE IN PRESS

Thermodynamic Design and Energy–Exergy Analysis of a Water-Cooled Photovoltaic–Thermal Systems under Tropical Conditions

M. M. Mundu[1*], J. I. Ssempewo[2], S. N. Nnamchi[3] and Daniel Ejim Uti[4*]

1. Department of Electrical, Telecommunication and Computer Engineering, Kampala International University, P. O. Box 20000, Kampala, Uganda, mundu.mustafa@kiu.ac.ug, ORCID; https://orcid.org/0000-0003-1345-9999.
2. Department of Civil and Environmental Engineering, College of Engineering, Design Art and Technology, Makerere University, P.O. Box 7062, Kampala, Uganda, jotham.sempewo@mak.ac.ug, ORCID; https://orcid.org/0000-0002-9897-211x.
3. Department of Mechanical and Industrial Engineering, Faculty of Science and Technology, Mbarara University of Science and Technology, snnamchi@must.ac.ug, ORCID; https://orcid.org/0000-0002-6368-2913
4. Daniel Ejim Uti (PhD). Department of Research and Publications, Kampala International University, P.O. Box 20000, Kampala, Uganda. Email: daniel.ejimuti@kiu.ac.ug

***Corresponding authors:** Mundu, M. M (PhD). Department of Electrical, Telecommunication and Computer Engineering, Kampala International University, P.O. Box 20000, Kampala, Uganda, mundu.mustafa@kiu.ac.ug.

Daniel Ejim Uti (PhD). Department of Research and Publications, Kampala International University, P. O. Box 20000, Kampala, Uganda. Email: dan4uti@gmail.com, daniel.ejimuti@kiu.ac.ug

Abstract

Photovoltaic–thermal (PVT) systems provide a promising approach for simultaneous electrical and thermal energy generation under high-irradiance tropical conditions. However, most existing studies primarily focus on first-law energy performance or global exergy indicators without detailed thermodynamic irreversibility diagnostics. This study presents a second-law thermodynamic analysis of a closed-loop water-cooled PVT system coupled to a well-mixed thermal storage tank under tropical climatic conditions. A coupled transient thermal–electrical numerical framework incorporating explicit Gibbs Tds thermodynamic relations is developed to evaluate entropy generation, exergy destruction, and subsystem-level thermodynamic irreversibilities within the PVT system. The model was applied to a representative tropical day using Typical Meteorological Year data for Kampala, Uganda. Under baseline operating conditions for a 1.66 m² collector integrated with a 100 L storage tank, the system maintained PV temperatures below approximately 43 °C while delivering about 1.9 kWh_{th} of useful thermal energy and 1.95 kWh_{el} of electrical energy. The second-law analysis further revealed that ambient heat rejection accounted for nearly 95% of the total exergy destruction, identifying it as the dominant thermodynamic irreversibility mechanism. Parametric analysis showed that increasing mass flow rate, solar irradiance, and ambient temperature reduced exergy efficiency despite relatively stable first-law energy efficiencies, confirming that energy-optimal and exergy-optimal operating conditions do not necessarily coincide. The thermodynamically favorable operating region was identified at low-to-moderate flow rates near 0.01 kg s^{-1} for the investigated configuration. Unlike many conventional PVT studies that primarily report overall energy or exergy efficiencies, the present work provides a mechanism-resolved second-law interpretation by explicitly linking entropy generation and exergy destruction to the governing thermodynamic processes within the collector and storage subsystems under tropical operating conditions. The results further demonstrate that the principal advantage of the proposed configuration lies in enhanced overall solar-energy utilization through simultaneous electrical and useful low-

ARTICLE IN PRESS

temperature thermal energy recovery rather than electrical enhancement alone. The study therefore provides second-law-based thermodynamic design guidance for optimization of tropical PVT systems, particularly regarding reduction of ambient thermal losses and improvement of PV–absorber thermal coupling.

Keywords: PVT systems; Exergy analysis; Entropy generation; Tds formulation; Second-law efficiency; Tropical climate; Thermodynamic optimization; Solar energy systems

1.0 Introduction

1.1 Background and Motivation

Photovoltaic (PV) technology is widely recognized as a major pillar of the global transition toward low-carbon energy systems. However, PV module efficiency decreases significantly with increasing cell temperature, typically by about 0.4–0.5% per °C above standard test conditions for crystalline silicon modules. Under tropical climatic conditions, high solar irradiance combined with elevated ambient temperature causes PV modules to operate substantially above nominal temperatures, resulting in considerable electrical performance degradation. Experimental and numerical studies in tropical regions have confirmed that elevated operating temperatures reduce PV electrical output, while cooling strategies such as phase change materials, green roofs, and active thermal management can mitigate thermal losses and improve system efficiency (Zm et al., 2025; Poongavanam et al., 2023; Arenandan et al., 2022; Dubey & Tay, 2013; Bian et al., 2025; Fashina et al., 2018). Additional environmental factors including humidity, dust accumulation, and particulate matter further degrade PV performance in tropical environments (Zm et al., 2025; Narkwatchara et al., 2020; Ballina & Go, 2025). Consequently, effective thermal management and site-specific operational strategies are essential for sustaining PV performance under high-temperature operating conditions.

In tropical regions, elevated solar irradiance and ambient temperature not only intensify PV thermal losses but also create substantial opportunities for low-grade thermal energy recovery. Consequently, photovoltaic–thermal (PVT) systems have attracted increasing attention because they simultaneously generate electrical and useful thermal energy from the same collector aperture area while reducing PV operating temperature. Such integrated energy utilization is particularly attractive for domestic hot water production, low-temperature thermal applications, building-integrated renewable-energy systems, and decentralized energy deployment in hot-climate environments.

In conventional PV modules, only a limited fraction of the incident solar radiation is converted into electricity, while the remaining energy is dissipated as heat, increasing cell temperature and reducing electrical efficiency. PVT systems address this limitation by integrating a thermal collector with the PV module to extract waste heat using a circulating working fluid, thereby simultaneously enhancing electrical performance and recovering useful thermal energy. Recent advances include spectral-splitting PVT configurations, thermally enhanced collectors, and PVT–heat-pump integrations for improved overall solar-energy utilization (Hong et al., 2022; Alessandro et al., 2021). Various cooling approaches involving air, water, nanofluids, and phase change materials have also been investigated to improve thermal extraction and combined system efficiency (Al-Waeli et al., 2020; Diwania et al., 2020; Bandaru et al., 2021; Muhamad et al., 2022; Kalateh et al., 2022; Al-Najjar et al., 2024; Bian et al., 2025). In addition, flow-channel modifications, enhanced absorber configurations, and integration with thermal storage systems have demonstrated further potential for improving PVT thermodynamic performance (Diwania et

ARTICLE IN PRESS

al., 2020; Jia et al., 2019; Asefi et al., 2022; Wang et al., 2024; Attia et al., 2025). Despite challenges associated with thermal losses, system complexity, and optimization trade-offs, PVT systems remain promising technologies for enhanced solar-energy utilization through simultaneous electricity generation and useful heat recovery (Hong et al., 2022; Bandaru et al., 2021; Samykano, 2023).

The fundamental energy flow in a PVT system is illustrated schematically in Figure 1, where the incident solar radiation is partitioned into three main components: electrical power output, useful thermal energy transferred to the working fluid, and unavoidable thermal losses to the environment.

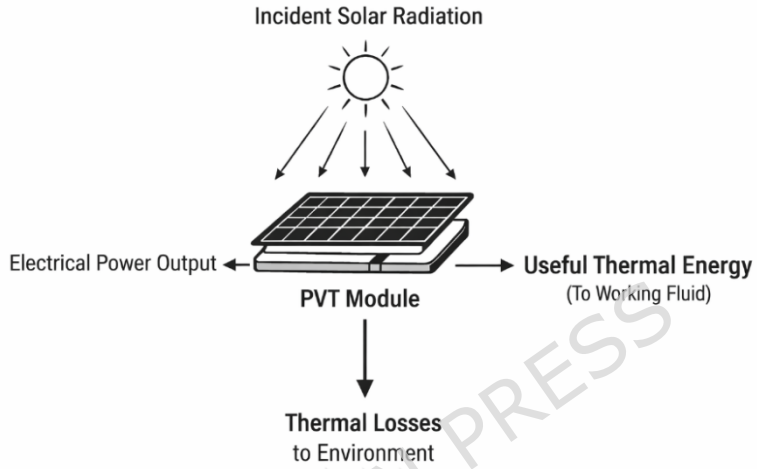

Figure 1 Conceptual energy flow diagram of the PVT system

1.2 Problem Statement and Research Gap

Photovoltaic–thermal systems have been widely investigated for simultaneous electrical and thermal energy generation; however, most existing studies remain dominated by first-law performance indicators such as thermal efficiency, electrical efficiency, and overall energy recovery, which quantify energy quantities without adequately addressing energy quality or thermodynamic irreversibility. Even in studies incorporating exergy analysis, the evaluation is commonly limited to global exergy efficiencies or generalized energy–exergy trade-offs without detailed identification of the irreversible thermodynamic mechanisms governing system degradation. Consequently, subsystem-level entropy generation associated with finite-temperature heat transfer, ambient thermal rejection, and fluid-flow dissipation remains insufficiently resolved in many existing PVT modeling frameworks (Joshi et al., 2009; Evola & Marletta, 2014; Kallio & Siroux, 2020; Kalateh et al., 2022; Rao et al., 2024; Al-Najjar et al., 2024). As a result, energy-based optimization alone is often insufficient for identifying true thermodynamic performance limits or guiding rational system design.

Second-law thermodynamics indicates that irreversibilities in PVT systems primarily originate from heat transfer across finite temperature differences, thermal losses to the ambient, and viscous dissipation within fluid channels (Maadi et al., 2017; Mundu et al., 2020; Liu et al., 2023; Hai et al., 2023; Ramírez-Minguela et al., 2023). Accordingly, recent studies emphasize that entropy generation analysis is essential for meaningful thermodynamic optimization of solar thermal and micro-thermofluidic systems (Torabi et al., 2020; Rashidi et al., 2020; Ramírez-Minguela et al.,

ARTICLE IN PRESS

2023). Although detailed CFD-based investigations have decomposed entropy generation into thermal and viscous contributions, such approaches are computationally intensive and rarely incorporated into design-oriented transient PVT frameworks (Maadi et al., 2017; Liu et al., 2023; Hai et al., 2023; Mundu et al., 2024).

Furthermore, relatively few studies have developed transient thermodynamic PVT models capable of simultaneously coupling thermal behavior, electrical performance, entropy generation, and exergy destruction under realistic tropical operating conditions. Existing analyses frequently rely on steady-state assumptions or simplified exergy formulations that provide limited diagnostic insight into the physical sources of irreversibility within collector and storage subsystems. More importantly, despite their fundamental thermodynamic significance, Gibbs Tdsrelations are seldom explicitly integrated into transient numerical PVT simulations. Instead, entropy generation is often treated using lumped or non-diagnostic formulations without direct linkage to the governing thermodynamic processes (Rashidi et al., 2020; Ramírez-Minguela et al., 2023; Mundu et al., 2022; Torabi et al., 2020; Osara & Bryant, 2024; Nnamchi et al., 2021). Consequently, many existing exergy-based studies remain focused primarily on global performance indicators and inlet-temperature optimization, providing limited guidance regarding collector design, thermal coupling, and thermodynamically optimal operating conditions under tropical high-irradiance environments (Kallio & Siroux, 2020; Al-Najjar et al., 2024; Rao et al., 2024; Nnamchi et al., 2022a; Nnamchi et al., 2022b).

In addition, many existing investigations implicitly treat thermal extraction mainly as a mechanism for improving PV electrical efficiency, with comparatively limited emphasis on the broader thermodynamic significance of simultaneous thermal energy recovery. Under tropical climatic conditions, however, useful recovery of low-grade thermal energy can represent a substantial component of the total solar-energy utilization potential of PVT systems. Therefore, there remains a need for a rigorous second-law-based framework capable of simultaneously evaluating electrical enhancement, thermal energy recovery, entropy generation, and exergy destruction in order to identify dominant irreversibility mechanisms and thermodynamically favorable operating conditions.

Accordingly, the present study develops a coupled transient thermal–electrical PVT framework that explicitly integrates Gibbs Tds thermodynamic relations, subsystem-level entropy generation diagnostics, and exergy destruction analysis under tropical climatic conditions. Unlike many conventional PVT investigations that primarily emphasize overall thermal or exergy efficiencies, the proposed framework provides a physically diagnostic second-law interpretation capable of explicitly linking entropy generation and exergy destruction to the governing irreversible thermodynamic processes within the collector and storage subsystems.

1.3 Aim and Objectives

The aim of this study is to develop a comprehensive first- and second-law-based numerical model of a water-cooled PVT system coupled to a closed-loop, well-mixed thermal storage tank, and to use this framework to evaluate and optimize its thermodynamic performance under tropical operating conditions. Specifically, the objectives are to (i) develop a coupled thermal–electrical model of the PVT collector and storage tank based on energy conservation principles, (ii) formulate entropy balances and entropy generation terms explicitly using the Gibbs (Tds) thermodynamic relations, (iii) evaluate exergy flows and exergy destruction rates in the system components through application of the Gouy–Stodola theorem, (iv) perform a parametric analysis to quantify the effects of key design and operating parameters, including mass flow rate, ambient

temperature, and solar irradiance, on energy efficiency, exergy efficiency, and entropy generation, and (v) identify thermodynamically optimal operating regions that maximize useful energy recovery while minimizing irreversible losses.

1.4 Contributions of the Present Study

The scientific contributions and novel aspects of the present study are as follows: (i) the development of a coupled transient thermal–electrical numerical framework for a closed-loop water-cooled PVT system under tropical climatic conditions, (ii) the explicit integration of Gibbs Tds thermodynamic relations into the entropy generation formulation of the PVT collector and storage system, (iii) the implementation of a mechanism-resolved second-law analysis capable of distinguishing entropy generation associated with finite-temperature heat transfer, ambient thermal rejection, and fluid friction, (iv) a detailed subsystem-level exergy destruction mapping based on the Gouy–Stodola theorem, and (v) a second-law-based thermodynamic optimization framework demonstrating that energy-optimal and exergy-optimal operating conditions do not necessarily coincide under tropical operating environments.

2.0 System Description and Design Configuration

2.1 System Architecture

The system considered in this study is a closed-loop, water-cooled PVT system coupled to a well-mixed thermal storage tank. The overall configuration consists of four main subsystems: (i) the PVT collector, (ii) the working fluid circulation loop, (iii) the storage tank, and (iv) the electrical load/inverter (Figure 2).

ARTICLE IN PRESS

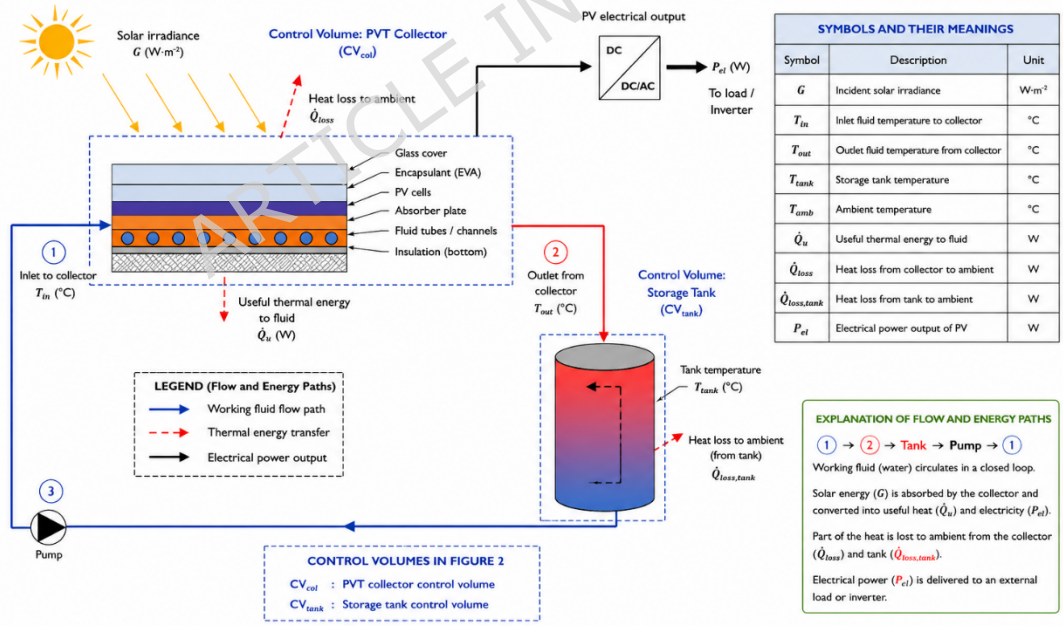

Figure 2. Schematic representation of the closed-loop water-cooled PVT system showing the collector, working-fluid circulation loop, storage tank coupling, thermal energy transfer paths, electrical output, and principal thermodynamic control volumes used in the analysis.

The conceptual energy flow paths and the main system components are illustrated in Figure 2, which also indicates the control volumes used later for the thermodynamic analysis. The notation

ARTICLE IN PRESS

adopted in Figure 2 is maintained consistently throughout the governing equations, thermodynamic formulations, and parameter tables presented in subsequent sections. The PVT collector is a flat-plate type and is composed, from top to bottom, of a glass cover, photovoltaic cells, a backsheet or bonding layer, a metallic absorber plate, and fluid channels or tubes attached to the absorber. Solar radiation G is incident on the PV surface, where a fraction is converted into electricity, while the remaining part is transformed into heat and conducted to the absorber. The circulating water removes this heat and transports it to the storage tank.

The hydraulic loop comprises a circulation pump, connecting pipes, and the storage tank. The water leaving the tank at temperature T_{tank} enters the PVT collector at T_{in}, absorbs heat, and exits the collector at T_{out} before returning to the tank. The storage tank is modeled as a well-mixed control volume, implying a spatially uniform tank temperature. The electrical output of the PV module is delivered to an external load or inverter.

2.2 Design Assumptions and Operating Modes

To obtain a tractable and robust numerical model, the following assumptions are adopted:

1. Heat transfer in the PVT collector is modeled using a one-dimensional (1D) thermal resistance network in the direction normal to the collector plane.
2. The system can be simulated in steady-state or transient mode; in the present formulation, the tank introduces time dependence, while the collector is treated in quasi-steady state at each time step.
3. The storage tank is assumed to be well-mixed, such that its temperature $T_{tank}(t)$ is spatially uniform.
4. Thermophysical properties of the working fluid and solid materials are either taken as constant or evaluated at mean operating temperature.
5. Heat losses from the collector to the ambient are represented by a lumped overall heat loss coefficient U_L.
6. Heat losses from the tank to the ambient are represented by a lumped coefficient $U_t A_t$.
7. Pressure losses in the fluid loop may be included to evaluate entropy generation due to friction, but they do not significantly affect the energy balance.

These assumptions were adopted to establish a computationally tractable transient thermodynamic framework while preserving the dominant heat transfer, thermal coupling, and irreversible loss mechanisms governing the operation of the investigated PVT system under tropical climatic conditions.

The system operates in a closed-loop recirculation mode, where the tank temperature determines the collector inlet temperature in Equation (1)

$$T_{in}(t) = T_{tank}(t) \tag{1}$$

where $T_{in}(t)$ is the inlet fluid temperature to the PVT collector and $T_{tank}(t)$ is the instantaneous temperature of the well-mixed storage tank. This relation provides the thermal coupling between the collector and the storage subsystem.

2.3 Geometric Design Parameters

The main geometric and design parameters of the PVT collector and storage tank are summarized in Table 1. These parameters define both the optical–thermal behavior of the collector and the thermal inertia of the storage system. The geometric configuration shown schematically in Figure 2 is used as the basis for the numerical model developed in Section 3.

ARTICLE IN PRESS

2.4 Working Fluid and Material Properties

The working fluid employed in the cooling loop is liquid water, selected because of its high specific heat capacity, relatively high thermal conductivity, low cost, wide availability, and suitability for low-temperature thermal energy applications. Water also exhibits favorable thermophysical behavior for heat extraction under moderate operating temperatures, making it a widely adopted benchmark fluid in photovoltaic–thermal systems. Furthermore, its relatively low viscosity contributes to reduced pumping requirements and lower hydraulic irreversibility during circulation, which is important for second-law thermodynamic assessment.

The thermophysical properties of water density ρ, specific heat capacity c_p, and thermal conductivity k are evaluated at the mean fluid temperature unless otherwise stated. The main solid materials and their properties are also listed in Table 1. These properties are required for the calculation of heat transfer rates, PV electrical efficiency, and overall system losses in the mathematical model presented in Section 3.

Table 1. Main design parameters, material properties, and PV module specifications used in the simulation (baseline case)

Table 1(a) System geometry and operating conditions (single-module PVT, DHW)

Parameter	Symbol	Baseline value	Unit
1. Collector gross area (single module)	A_c	1.66	m^2
2. Module dimensions (L × W × H)	–	1675 × 992 × 35	mm
3. Tilt angle (Kampala near-equator baseline)	β	10	°
4. Working fluid	–	Water	–
5. Tank volume (well-mixed)	V_{tank}	100	L
6. Tank volume	V_{tank}	0.10	m^3
7. Tank initial temperature	$T_{tank,0}$	26	$°C$
8. Ambient temperature (baseline daytime)	T_{amb}	26	$°C$
9. Wind speed (baseline)	v_w	2.4	ms^{-1}
10. Mass flow rate (closed loop)	$\dot{m}$	0.034	kgs^{-1}

Table 1(a) summarizes the geometry and operating conditions of the reference single-module PVT system modeled for domestic hot water (DHW) production in Kampala. The collector gross area (1.66 m²) and module dimensions correspond to a standard residential PV module footprint, in line with many experimental and numerical PVT studies that use single flat-plate modules of roughly $1.5 - 1.7\ m\ \times\ 1.0\ m$ (Wang et al., 2024; Yan et al., 2022; Maoulida et al., 2022). The tilt angle of 10° represents a near-equatorial installation, comparable to other tropical and subtropical PVT investigations in Ghana, Malaysia, and Comoros, where low tilt angles are adopted to reflect local latitude and maximize annual irradiation on the collector surface (Abdul-Ganiyu et al., 2021; Basuhaib et al., 2024; Misha et al., 2019; Maoulida et al., 2022; Mundu et al., 2025a; Mundu et al., 2025b).

The system is configured as a closed-loop water-based PVT for DHW, with a well-mixed 100 L storage tank ($0.10\ m^3$). Similar storage volumes (100–200 L) are widely used in residential PVT DHW simulations and field tests, providing a realistic match to typical household hot water

ARTICLE IN PRESS

demand (Bigorajski & Chwieduk, 2018; Yan et al., 2022; Maoulida et al., 2022). The baseline ambient temperature is set to 26 °C, consistent with typical daytime conditions in tropical locations where reported ambient temperatures during PVT testing range from about 25–30 °C (Rao et al., 2024; Basuhaib et al., 2024; Wang et al., 2024; Misha et al., 2019; Kenfack et al., 2023; Maoulida et al., 2022). The baseline wind speed of 2.4 ms^{-1} is also representative of moderate natural convection conditions used in PVT performance analyses and NOCT/thermal characterizations, where values between about $2-3\ ms^{-1}$ are commonly assumed or measured (Wang et al., 2024; Kenfack et al., 2023; Kramer et al., 2023; Sun et al., 2021).

The closed-loop mass flow rate of 0.034 kgs^{-1} lies within the lower range of water flow rates investigated in tropical PVT experiments and optimization studies (typically $0.025-0.083\ kgs^{-1}$ for single modules), where such values have been shown to provide effective cooling without excessive pumping power or diminishing returns in electrical/thermal performance (Abdul-Ganiyu et al., 2021; Basuhaib et al., 2024; Misha et al., 2019; Abdullah et al., 2020; Soliman, 2023). This choice therefore represents a realistic baseline operating point for subsequent parametric and second-law analyses under Kampala-type tropical conditions (for all simulations presented in Section 6).

Table 1(b) PVT collector construction (sheet-and-tube absorber)

Parameter	Symbol	Baseline value	Unit
1. Glass cover thickness (tempered)	δ_g	3.2	mm
2. Absorber plate material	–	Copper	–
3. Absorber plate thickness	δ_{abs}	0.5	mm
4. Tube inner diameter	D_i	8	mm
5. Tube outer diameter	D_o	10	mm
6. Number of parallel tubes	N_t	10	–
7. Tube spacing (center-to-center)	s_t	0.10	m
8. Back insulation thickness	δ_{ins}	50	mm

ARTICLE IN PRESS

The PVT collector construction in Table 1(b) reflects a conventional sheet-and-tube flat-plate design, widely used in commercial and research PVT systems due to its proven thermal performance and manufacturability (Herrando et al., 2019; Guarracino et al., 2016; Kim & Kim, 2012). The 3.2 mm tempered glass cover thickness is typical for durability and optical transmittance balance, protecting the PV cells while minimizing solar radiation losses (Guarracino et al., 2019; Kim & Kim, 2012). The copper absorber plate with a thickness of 0.5 mm offers excellent thermal conductivity, enhancing heat transfer from the PV cells to the fluid, which is consistent with common practice in high-performance PVT collectors (Herrando et al., 2019; Alami et al., 2025; Kim & Kim, 2012). Its high thermal conductivity also improves thermal coupling between the absorber and working fluid, and contributes to reduced temperature gradients and entropy generation within the collector. The tube dimensions (8 mm inner diameter, 10 mm outer diameter) and spacing (0.10 m center-to-center) align with standard sheet-and-tube configurations designed to optimize fluid flow and heat extraction without excessive pressure drop (Herrando et al., 2019; Guarracino et al., 2016; Francisco et al., 2024). The use of 10 parallel tubes ensures sufficient coolant coverage across the absorber area, balancing hydraulic and thermal performance (Guarracino et al., 2016; Francisco et al., 2024). Finally, the 50 mm back insulation

ARTICLE IN PRESS

thickness is chosen to minimize rear heat losses, making top losses dominant as typical for flat-plate collectors aiming to maximize thermal efficiency under steady-state conditions (Alami et al., 2025; Guarracino et al., 2019). Moreover, these parameters are consistent with those reported in detailed numerical and experimental studies of sheet-and-tube PVT collectors, which emphasize copper absorbers, tempered glass covers around 3 mm thick, and back insulation thicknesses between 40–60 mm to optimize thermal performance while maintaining structural integrity (Herrando et al., 2019; Guarracino et al., 2016; Alami et al., 2025; Nnamchi et al., 2020; Guarracino et al., 2019; Kim & Kim, 2012).

Table 1(c) Optical properties

Parameter	Symbol	Baseline value	Unit
1. Glass transmittance	τ_g	0.90	–
2. Effective absorptance (PV/absorber)	α_{eff}	0.90	–
3. Effective emissivity (outer surface)	ε_{eff}	0.88	–

Table 1(c) summarizes the key optical properties that control both solar energy capture and radiative heat exchange with the surroundings. The glass transmittance of 0.90 represents high-quality low-iron glazing, consistent with commercially available covers that transmit around 90% of incident solar radiation and are widely used in flat-plate collectors for enhanced thermal performance (Giovannetti et al., 2014; Shaik et al., 2021; Bakari et al., 2014). Tempered low-iron glass was selected because of its high solar transmittance, mechanical durability, and favorable optical performance under outdoor tropical operating conditions. The effective absorptance of the combined PV/absorber surface is also set to 0.90, reflecting a well-coupled interface with high solar absorptivity, in line with values typically targeted for efficient solar absorbers (Hellström et al., 2003). The effective emissivity of the outer surface, $\varepsilon_{eff} = 0.88$, characterizes its long-wave infrared behavior and is comparable to standard clear or low-iron glass, which typically exhibits mid-infrared emissivity around 0.8–0.85 (Giovannetti et al., 2014; Khoukhi & Maruyama, 2006; Khoukhi & Maruyama, 2005). This parameter is essential for accurately predicting radiative heat losses, especially at elevated operating temperatures where long-wave radiation can dominate over convection. Thus, these baseline values are representative of conventional, high-quality flat-plate solar collector glazing and provide a realistic basis for performance modeling.

Table 1(d) Material and fluid properties (evaluated near 25–60°C)

Parameter	Symbol	Baseline value	Unit
1. Water density	ρ	997	kg/m³
2. Water specific heat	c_p	4180	J/kg·K
3. Water thermal conductivity	k_f	0.60	W/m·K
4. Water dynamic viscosity	μ	0.89×10^{-3}	Pa·s
5. Copper conductivity	k_{cu}	385	W/m·K
6. Glass conductivity	k_g	1.0	W/m·K
7. Insulation conductivity	k_{ins}	0.040	W/m·K

ARTICLE IN PRESS

Table 1(d) reports the thermophysical properties of the working fluid and structural materials adopted in the model over the representative operating range of 25–60 °C. Water is selected as the heat transfer fluid because of its high specific heat capacity, relatively high thermal conductivity, low viscosity, and low cost, which make it a standard choice and performance benchmark for solar thermal and flat-plate collector systems (Unar et al., 2020; Jamshed et al., 2021; Chyngyzbekkyzy & Satybaldyev, 2025). The listed water density, specific heat, thermal conductivity, and dynamic viscosity are consistent with reference values commonly used in modeling and CFD studies of solar collectors near ambient and moderate operating temperatures (Unar et al., 2020; Jamshed et al., 2021). The thermal conductivities of copper, glass, and insulation define the main conductive heat transfer pathways in the collector, with copper providing highly conductive channels for heat removal, glass acting as a moderate-conductivity cover, and the low-conductivity insulation minimizing heat losses to the surroundings (Costa & Kenisarin, 2022; Unar et al., 2020). The insulation layer was selected primarily to minimize rear conductive heat losses, thereby improving thermal energy retention and reducing irreversible exergy losses to the surroundings. These properties form the basis for the thermal resistance network described in Section 3.3 and are necessary for accurate prediction of fluid temperatures, collector efficiency, and overall system performance.

Table 1(e) PV electrical parameters c-Si modules

Parameter	Symbol	Baseline value	Unit
Reference PV efficiency (STC baseline)	η_{ref}	0.18	–
Reference temperature	T_{ref}	25	°C
Power temperature coefficient	β	−0.0037	1/°C

Table 1(e) specifies the PV electrical parameters used to couple the thermal and electrical sub-models. The reference efficiency $\eta_{ref} = 0.18$ at STC (1000 W/m², 25 °C, AM1.5) is representative of commercial crystalline silicon modules and lies within the typical 15–22 % range reported for modern c-Si technologies (Skoplaki & Palyvos, 2009; Elsabahy et al., 2024; Cotfas et al., 2018). Crystalline silicon PV technology was selected because of its widespread commercial deployment, well-characterized thermal behavior, established temperature-dependent electrical performance relationships, and suitability for coupled thermodynamic analysis under tropical operating conditions. The reference temperature $T_{ref} = 25\,°C$ corresponds to the standard test condition used for rating and translating PV performance (Ozcan & Seval, 2022; Skoplaki & Palyvos, 2009). The power temperature coefficient $\beta = -0.0037\,°C^{-1}$ (−0.37 %/°C) falls within the commonly reported interval of roughly −0.3 to −0.5 %/°C for crystalline silicon cells and modules, reflecting the well-known decrease of maximum power and efficiency with increasing cell temperature (Skoplaki & Palyvos, 2009; Takyi & Nyarko, 2020; Chander et al., 2015; Mohammad & Al-Shohani, 2022). Therefore, η_{ref} and β define the linear sensitivity of electrical output to operating temperature and thus provide the key linkage between the thermal model and the electrical performance formulation in Section 3.2, ensuring that simulated power output remains consistent with realistic, datasheet-based PV behavior across the expected operating temperature range.

Thus, the selected materials and component configurations were intentionally chosen to represent a realistic and thermodynamically representative water-cooled flat-plate PVT system suitable for tropical climatic environments and low-temperature thermal energy applications.

ARTICLE IN PRESS

3.0 Mathematical and Thermodynamic Modeling

The overall numerical implementation procedure adopted in the present study consists of the following sequential stages: (i) specification of the meteorological and operating boundary conditions, (ii) solution of the coupled thermal–electrical energy balances for the PVT collector and storage tank, (iii) evaluation of the PV temperature and useful thermal energy transfer, (iv) computation of entropy generation and subsystem exergy destruction using the Gibbs Tds formulation, and (v) thermodynamic performance assessment through parametric and second-law analyses. This structured workflow ensures consistent coupling between the thermal, electrical, and thermodynamic components of the model.

In the present study, the reported thermal, electrical, entropy-generation, and exergy-related parameters were obtained numerically through the developed thermodynamic modeling framework using the governing conservation equations, thermophysical property relations, and meteorological boundary conditions described in the manuscript. The simulation procedure was implemented under transient operating conditions representative of tropical climatic environments.

3.1 Governing Conservation Equations

The thermodynamic model is developed by applying the conservation laws to the two principal control volumes shown in Figure 2: (i) the PVT collector control volume, and (ii) the storage tank control volume. The geometric parameters and material properties required by the model are provided in Table 1.

3.1.1 Energy Balance (Control Volume Form)

(a) General steady-flow energy equation

For a control volume operating under quasi-steady conditions (valid for the collector at each time step), the steady-flow energy equation is written as in Equation (2). This equation accounts for internal energy changes as well as kinetic and potential energy variations in the fluid flow (David et al., 2021; Kumar, 2022). It provides a comprehensive framework to model energy conversion and transport in engineering applications involving fluid flow with heat and work interactions (Wang & Wang, 2020; Kumar, 2022).

$$\dot{Q} - \dot{W} + \sum \dot{m}\left(h + \frac{V^2}{2} + gz\right)_{in} = \sum \dot{m}\left(h + \frac{V^2}{2} + gz\right)_{out} \quad (2)$$

where $\dot{Q}_{cv}$ is the heat transfer rate to the control volume (W), $\dot{W}$ is the work transfer rate from the control volume (W), $\dot{m}$ is the mass flow rate (kgs^{-1}), h is the specific enthalpy (Jkg^{-1}), V is the flow velocity (ms^{-1}), g is the gravitational acceleration (ms^{-2}), and z is the elevation (m), while the subscripts "in" and "out" denote inlet and outlet states, respectively. Extensions of this equation also support dynamic modeling of integrated energy systems by coupling thermal and hydraulic behaviors (Dancker & Wolter, 2021; Huang et al., 2023).

For the PVT collector, kinetic and potential energy changes are negligible, and shaft work across the collector is zero. Hence, Equation (2) reduces to Equation (3):

$$\dot{Q}_{cv} = \dot{m}(h_{out} - h_{in}) \quad (3)$$

where h_{in} and h_{out} are the specific enthalpies of the fluid at the collector inlet and outlet, respectively.

(b) Useful heat gain to the working fluid

For liquid water, the enthalpy difference is approximated by Equation (4):

$$h_{out} - h_{in} = c_p(T_{out} - T_{in}) \quad (4)$$

ARTICLE IN PRESS

where c_p is the specific heat capacity of the working fluid at constant pressure ($J\ kg^{-1}K^{-1}$), and T_{in} and T_{out} are the inlet and outlet fluid temperatures, respectively (K).
Accordingly, the useful thermal gain of the collector becomes(Equation (5)):

$$\dot{Q}_u = \dot{m} c_p (T_{out} - T_{in}) \quad (5)$$

(c) Solar energy partition in the PVT collector
The absorbed solar power by the collector is defined by Equation (6)

$$\dot{Q}_{abs} = (\tau\alpha) A_c G \quad (6)$$

where τ is the effective transmittance of the cover, α is the effective absorptance of the absorber-PV surface, A_c is the collector aperture area (m^2), and G is the global solar irradiance incident on the collector plane (Wm^{-2}). The product $(\tau\alpha)$ represents the overall optical efficiency of the collector.
The absorbed energy is partitioned into electrical output, useful thermal gain, and thermal losses to the ambient (Equation (7)):

$$\dot{Q}_{abs} = P_{el} + \dot{Q}_u + \dot{Q}_{loss} \quad (7)$$

where $\dot{Q}_{abs}$ is the absorbed solar power (W), P_{el} is the electrical power output of the PV module (W), $\dot{Q}_u$ is the useful thermal power transferred to the working fluid (W), and $\dot{Q}_{loss}$ is the total thermal loss to the surroundings (W).

The lumped thermal loss term is modeled as (Equation (8)):

$$\dot{Q}_{loss} = U_L A_c (T_{pvt} - T_{amb}) \quad (8)$$

where T_{pvt} represents a characteristic collector temperature (e.g., PV cell or absorber mean temperature, depending on the implemented resistance network) and U_L is the overall heat loss coefficient of the collector ($Wm^{-2}K^{-1}$). The overall heat loss coefficient U_L accounts for the combined effects of convective, radiative, and conductive heat losses from the collector to the environment.

(d) Storage tank energy balance (well-mixed)
The tank is modeled as a well-mixed thermal capacitance with uniform temperature $T_{tank}(t)$. The transient tank energy balance is (Equation (9)):

$$m_t c_p \frac{dT_{tank}}{dt} = \dot{m} c_p (T_{out} - T_{tank}) - U_t A_t (T_{tank} - T_{amb}) \quad (9)$$

where $m_t = \rho V_t$ and ρ and c_p are evaluated at the mean tank temperature.

3.1.2 Mass and Momentum

(a) Mass conservation
Since the system operates in a closed loop with incompressible water, the mass flow rate is constant along the loop (Equation (10)):

$$\dot{m}_{in} = \dot{m}_{out} = \dot{m} \quad (10)$$

(b) Pressure drop model

ARTICLE IN PRESS

Pressure losses in the collector tubes (and optionally pipes) are modeled to enable frictional entropy generation terms later in the second-law analysis. The Darcy–Weisbach equation is applied (Equation (11)). This equation is widely used due to its broad applicability in pressurized pipe flow and forms a basis for calculating head loss in engineering systems (De Almeida Minhoni et al., 2020; Abdulameer et al., 2022).

$$\Delta P = f\frac{L}{D_h}\frac{\rho v^2}{2} + \sum K\frac{\rho v^2}{2} \tag{11}$$

where f is the friction factor, L is the flow length, D_h is the hydraulic diameter, v is the mean velocity, and K represents minor loss coefficients. Experimental studies confirm that Darcy–Weisbach accurately predicts head loss in various pipe materials and flow regimes, including turbulent flows in small-diameter pipes common in irrigation systems (Lima et al., 2025; Ciprian, 2019).

The mean velocity is expressed as (Equation (12)):

$$v = \frac{\dot{m}}{\rho A_f} \tag{12}$$

with A_f being the flow cross-sectional area.

For laminar flow ($Re < 2300$):

$$f = \frac{64}{Re} \tag{13}$$

For turbulent flow, f may be computed using a standard explicit correlation (e.g., Blasius for smooth tubes) for appropriate Reynolds number ranges (Equation (14)):

$$f = 0.3164\, Re^{-0.25} \tag{14}$$

The Reynolds number is (Equation (15)):

$$Re = \frac{\rho v D_h}{\mu} \tag{15}$$

The pressure drop formulation in Equations (11) – (15) is used in Section 3.4 to quantify frictional irreversibility through entropy generation and exergy destruction.

ARTICLE IN PRESS

3.1.3 Boundary Conditions

The model requires time-dependent environmental inputs and specified operating conditions.

(a) Meteorological boundary conditions

At each simulation time step (Equation (16)):

$$G = G(t),\ T_{amb} = T_{amb}(t) \tag{16}$$

If wind speed is used to evaluate convective losses (Equation (17)):

$$v_w = v_w(t) \tag{17}$$

(b) Hydraulic boundary conditions

The mass flow rate is specified (constant or time-dependent) (Equation (18)):

$$\dot{m} = \dot{m}(t) \tag{18}$$

(c) Thermal coupling condition (tank–collector)

For the closed-loop well-mixed tank configuration in Figure 2, the collector inlet temperature equals the tank temperature (Equation (18)):

ARTICLE IN PRESS

$$T_{in}(t) = T_{tank}(t) \tag{19}$$

(d) Initial condition for transient simulation
For simulations including the tank transient (Equation (20)):

$$T_{tank}(t = 0) = T_{tank,0} \tag{20}$$

Equations (2) – (20) define the conservation-law foundation of the model. In the next subsection, the electrical behavior of the PV layer is introduced and coupled to the thermal model through the temperature-dependent electrical efficiency relation.

3.2 PV Electrical Model

The electrical behavior of the photovoltaic layer is strongly dependent on the cell operating temperature, which is governed by the thermal balance of the PVT collector described in Section 3.1. In this study, the PV electrical model is therefore fully coupled to the thermal model through the PV cell temperature T_{pv}, as indicated schematically in Figure 2.

3.2.1 PV Temperature Model

The PV cell temperature is not an independent variable but results from the heat transfer processes within the PVT collector. It is determined from the collector thermal balance through the thermal resistance network between the PV cells, absorber, working fluid, and ambient environment.
In lumped-parameter form, the energy balance on the PV layer can be expressed as (Equation (21)):

$$(\tau\alpha)A_c G = P_{el} + \dot{Q}_{pv\to f} + \dot{Q}_{pv\to amb} \tag{21}$$

Where $\dot{Q}_{pv\to f}$ is the heat transferred from the PV layer to the absorber/fluid and $\dot{Q}_{pv\to amb}$ is the heat lost from the PV layer to the ambient.
Using a thermal resistance representation, these heat transfer terms are written as (Equation (22)):

$$\dot{Q}_{pv\to f} = \frac{T_{pv} - T_f}{R_{pv-f}} \tag{22}$$

And (Equation (23))

$$\dot{Q}_{pv\to amb} = \frac{T_{pv} - T_{amb}}{R_{pv-amb}} \tag{23}$$

where T_f is a representative mean fluid temperature (e.g., $T_f \approx (T_{in} + T_{out})/2$), and R_{pv-f} and R_{pv-amb} are equivalent thermal resistances, constructed from the material layers and convection/radiation coefficients.
Substituting Equations (22) and (23) into Equation (21) yields Equation (24):

ARTICLE IN PRESS

$$(\tau\alpha)A_cG = P_{el} + \frac{T_{pv} - T_f}{R_{pv-f}} + \frac{T_{pv} - T_{amb}}{R_{pv-amb}} \quad (24)$$

Equation (24) is solved simultaneously with the collector energy equations (Section 3.1) to obtain the PV cell temperature T_{pv} at each time step.
For numerical implementation, the mean fluid temperature is approximated as:

$$T_f = \frac{T_{in} + T_{out}}{2} \quad (25)$$

3.2.2 Electrical Power and Efficiency Relations

The electrical efficiency of the PV module decreases approximately linearly with increasing cell temperature. This effect is modeled using the standard temperature-corrected efficiency relation (Equation (26)):

$$\eta_{el}(T_{pv}) = \eta_{ref}[1-\beta(T_{pv}-T_{ref})] \quad (26)$$

Where η_{ref} is the reference efficiency at temperature T_{ref} (usually 298.15 K) and β is the temperature coefficient of the PV module.
The instantaneous electrical power output of the PVT collector is then given by (Equation (27)):

$$P_{el} = \eta_{el}(T_{pv})A_cG \quad (27)$$

Substituting Equation (26) into Equation (27) yields Equation (28)

$$P_{el} = \eta_{ref}[1-\beta(T_{pv}-T_{ref})]A_cG \quad (28)$$

Equations (26) – (28) establish the direct coupling between the thermal and electrical performances of the PVT collector: any reduction in T_{pv} achieved through enhanced heat extraction by the working fluid (Equation. (5)) leads to an increase in electrical efficiency and power output.
The electrical model given by Equations (21) – (28) is fully coupled to the thermal balances presented in Section 3.1 through the PV cell temperature T_{pv}. In the next subsection, the detailed heat transfer mechanisms within the PVT collector and the associated loss terms are formulated.

3.3 Heat Transfer Sub-Models

The thermal behavior of the PVT collector is governed by a combination of optical absorption, conduction through solid layers, convection to the ambient air, radiation exchange with the surroundings, and convection to the circulating working fluid. These mechanisms are represented using a lumped thermal resistance network consistent with the schematic shown in Figure 2 and the energy balances formulated in Sections 3.1 and 3.2.
In the present study, the heat transfer relations are introduced primarily to establish the coupled thermal interactions governing PV temperature regulation, useful heat extraction, and entropy generation within the PVT collector. Accordingly, emphasis is placed on the thermodynamic implications of these mechanisms rather than on detailed derivational treatment of standard heat transfer correlations.

ARTICLE IN PRESS

3.3.1 Solar Absorption and Optical Losses

The solar radiation incident on the collector surface is partially transmitted through the glass cover and absorbed by the PV cells and the absorber. The effective absorbed solar power is expressed as (Equation (29)):

$$\dot{Q}_{abs} = (\tau\alpha)_{eff} A_c G \tag{29}$$

where $(\tau\alpha)_{eff}$ is the effective transmittance–absorptance product of the glass–PV–absorber assembly.

The optical losses are therefore (Equation (30)):

$$\dot{Q}_{opt,loss} = A_c G\left[1 - (\tau\alpha)_{eff}\right] \tag{30}$$

Only the absorbed part given by Equation (29) contributes to electrical generation and thermal heating in the PVT collector, as already used in Equation (6).

3.3.2 Convection to the Ambient (Wind Correlation)

Convective heat loss from the top surface of the PVT collector to the ambient air is modeled as (Equation (31)):

$$\dot{Q}_{conv,amb} = h_{c,amb} A_c \left(T_{pvt} - T_{amb}\right) \tag{31}$$

The convective heat transfer coefficient is correlated to wind speed using a widely adopted empirical relation (Equation (32)):

$$h_{c,amb} = 5.7 + 3.8\, v_w \tag{32}$$

where v_w is the wind speed in m/s and $h_{c,amb}$ is in W/m²·K.

3.3.3 Radiation Losses

Radiative heat exchange between the PVT surface (or glass cover) and the sky is expressed as (Equation (33)):

$$\dot{Q}_{rad,amb} = \varepsilon_{eff} \sigma A_c \left(T_{pvt}^4 - T_{sky}^4\right) \tag{33}$$

Where ε_{eff} is the effective emissivity of the top surface and σ is the Stefan–Boltzmann constant. This formulation captures long-wave radiative cooling effects that can significantly influence PVT system performance, especially at night or under clear-sky conditions (Eicker & Dalibard, 2011; Zhao et al., 2020). Radiative cooling also plays a role in reducing building energy consumption when integrated into ventilated PVT roofs or ground-coupled heat exchangers, improving thermal efficiency through passive heat rejection to the sky (Shao et al., 2022; Jia et al., 2022). Thus, radiative heat exchange with the sky is a critical factor in optimizing PVT system thermal management and enhancing renewable energy utilization (Hu et al., 2022).

The effective sky temperature is approximated by (Equation (34)):

ARTICLE IN PRESS

$$T_{sky} = 0.0552\, T_{amb}^{1.5} \tag{34}$$

with all temperatures in Kelvin.

3.3.4 Convection to the Fluid (Internal Heat Transfer Coefficient)

The heat transferred from the absorber to the working fluid is modeled as (Equation (35)):

$$\dot{Q}_f = h_f A_f \left(T_{abs} - T_f\right) \tag{35}$$

Where h_f is the internal convective heat transfer coefficient, A_f is the effective heat transfer area, T_{abs} is the absorber temperature and T_f is the mean fluid temperature given by Equation (25). The internal convective heat transfer coefficient is evaluated using standard dimensionless heat transfer correlations based on Reynolds, Prandtl, and Nusselt numbers for laminar and turbulent internal flow conditions (David et al., 2021; Van Zyl et al., 2013):

$$h_f = \frac{Nu\, k_f}{D_h} \tag{36}$$

where Nu is the Nusselt number and D_h is the hydraulic diameter of the flow channel (m).
The Reynolds number is (Saldaña et al., 2024; Tamburrino & Niño, 2025; Abimanyu et al., 2025):

$$Re = \frac{\rho v D_h}{\mu} \tag{37}$$

where μ is the dynamic viscosity of the working fluid (Pas).
For laminar flow ($Re < 2300$):

$$Nu = 4.36 \tag{38}$$

For turbulent flow ($Re > 3000$) (Dittus–Boelter correlation):

$$Nu = 0.023 Re^{0.8} Pr^{0.4} \tag{39}$$

where the Prandtl number is:

$$Pr = \frac{c_p \mu}{k_f} \tag{40}$$

3.3.5 Overall Heat Loss Coefficient

The total heat loss from the collector to the ambient is the sum of convective and radiative losses (Equation (41))::

$$\dot{Q}_{loss} = \dot{Q}_{conv,amb} + \dot{Q}_{rad,amb} \tag{41}$$

This total loss is represented in lumped form by (Equation (42)):

$$\dot{Q}_{loss} = U_L A_c \left(T_{pvt} - T_{amb}\right) \tag{42}$$

ARTICLE IN PRESS

Thus, the overall heat loss coefficient is (Equation (43)):

$$U_L = h_{c,amb} + h_{r,amb} \tag{43}$$

where the equivalent radiative heat transfer coefficient is (Equation (44)):

$$h_{r,amb} = \varepsilon_{eff}\sigma\left(T_{pvt} + T_{sky}\right)\left(T_{pvt}^2 + T_{sky}^2\right) \tag{44}$$

3.3.6 Thermal resistance network formulation

The conduction and convection processes between the PV layer, absorber, fluid, and ambient are represented by an equivalent thermal resistance network. The dominant resistances include (Equation (45)):

$$R_{pv-f} = R_{cond,layers} + \frac{1}{h_f A_f} \tag{45}$$

And (Equation (46)):

$$R_{pv-amb} = \frac{1}{(h_{c,amb} + h_{r,amb})A_c} \tag{46}$$

These resistances are used directly in the PV temperature equation (Equation (24)) and in the global energy balance relations in Section 3.1.

The heat transfer sub-models defined by Equations (29) – (46) close the thermal description of the PVT collector and provide the temperature fields required for the electrical model (Section 3.2) and the second-law analysis developed in the next section.

ARTICLE IN PRESS

3.4 Entropy Generation and Tds-Based Thermodynamic Formulation

The second-law analysis of the PVT system is developed using the fundamental Gibbs relations, also known as the Tds equations. These relations provide the link between entropy variations and changes in internal energy, enthalpy, pressure, and temperature, and form the theoretical basis for the rigorous quantification of irreversibilities in the system components shown in Figure 2.

Unlike conventional PVT analyses that treat entropy generation using simplified global exergy balances, the present formulation directly employs the Gibbs Tds relations to resolve subsystem-level irreversible processes associated with coupled thermal transport, ambient heat rejection, and fluid-flow dissipation. This enables a more physically diagnostic interpretation of thermodynamic losses within the PVT system.

3.4.1 Tds Equations (Gibbs Relations)

For a simple compressible system, the fundamental thermodynamic relations are written as (Equation (47)):

$$T\,dS = dU + P\,dV \tag{47}$$

where T is the absolute temperature (K), S is the entropy (JK^{-1}), U is the internal energy (J), P is the pressure (Pa), and V is the volume (m^3). This form is especially convenient when ($U = U(S,V$)) and underpins entropy balances and entropy generation expressions in second-law analysis of closed or simple PVT systems (Moran et al., 2010; Bejan, 2013).

ARTICLE IN PRESS

And (Equation (48)):

$$T\,dS = dH - V\,dP \tag{48}$$

where H is the enthalpy (J), suitable when ($H = H(S,P)$), as in many flow and control-volume applications (Moran et al., 2010, 2014; Bejan, 2013), while all other symbols have their usual thermodynamic meanings. The Tds underpin entropy balance, entropy generation, and exergy analysis, and are treated as central tools for second-law and optimization-based design in both Moran et al. (2010) and Bejan's (2013) thermodynamics frameworks.

Equations (47) and (48) are equivalent forms of the Gibbs fundamental relation and are used in this work to derive the entropy balance and entropy generation terms for the solid and fluid control volumes.

For an incompressible liquid such as water, the differential entropy change can be approximated as (Equation (49)):

$$ds = c_p \frac{dT}{T} \tag{49}$$

which is consistent with the enthalpy relation $dh = c_p dT$ and is used in the subsequent formulations for the working fluid.

3.4.2 Entropy Balance for System Components

The general entropy balance for a control volume is in Equation (50) (Çengel & Boles, 2002; Nasrin et al., 2016; Malekan et al., 2019; Mwesigye et al., 2018; Krishna et al., 2020; Kalateh et al., 2022; Al-Najjar et al., 2024; Rao et al., 2024):

$$\frac{dS_{cv}}{dt} = \sum \dot{m}_{in} s_{in} - \sum \dot{m}_{out} s_{out} + \sum_k \frac{\dot{Q}_k}{T_k} + \dot{S}_{gen} \tag{50}$$

where S_{cv} is the total entropy within the control volume ($J\,K^{-1}$), s is specific entropy ($Jkg^{-1}\,K^{-1}$), T_k is the boundary temperature at which heat transfer $\dot{Q}_k$ occurs (K), and $\dot{S}_{gen}$ is the entropy generation rate due to irreversibilities (WK^{-1}).

Under quasi-steady conditions for the PVT collector control volume, Equation (51) reduces to:

$$\dot{S}_{gen,cv} = \dot{m}(s_{out} - s_{in}) - \sum_k \frac{\dot{Q}_k}{T_k} \tag{51}$$

(a) Fluid control volume (inside collector tubes)

For the working fluid flowing through the collector (Equation (52)):

$$\dot{S}_{gen,f} = \dot{m}(s_{out} - s_{in}) - \frac{\dot{Q}_u}{T_b} \tag{52}$$

where T_b is a representative boundary temperature at which heat is transferred from the solid to the fluid (e.g., absorber mean temperature).

ARTICLE IN PRESS

Using Equation (49), the entropy change of the fluid becomes:

$$s_{out} - s_{in} = c_p \ln\left(\frac{T_{out}}{T_{in}}\right) \tag{53}$$

Substituting Equation (53) into Equation (52) yields Equation (54),

$$\dot{S}_{gen,f} = \dot{m}\, c_p \ln\left(\frac{T_{out}}{T_{in}}\right) - \frac{\dot{Q}_u}{T_b} \tag{54}$$

(b) Solid control volume (PV + absorber assembly)
For the solid part of the PVT collector, operating under steady conditions (Equation (55)):

$$\dot{S}_{gen,s} = \frac{\dot{Q}_{abs}}{T_{sun}} - \frac{\dot{Q}_{pv\to f}}{T_b} - \frac{\dot{Q}_{loss}}{T_{amb}} \tag{55}$$

where T_{sun} is the effective blackbody temperature of the sun and the terms represent entropy inflow with radiation, entropy outflow to the fluid, and entropy rejected to the ambient, respectively.

3.4.3 Sources of Entropy Generation

In the present system, entropy generation arises from three main physical mechanisms:

(a) Heat transfer across finite temperature differences
This contribution is inherently captured in Equations (54) and (55). In compact form, the contribution associated with finite-temperature heat transfer within the PVT collector can be expressed as (Çengel & Boles, 2002; Nasrin et al., 2016; Malekan et al., 2019; Mwesigye et al., 2018; Krishna et al., 2020; Wang et al., 2024; Satpute et al., 2025) in Equation (56)

$$\dot{S}_{\Delta T} = \dot{m}\, c_p \ln\left(\frac{T_{out}}{T_{in}}\right) - \frac{\dot{Q}_u}{T_b} + \frac{\dot{Q}_{loss}}{T_{amb}} - \frac{\dot{Q}_{abs}}{T_{sun}} \tag{56}$$

This expression explicitly accounts for entropy changes associated with sensible heating of the working fluid, useful heat transfer at the absorber–fluid interface, thermal losses to the ambient, and the exergy content of the absorbed solar radiation, thereby providing a direct second-law measure of thermal irreversibility within the collector.

(b) Viscous friction (pressure drop in tubes)
Using the second Gibbs relation (Equation (48)) for the flowing liquid, the entropy generation associated with pressure drop is approximated by (Equation (57)):

$$\dot{S}_{fr} = \frac{\dot{m}}{\rho}\frac{\Delta P}{T_f} \tag{57}$$

where ΔP is given by Equation (11) and T_f is the mean fluid temperature.

ARTICLE IN PRESS

(c) Thermal losses to the ambient

The entropy generation associated with heat rejection to the ambient is (Equation (58)):

$$\dot{S}_{loss} = \dot{Q}_{loss}\left(\frac{1}{T_{amb}} - \frac{1}{T_{pvt}}\right) \tag{58}$$

3.4.4 Total Entropy Generation Rate (System Level)

The total entropy generation rate of the PVT system is obtained by summing all contributions (Bejan, 2013; Kalateh et al., 2022):

$$\dot{S}_{gen,tot} = \dot{S}_{\Delta T} + \dot{S}_{fr} \tag{59}$$

where $\dot{S}_{\Delta T}$ is the entropy generation rate due to heat transfer across finite temperature differences, and $\dot{S}_{fr}$ is the entropy generation rate due to fluid friction (viscous dissipation). This expression separates thermal irreversibility from hydraulic irreversibility within the PVT system (Equation (60)).

or, equivalently, by summing the component-wise terms:

$$\dot{S}_{gen,tot} = \dot{S}_{gen,f} + \dot{S}_{gen,s} + \dot{S}_{fr} \tag{60}$$

Equations (59) and (60) provide the basis for identifying the dominant irreversibility mechanisms in the system and for the subsequent exergy destruction analysis presented in Section 3.5.

Once the total entropy generation rate is known from Equations (59) – (60), the corresponding exergy destruction can be evaluated using the Gouy–Stodola theorem, as formulated in the next section.

Unlike conventional first-law-based PVT analyses that primarily quantify energy quantities, the present formulation enables direct identification of the dominant irreversibility mechanisms governing thermodynamic performance degradation. This provides a physically meaningful basis for interpreting how thermal coupling, ambient heat rejection, and fluid transport processes influence overall system optimization under tropical operating conditions.

3.5 Exergy Analysis

The exergy analysis provides a second-law measure of the quality of energy flows and quantifies the thermodynamic losses associated with irreversibilities. In this study, the exergy framework is built directly upon the entropy generation model developed in Section 3.4 and the energy balances presented in Sections 3.1–3.3.

The exergy framework is employed not merely to quantify energy conversion performance, but to evaluate the thermodynamic quality of the recovered electrical and thermal energy streams and to identify the irreversible losses limiting useful energy utilization within the PVT system.

All exergy quantities are evaluated relative to the reference (dead) state defined by the ambient conditions (Equation (61)):

$$T_0 = T_{amb},\ P_0 = P_{amb} \tag{61}$$

3.5.1 Flow Exergy of the Working Fluid

ARTICLE IN PRESS

The specific flow exergy of a stream is defined as (Moran et al., 2010, 2014; Bejan, 2013; Kalateh et al., 2022):

$$ex = (h - h_0) - T_0(s - s_0) \tag{62}$$

where ex is the specific flow exergy (Jkg^{-1}), the subscript 0 denotes properties evaluated at the environmental (dead-state) conditions, and T_0 is the ambient reference temperature (K). This expression represents the maximum useful work obtainable as the fluid is brought reversibly to the environmental state.
Accordingly, the exergy rate associated with the working fluid flowing through the PVT collector is (Bejan, 2013; Kalateh et al., 2022):

$$\dot{E}x_f = \dot{m}[(h_{out} - h_{in}) - T_0(s_{out} - s_{in})] \tag{63}$$

where $\dot{E}_{x,f}$ is the rate of flow exergy gain of the working fluid (W).
For liquid water with constant properties, using (Çengel & Boles, 2002; Moran et al., 2010):

$$h_{out} - h_{in} = c_p(T_{out} - T_{in}) \tag{64}$$

This approximation is valid for incompressible liquids over the investigated temperature range, for which variations of c_p are negligible (Moran et al., 2010, Bejan, 2013).

$$s_{out} - s_{in} = c_p \ln\left(\frac{T_{out}}{T_{in}}\right) \tag{65}$$

Equation (63) becomes:

$$\dot{E}x_{th} = \dot{m}c_p\left[(T_{out} - T_{in}) - T_0 \ln\left(\frac{T_{out}}{T_{in}}\right)\right] \tag{66}$$

Equation (66) represents the useful thermal exergy gain of the working fluid.

3.5.2 Solar Radiation Exergy Input

The exergy associated with the incident solar radiation is evaluated using the Petela–Landsberg exergy of solar radiation formulation (Bejan, 2016; Çengel & Boles, 2019; Duffie & Beckman, 2013):

$$\dot{E}x_{solar} = A_c G\left[1 - \frac{4}{3}\left(\frac{T_0}{T_{sun}}\right) + \frac{1}{3}\left(\frac{T_0}{T_{sun}}\right)^4\right] \tag{67}$$

where T_{sun} is the effective temperature of the sun, taken as $T_{sun} = 5777$ K and $T_0 = 298\ K$

3.5.3 Exergy Destruction (Gouy–Stodola Theorem)

ARTICLE IN PRESS

The exergy destruction rate associated with irreversibilities in the system is directly related to the total entropy generation rate obtained in Section 3.4, it is given by Equation (68) by Gouy–Stodola theorem as in (Bejan, 2002; Kotas, 2012; Pal, 2017, Pal, 2018; Pal, 2019).

$$\dot{E}x_{dest} = T_0 \, \dot{S}_{gen,tot} \tag{68}$$

where $\dot{S}_{gen,tot}$ is given by Equations (59) – (60).
Equation (68) provides the quantitative measure of lost work potential due to heat transfer across finite temperature differences, thermal losses, and viscous friction in the PVT system.

3.5.4 Exergy Efficiency Definitions

(a) Electrical exergy output

Since electrical power is a fully convertible (high-grade) form of energy, its exergy is equal to the electrical power itself:

$$\dot{E}x_{el} = P_{el} \tag{69}$$

where $\dot{E}_{x,el}$ is the exergy rate associated with the electrical output (W).

(b) Thermal exergy efficiency

The thermal exergy efficiency is defined as the ratio of useful thermal exergy gain of the fluid to the solar exergy input (Equation (70)):

$$\eta_{ex,th} = \frac{\dot{E}x_{th}}{\dot{E}x_{solar}} \tag{70}$$

where $\dot{E}x_{th}$ is given by Equation (66).

(c) Electrical exergy efficiency

The electrical exergy efficiency is defined as (Equation (71)):

$$\eta_{ex,el} = \frac{P_{el}}{\dot{E}x_{solar}} \tag{71}$$

where $\eta_{ex,el}$ is the electrical exergy efficiency.

(d) Overall exergy efficiency

The overall exergy efficiency of the PVT system is defined as (Equation (72)):

$$\eta_{ex,tot} = \frac{P_{el} + \dot{E}x_{th}}{\dot{E}x_{solar}} \tag{72}$$

where $\eta_{ex,tot}$ is the total exergy efficiency of the PVT system. This definition accounts simultaneously for the useful electrical and thermal exergy outputs relative to the exergy content of the incident solar radiation.

ARTICLE IN PRESS

Consistency relation
From the exergy balance of the system (Equation (73)):

$$\dot{E}x_{solar} = P_{el} + \dot{E}x_{th} + \dot{E}x_{dest} \tag{73}$$

which provides a useful check on numerical accuracy and thermodynamic consistency.

Table 2. Summary of governing thermodynamic relations and their primary outputs used in the numerical model.

Category	Equation No.	Relation	Primary Output
Useful heat gain	(5)	$\dot{Q}_u = \dot{m}c_p(T_{out} - T_{in})$	Thermal power
PV temperature	(24)	Energy balance on PV layer	T_{pv}
Electrical power	(28)	$P_{el} = \eta_{ref}[1 - \beta(T_{pv} - T_{ref})]A_c G$	Electrical power
Tank temperature	(9)	Tank energy balance	$T_{tank}(t)$
Fluid entropy change	(53)	$s_{out} - s_{in} = c_p \ln(T_{out}/T_{in})$	Entropy rise
Fluid entropy generation	(54)	Entropy balance (fluid CV)	$\dot{S}_{gen,f}$
Friction entropy	(57)	$\dot{S}_{fr} = \dot{m}\Delta P/(\rho T_f)$	Friction irreversibility
Total entropy gen.	(60)	Sum of contributions	$\dot{S}_{gen,tot}$
Thermal exergy gain	(66)	Flow exergy rise	$\dot{E}x_{th}$
Solar exergy input	(67)	Petela equation	$\dot{E}x_{solar}$
Exergy destruction	(68)	$T_0 \dot{S}_{gen,tot}$	$\dot{E}x_{dest}$
Overall exergy efficiency	(72)	$(P_{el} + \dot{E}x_{th})/\dot{E}x_{solar}$	$\eta_{ex,tot}$

ARTICLE IN PRESS

With the formulations presented in Sections 3.1–3.5, the complete coupled energy–entropy–exergy model of the PVT system is fully defined. The next section describes the numerical solution procedure used to solve the governing equations and perform the parametric simulations

4.0 Numerical Simulation Procedure

The coupled thermal–electrical and thermodynamic equations developed in the present study were solved numerically under transient operating conditions using time-dependent meteorological inputs representative of Kampala, Uganda. At each simulation time step, the collector energy balances, PV electrical performance relations, storage tank energy equation, entropy generation expressions, and exergy balance equations were solved sequentially to obtain the instantaneous thermodynamic state of the system. The collector inlet temperature was continuously updated from the well-mixed storage tank temperature, thereby maintaining dynamic thermal coupling between the collector and storage subsystems throughout the simulation period. The numerical implementation was used to evaluate temperature evolution, useful thermal energy recovery, electrical output, entropy generation, exergy destruction, and overall thermodynamic performance under varying operating conditions.

ARTICLE IN PRESS

Thermophysical properties, operating parameters, and environmental boundary conditions employed in the simulations were obtained from standard literature correlations, established photovoltaic–thermal modeling practices, and representative meteorological conditions for Kampala, Uganda. The developed numerical framework was subsequently used to evaluate collector temperatures, electrical efficiency, useful thermal energy recovery, entropy generation, and exergy destruction throughout the analysis.

The coupled energy–entropy–exergy model (Sections 3.1–3.5) is solved numerically to obtain transient and steady-state performance metrics of the closed-loop, water-cooled PVT system with well-mixed storage tank shown in Figure 2. This section details the solution strategy, algorithm, inputs, convergence criteria, and validation plan.

4.1 Solution Approach

The model is implemented in a time-marching framework using a lumped parameter solver that advances the tank temperature in time while solving the collector thermal–electrical balance quasi-steadily at each time step.

At each time step t_n:

1. Read meteorological inputs $G(t_n)$,$T_{amb}(t_n)$,$v_w(t_n)$ (Equations 16–17).
2. Solve the thermal–electrical balance (Equations 5, 24, 28) to update T_{pv},T_{out}, and P_{el}.
3. Update entropy generation terms (Equations 54, 57–60).
4. Evaluate exergy flows (Equations 66, 67, 68).
5. Integrate the storage tank energy balance (Equation 9) to find $T_{tank}(t_{n+1})$.

This transient time-marching approach captures dynamic behavior while maintaining computational efficiency because the PVT collector itself is treated as quasi–steady state relative to the slower tank dynamics. Similar lumped-parameter transient approaches are widely adopted in PVT simulation studies due to acceptable accuracy and reduced computational cost compared to full CFD/2-D models.

4.2 Algorithm and Flowchart

The numerical procedure follows an iterative solution within each time step until convergence of key state variables:

Algorithm 4.1 (per time step)

1. Initialize: Set $T_{tank}(t_0) = T_{tank,0}$ (Equation 20).
2. Loop over time: for $t_n = t_0$ to t_{end} with Δt:
   2.1 Assign boundary conditions $G(t_n)$,$T_{amb}(t_n)$,$v_w(t_n)$.
   2.2 Set $T_{in} = T_{tank}(t_n)$ (Equation 19).
   2.3 Guess initial T_{pv} and T_{out}.
   2.4 Inner iteration:
      a. Solve thermal network (Equation 24) for T_{pv}.
      b. Update electrical output P_{el} (Equation 28).
      c. Solve fluid energy balance for T_{out} (Equation 5).
      d. Check inner convergence: $\left|T_{pv}^{k+1} - T_{pv}^{k}\right| < \epsilon_T$, $|T_{out}^{k+1} - T_{out}^{k}| < \epsilon_T$.
   2.5 Compute entropy generation $\dot{S}_{gen,tot}$ (Equation 59–60) and exergy terms (Equations 66 – 68).
   2.6 Advance tank temperature using tank ODE (Equation 9).
   2.7 Store results.

ARTICLE IN PRESS

Convergence criteria for inner iteration are typically set to $\epsilon_T = 10^{-4}$ K and energy balance residuals < 1 W.

4.3 Model Inputs and Datasets

The transient simulation is driven by time-resolved meteorological boundary conditions and a fixed set of system parameters. The required environmental inputs are global solar irradiance $G(t)$, ambient temperature $T_{amb}(t)$, and wind speed $v_w(t)$, while all geometric, thermal, and electrical properties of the collector and storage system are prescribed from the baseline configuration in Table 1.

A Typical Meteorological Year (TMY) dataset representative of the Kampala region is used to impose realistic tropical boundary conditions, obtained from standard satellite-based reanalysis or regional meteorological sources. All optical, thermal, and electrical properties, as well as tank and fluid parameters, are treated as fixed inputs. Owing to the one-dimensional lumped-parameter formulation, no spatial discretization is required, resulting in a computationally efficient framework consistent with most transient PVT models in the literature.

The numerical simulation was conducted over a representative diurnal operating period extracted from the Kampala TMY dataset. Therefore, the "test duration" in the present study refers to the simulated daily operating period rather than an experimental measurement campaign. Time-resolved meteorological inputs, including solar irradiance, ambient temperature, and wind speed, were applied at each simulation time step. Time-step independence was assessed using 3600 s, 1800 s, and 900 s intervals, and a 900 s time step was adopted for the final simulations because it provided stable results with acceptable computational efficiency.

4.4 Numerical Convergence and Independence Tests

Because the model is lumped-parameter, mesh independence is not applicable. Numerical robustness is ensured through time-step independence testing and strict convergence of the inner iterative solution of the coupled collector equations.

Time-step independence is verified by repeating simulations with decreasing time steps until the predicted tank temperature, electrical power, useful thermal output, and exergy efficiency change by less than 1%. Time steps of 3600 s, 1800 s, and 900 s were tested, and 900 s was adopted as a compromise between accuracy and computational cost.

At each time step, the nonlinear algebraic equations governing the thermal coupling between the PV layer, absorber, and working fluid are solved iteratively. Convergence is declared when

$$\left|T_{pv}^{k+1} - T_{pv}^{k}\right| < \varepsilon_T,\ \left|T_{out}^{k+1} - T_{out}^{k}\right| < \varepsilon_T \tag{73.1}$$

with ε_T in the range $10^{-4} - 10^{-3}\ K$.

4.5 Model Verification and Validation

Model credibility is established through internal verification and literature-based validation. Verification is ensured by strict adherence to energy, entropy, and exergy balance relations, with closure confirmed between absorbed solar energy, electrical output, useful thermal gain, and losses, and consistency enforced with the Gibbs (Tds) relations and the Gouy–Stodola theorem. Numerical robustness is further supported by the convergence and time-step independence tests described in Section 4.4.

ARTICLE IN PRESS

Validation is conducted through comparison of predicted transient PV temperature, outlet fluid temperature, useful thermal output, and electrical power with reference results reported in the literature for water-cooled PVT systems modeled using lumped-parameter or experimentally calibrated approaches. Agreement within commonly reported error margins, such as RMSE values below approximately 5% for temperatures and thermal outputs, is considered acceptable for system-level assessment. In the absence of experimental data under identical tropical conditions, the model is validated against high-quality numerical results from published PVT energy and exergy studies, which is appropriate for evaluating thermodynamic trends, irreversibility distributions, and optimization behavior.

ARTICLE IN PRESS

ARTICLE IN PRESS

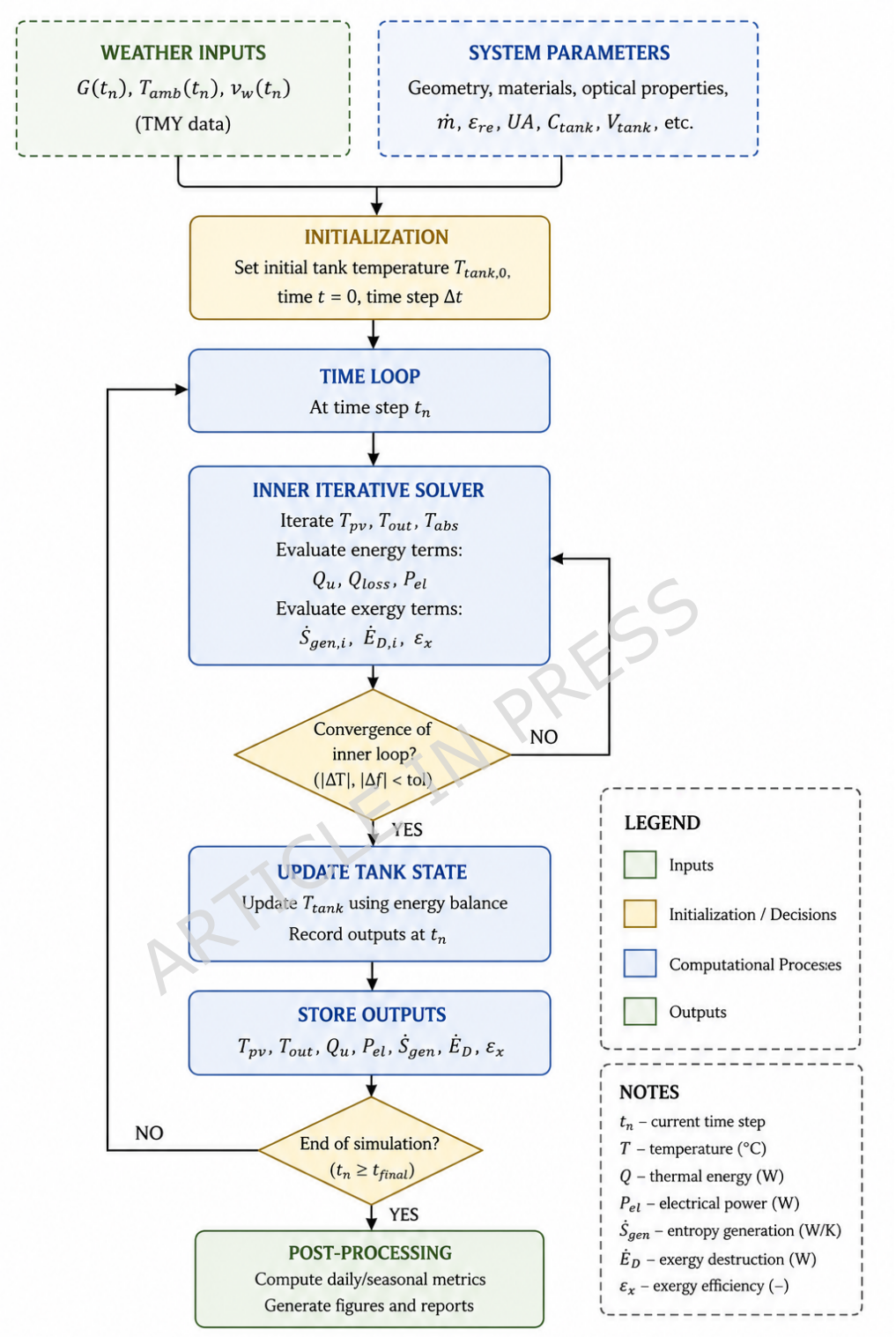

Figure 3 Workflow diagram of the numerical simulation procedure

The workflow (Figure 3) begins with the specification of time-resolved input data, including meteorological variables (G,T_{amb},v_w) and system parameters defined in Table 1. The simulation is initialized by prescribing the initial storage tank temperature $T_{tank,0}$. The solution then advances

ARTICLE IN PRESS

through a time-marching loop, within which an inner iterative solver is employed at each time step to resolve the coupled collector temperatures T_{pv} and T_{out}. Upon convergence, the instantaneous energy and exergy terms are evaluated, followed by a convergence check on the state variables. The storage tank temperature is subsequently updated, and all relevant outputs are recorded before proceeding to the next time step.

4.6 Numerical Uncertainty and Modeling Limitations

The present study is based on a transient numerical thermodynamic framework and therefore does not involve direct experimental measurement uncertainty associated with sensors or instrumentation. Nevertheless, several sources of modeling uncertainty may influence the obtained results. These include assumptions associated with thermophysical property correlations, convective heat-transfer coefficients, meteorological boundary conditions, uniform flow distribution within the absorber tubes, neglect of localized thermal contact resistances, and the use of a well-mixed storage-tank approximation. In addition, uncertainty may arise from temporal discretization and numerical convergence behavior during transient simulation. To improve robustness, parametric analyses were conducted over a range of operating conditions, including variations in solar irradiance, ambient temperature, and mass flow rate. Accordingly, the presented results should be interpreted within the assumptions and operating conditions adopted in the developed thermodynamic model.

5.0 Performance Indicators and Evaluation Metrics

To evaluate the thermodynamic performance of the PVT system shown in Figure 2, a set of energy- and exergy-based performance indicators is defined. These indicators are derived directly from the energy balances (Section 3.1), the electrical model (Section 3.2), the heat transfer sub-models (Section 3.3), and the entropy–exergy framework (Sections 3.4 and 3.5).

To ensure fair comparison with conventional PV and published PVT systems, all energy, exergy, and efficiency indicators in this study are evaluated with respect to the total solar receiving area of the collector, represented by the aperture area A_c, rather than the PV cell area alone. This normalization is essential because the PVT collector receives solar radiation over the entire collector aperture and simultaneously produces electrical and thermal outputs from the same receiving area.

5.1 Thermal Performance Metrics

(a) Useful thermal power

The useful thermal power transferred to the working fluid is given by Equation (5), repeated here for clarity (Equation (74)):

$$\dot{Q}_u = \dot{m} c_p (T_{out} - T_{in}) \tag{74}$$

(b) Thermal efficiency

The instantaneous thermal efficiency of the PVT collector is defined as the ratio of useful thermal power to the incident solar power (Equation (75)):

$$\eta_{th} = \frac{\dot{Q}_u}{A_c G} \tag{75}$$

ARTICLE IN PRESS

This indicator measures the capability of the system to recover the thermal part of the solar energy.

5.2 Electrical Performance Metrics

(a) Electrical power output

The electrical power output of the PVT collector is computed from Equation (28):

$$P_{el} = \eta_{ref}\left[1 - \beta(T_{pv} - T_{ref})\right]A_c G \tag{76}$$

The area-normalized useful thermal and electrical energy outputs are evaluated as: $E_{th,A} = \frac{E_{th}}{A_c}$ and $E_{el,A} = \frac{E_{el}}{A_c}$, where $E_{th,A}$ and $E_{el,A}$ represent the daily useful thermal and electrical energy outputs per unit solar receiving area, respectively.

(b) Electrical efficiency

The instantaneous electrical efficiency is defined as in Equation (77):

$$\eta_{el} = \frac{P_{el}}{A_c G} \tag{77}$$

This indicator reflects the effect of PV cell temperature on the electrical performance.

5.3 Overall Energy Efficiency

Since the PVT system delivers two useful energy products (electricity and heat), the overall energy efficiency is defined as the sum of thermal and electrical contributions (Equation (78)):

$$\eta_{en} = \frac{P_{el} + \dot{Q}_u}{A_c G} \tag{78}$$

Equivalently (Equation (79)):

$$\eta_{en} = \eta_{el} + \eta_{th} \tag{79}$$

In applications where a weighting factor is needed to reflect different energy values, a generalized form may be used (Equation (80)):

$$\eta_{en,w} = \frac{w_{el}P_{el} + w_{th}\dot{Q}_u}{A_c G} \tag{80}$$

where w_{el} and w_{th} are application-dependent weighting coefficients.

5.4 Exergy Performance Metrics

(a) Thermal exergy rate

From Equation (66):

ARTICLE IN PRESS

$$\dot{E}x_{th} = \dot{m}c_p\left[(T_{out} - T_{in}) - T_0 \ln\left(\frac{T_{out}}{T_{in}}\right)\right] \quad (81)$$

(b) Electrical exergy rate
Since electricity is high-grade energy (Equation (82)):

$$\dot{E}x_{el} = P_{el} \quad (82)$$

(c) Exergy destruction rate
From the Gouy–Stodola theorem (Equation 68):

$$\dot{E}x_{dest} = T_0 \dot{S}_{gen,tot} \quad (83)$$

(d) Exergy efficiencies
Thermal exergy efficiency (Equation (84)):

$$\eta_{ex,th} = \frac{\dot{E}x_{th}}{\dot{E}x_{solar}} \quad (84)$$

Electrical exergy efficiency (Equation (85)):

$$\eta_{ex,el} = \frac{P_{el}}{\dot{E}x_{solar}} \quad (85)$$

Overall exergy efficiency (Equation (86)):

$$\eta_{ex,tot} = \frac{P_{el} + \dot{E}x_{th}}{\dot{E}x_{solar}} \quad (86)$$

ARTICLE IN PRESS

5.5 Thermodynamic Optimization Criteria

The thermodynamic optimization of the PVT system is formulated based on the following competing objectives:

(a) Minimization of entropy generation

$$\min\left(\dot{S}_{gen,tot}\right) \quad (87)$$

or equivalently (Equation (88)):

$$\min\left(\dot{E}x_{dest}\right) \quad (88)$$

(b) Maximization of overall exergy efficiency

$$\max\left(\eta_{ex,tot}\right) \quad (89)$$

ARTICLE IN PRESS

(c) Trade-off criterion

Because increasing mass flow rate or heat extraction may improve electrical efficiency but reduce thermal quality (or vice versa), the optimal operating point is identified from a multi-objective compromise between: maximizing $\eta_{ex,tot}$, minimizing $\dot{S}_{gen,tot}$ and maintaining high η_{en}.
Thus, the optimal operating region is determined from parametric studies rather than a single-variable extremum.

Table 3. Performance indicators used for the thermodynamic evaluation of the PVT system

Indicator	Symbol	Definition	Unit	Physical Meaning
Useful thermal power	$\dot{Q}_u$	Eq. (74)	W	Recovered heat
Thermal efficiency	η_{th}	Eq. (75)	–	Fraction of solar energy converted to heat
Electrical power	P_{el}	Eq. (76)	W	Electrical output
Electrical efficiency	η_{el}	Eq. (77)	–	Fraction of solar energy converted to electricity
Overall energy efficiency	η_{en}	Eq. (78)	–	Total first-law performance
Thermal exergy rate	$\dot{E}x_{th}$	Eq. (81)	W	Useful thermal work potential
Solar exergy input	$\dot{E}x_{solar}$	Eq. (67)	W	Maximum theoretical work from sun
Exergy destruction	$\dot{E}x_{dest}$	Eq. (83)	W	Lost work due to irreversibility
Overall exergy efficiency	$\eta_{ex,tot}$	Eq. (86)	–	Second-law performance indicator
Entropy generation	$\dot{S}_{gen,tot}$	Eq. (60)	W/K	Measure of irreversibility

The performance indicators defined in Equations (74) – (89) and summarized in Table 3 are used in the next section to analyze the baseline performance, parametric sensitivity, and thermodynamic optimization of the PVT system.

6.0 Results and Discussion

This section presents the thermal, electrical, and thermodynamic performance characteristics of the proposed water-cooled photovoltaic–thermal system under tropical operating conditions. The analysis focuses on the coupled behavior of heat transfer, electrical generation, entropy generation, and exergy destruction within the collector and storage subsystems.

Parametric simulations were performed by systematically varying key operating parameters, including mass flow rate, solar irradiance, and ambient temperature, while monitoring their effects on thermal performance, electrical output, entropy generation, exergy destruction, and overall second-law efficiency. This approach enabled identification of the dominant thermodynamic mechanisms and operating conditions governing system optimization under tropical climatic environments. The adopted parametric framework further enabled comparative assessment of competing thermodynamic behaviors under varying operating conditions rather than merely demonstrating functional operation of the integrated PVT configuration.

6.1 Baseline Case Performance

The baseline performance of the single-module PVT system is evaluated using the fixed design and operating parameters summarized in Table 1 and a representative day extracted from the Kampala Typical Meteorological Year (TMY) dataset. The system consists of a $1.66\ m^2$ PVT

ARTICLE IN PRESS

collector coupled to a 100 L well-mixed storage tank operating in a closed loop without draw-off during the simulated day. The numerical results presented in this section are obtained from the two-node transient model described in Section 3, which explicitly resolves the PV layer and absorber temperatures and their thermal coupling to the working fluid.

Based on the total collector aperture area of 1.66 m^2, the baseline daily useful thermal and electrical outputs correspond to approximately 1.14 $kWh_{th}m^{-2}day^{-1}$and 1.17 $kWh_{el}m^{-2}day^{-1}$, respectively. These area-normalized values provide a more appropriate basis for comparison with conventional PV and other PVT systems because they refer to the same total solar receiving area.

6.1.1 Temperature Profiles

The diurnal evolution of the PV cell temperature T_{pv} and the fluid outlet temperature T_{out} is shown in Figure 4 for the baseline case.

Both temperatures increase from their early-morning values as solar irradiance rises, reach a maximum around solar noon, and decrease in the afternoon following the irradiance profile. Owing to the two-node thermal formulation, the PV temperature remains consistently higher than the fluid outlet temperature, reflecting the finite thermal resistance between the PV layer and the absorber–fluid interface.

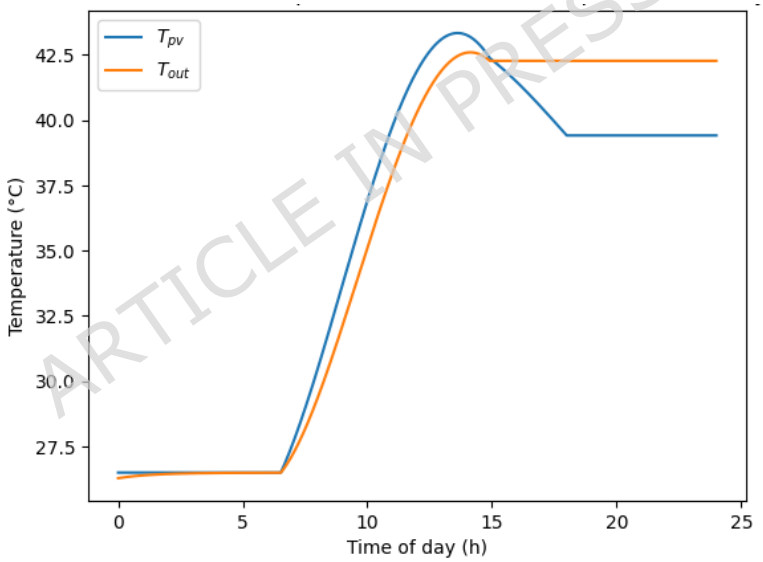

Figure 4. PV cell and outlet fluid temperatures vs time (TMY representative day, baseline case)

For the present baseline configuration, the PV temperature reaches a peak value of approximately 43.3°C, while the outlet fluid temperature peaks at about 42.6°C. These relatively moderate temperatures demonstrate the effectiveness of the active water cooling in limiting the thermal loading of the PV cells, which would otherwise operate at significantly higher temperatures in a standalone PV module under the same climatic conditions.

The gradual convergence of T_{out} and the storage tank temperature in the late afternoon reflects the absence of hot water draw-off in the present simulation and indicates that the system approaches a quasi-steady charged state. This behavior is representative of a domestic hot water system during periods of low demand and is consistent with the governing tank energy balance in Equation (58).

ARTICLE IN PRESS

6.1.2 Energy Outputs

The corresponding useful thermal power $\dot{Q}_u$ delivered to the fluid and the electrical power output P_{el} are shown in Figure 5 for the same representative day.

Both outputs follow the characteristic diurnal pattern of solar irradiance, increasing in the morning, peaking around solar noon, and decreasing thereafter. The useful thermal power, computed from Equation (74), attains significantly higher instantaneous values than the electrical power because a large fraction of the absorbed solar radiation is recovered in the form of low-grade heat in addition to electricity.

The electrical power output, evaluated using Equation (76), is slightly moderated around peak solar hours by the increase in PV operating temperature, illustrating the thermal–electrical coupling inherent to PVT systems. Nevertheless, the combined production of heat and electricity results in a substantially higher overall energy utilization compared to a standalone PV module of the same area.

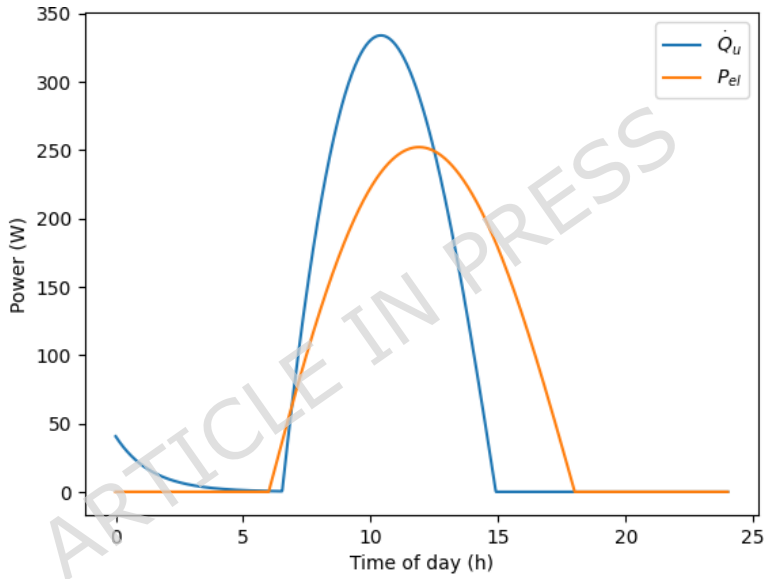

Figure 5. Useful thermal power and electrical power vs time (TMY representative day, baseline case)

When integrated over the day, the baseline system delivers approximately 1.88 kWh of thermal energy to the storage tank and about 1.95 kWh of electrical energy, confirming the suitability of the system for small-scale domestic hot water and on-site electricity supply in tropical climates.

6.1.3 Loss Breakdown

To clarify the physical origin of the performance limitations, the main heat loss components at peak operating conditions are decomposed in Figure 6.

ARTICLE IN PRESS

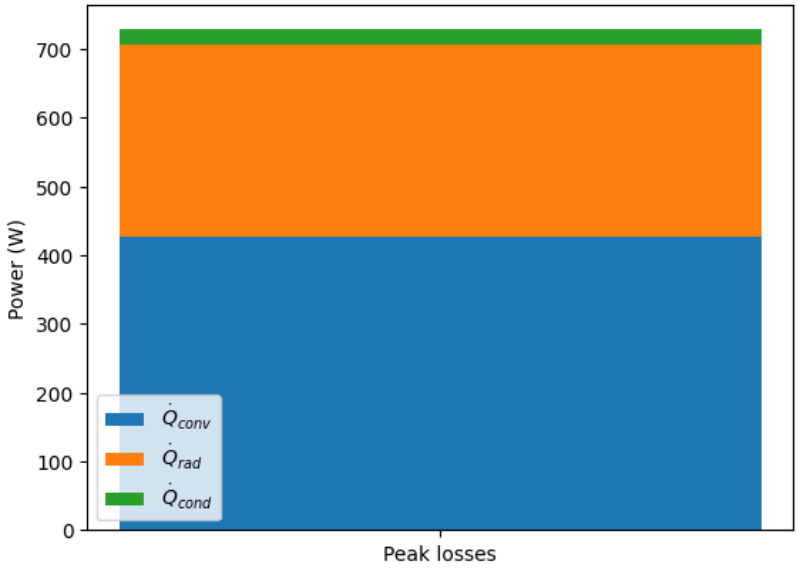

Figure 6. Breakdown of thermal losses at peak operating conditions (baseline case)

The total thermal losses are dominated by top losses, namely convective heat transfer to the ambient air and radiative heat exchange with the sky. Among these, convective losses represent the largest single contribution under the baseline wind speed of 2.4 ms^{-1}, while radiative losses constitute a comparable fraction due to the elevated surface temperature around solar noon. In contrast, conductive losses through the back insulation are relatively small, confirming the adequacy of the selected insulation thickness in Table 1.

This loss structure explains why, despite effective fluid cooling, the PV and absorber temperatures cannot be reduced indefinitely: as the surface temperature rises, an increasing fraction of the absorbed solar energy is irreversibly rejected to the environment rather than being converted into useful heat or electricity. This observation motivates the second-law analysis presented in the next section, where the same processes are examined in terms of entropy generation and exergy destruction.

ARTICLE IN PRESS

6.2 Second-Law (Entropy and Exergy) Results

While the first-law analysis in Section 6.1 quantifies how much energy is produced and lost, it does not reveal the thermodynamic quality of these energy flows or identify the true sources of performance degradation. The second-law analysis presented in this section addresses this limitation by examining the system in terms of entropy generation and exergy destruction, using the formulations introduced in Sections 3.4 and 3.5.

All results in this section correspond to the same baseline case and two-node transient simulation used to generate Figures 3–5.

6.2.1 Entropy Generation Breakdown by Mechanism

The total entropy generation rate of the system, $\dot{S}_{gen}$, is decomposed into contributions associated with the main irreversible processes, namely: (1) heat transfer between the collector surface and the ambient across a finite temperature difference, (2) heat transfer between the absorber and the working fluid, and (3) internal entropy production within the fluid due to temperature rise.

For the baseline case, the results show that heat rejection to the ambient environment constitutes the dominant source of entropy generation. This is primarily due to the relatively large temperature

ARTICLE IN PRESS

difference between the collector surface and the ambient air/sky during peak solar hours, which leads to strong irreversibility according to Equation (64).

The second most important contribution arises from heat transfer from the absorber to the fluid, which, although beneficial from an energy recovery perspective, still occurs across a finite temperature difference and therefore produces entropy internally. In contrast, the entropy generation associated with the temperature increase of the fluid itself is comparatively small.

The diurnal evolution of $\dot{S}_{gen}$ closely follows the solar irradiance profile, with negligible values during early morning and evening hours and a pronounced peak around solar noon. This behavior confirms that irreversibility is driven primarily by high-temperature operation under strong solar input, rather than by low-load operating periods. The diurnal evolution of the total entropy generation rate and its main components is shown in Figure 7.

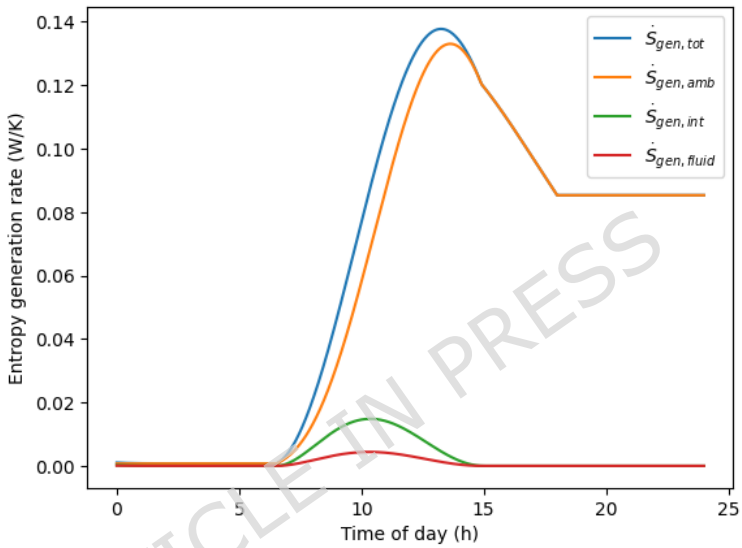

Figure 7. Diurnal evolution of entropy generation and its main components (baseline case)

ARTICLE IN PRESS

6.2.2 Exergy Destruction by Component

Using the Gouy–Stodola relation, Equation (85), the local entropy generation rates are mapped into exergy destruction rates for the main components of the system, namely: the collector (including PV surface, absorber, and top losses), the heat transfer process to the working fluid, and the thermal rejection to the environment.

ARTICLE IN PRESS

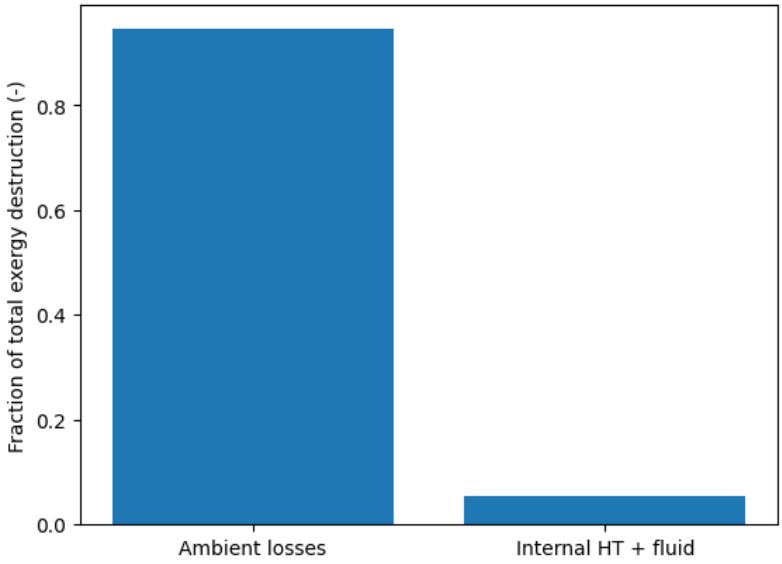

Figure 8. Distribution of exergy destruction by main components (baseline case)

Daily-integrated exergy destruction results (Figure 8) show that approximately 95% of the total destroyed exergy is associated with ambient heat losses, while only about 5% originates from internal heat transfer processes and fluid heating.

The results indicate that the collector–environment interface (i.e., combined convective and radiative top losses) accounts for the largest fraction of total exergy destruction in the system. This is expected, since rejecting heat to the ambient at a temperature close to the dead-state temperature T_0 destroys almost all of the work potential associated with that heat.

The second largest share of exergy destruction occurs within the collector heat transfer chain (PV → absorber → fluid), where finite temperature differences are required to drive heat into the fluid. Although this process produces useful thermal energy, it still degrades part of the available work potential.

In contrast, the storage tank contributes only marginally to the total exergy destruction in the present baseline case, owing to the assumption of a well-mixed tank and the absence of strong internal temperature gradients.

6.2.3 Major Irreversibility Drivers

The combined entropy-generation and exergy analyses reveal that the dominant irreversibility mechanisms in the baseline PVT system arise primarily from ambient thermal rejection and finite-temperature-difference heat transfer within the collector. Quantitatively, ambient heat rejection contributes approximately 95% of the total exergy destruction, clearly identifying external thermal losses as the principal thermodynamic limitation under tropical operating conditions. The underlying mechanism is that heat rejected from the collector to the ambient occurs across finite temperature differences, causing irreversible degradation of useful energy quality. Under high irradiance conditions, elevated absorber and PV temperatures intensify thermal gradients between the collector, working fluid, and surroundings, thereby increasing entropy generation and exergy destruction. Consequently, improvements in thermal insulation, selective coatings, reduced external heat-transfer coefficients, and enhanced PV–absorber thermal coupling may provide greater thermodynamic benefits than simply increasing heat extraction rates.

ARTICLE IN PRESS

Although higher coolant flow rates improve PV cooling and electrical performance through enhanced convective heat removal, the reduced fluid residence time lowers the outlet temperature rise and consequently decreases the thermodynamic quality of the recovered heat. Therefore, operating conditions associated with improved first-law cooling performance do not necessarily correspond to thermodynamically optimal second-law performance. Similarly, increasing solar irradiance enhances both electrical generation and thermal energy recovery, but simultaneously intensifies irreversible heat transfer due to larger collector temperature gradients. These findings confirm that energy-optimal and exergy-optimal operating conditions may diverge significantly in tropical PVT systems.

The significance of the proposed cooling strategy should therefore not be interpreted solely in terms of electrical efficiency enhancement relative to conventional PV modules. Rather, the principal thermodynamic advantage of the investigated configuration lies in simultaneous recovery of useful low-temperature thermal energy while maintaining improved PV electrical performance through temperature regulation. Consequently, the proposed system functions not only as a PV cooling mechanism but also as an integrated solar-energy recovery framework suitable for applications such as domestic hot water production and other low-temperature thermal uses under tropical climatic conditions.

Comparison with previous thermodynamic PVT investigations indicates that the present findings are consistent with reported trends in water-cooled PVT systems, where enhanced cooling improves electrical performance while simultaneously enabling useful thermal energy recovery (Rashidi et al., 2020; Rao et al., 2024; Wang et al., 2024). Similar studies also reported that entropy generation and exergy destruction are strongly influenced by thermal losses and finite-temperature-difference heat transfer processes within the collector (Ramírez-Minguela et al., 2023; Al-Najjar et al., 2024). However, unlike many existing investigations that primarily report global energy or exergy efficiencies, the present work provides a mechanism-resolved second-law interpretation by explicitly linking subsystem-level entropy generation and exergy destruction to Gibbs Tds-based thermodynamic relations under tropical operating conditions. For consistency, literature comparisons were based on aperture-area-normalized outputs or efficiency indicators where sufficient collector-area information was available.

Fluid friction and pumping losses were intentionally excluded; therefore, the identified irreversibility structure reflects predominantly thermal and thermoelectric effects. Overall, the results demonstrate that system performance is constrained less by solar absorption itself than by irreversible energy degradation associated with ambient heat rejection and finite-temperature heat transfer processes. This second-law insight, which cannot be fully inferred from first-law efficiency analysis alone, provides a rigorous thermodynamic basis for optimization of PVT systems operating in tropical environments.

6.3 Parametric and Sensitivity Analysis

To assess the robustness of the baseline conclusions and identify thermodynamically meaningful improvement directions, a parametric study was conducted by varying a limited set of key operational, environmental, and design parameters while keeping all others fixed at the baseline values (Table 1). For each case, the system was simulated over the same representative day, and the daily integrated entropy generation $S_{gen,day}$ and exergy efficiency $\eta_{ex,day}$ were evaluated.

The main trends and resulting thermodynamic design recommendations based on daily-integrated entropy generation and exergy efficiency for the baseline PVT system are summarized in Table 4.

ARTICLE IN PRESS

Table 4. Summary of parametric sensitivity results and thermodynamic optimization recommendations

Parameter	Tested range	Effect on S_{gen}	Effect on η_{ex}	Recommended baseline / optimal setting
Mass flow rate, $\dot{m}$(kg/s)	0.01 – 0.10	Increases with $\dot{m}$ (minimum at lowest $\dot{m}$)	Decreases with $\dot{m}$; maximum at lowest $\dot{m}$	$\dot{m} = 0.01$ kg/s (thermodynamically optimal in this configuration)
Wind speed, v_w(m/s)	0.5 – 5.0	Decreases strongly with v_w	Weak, shallow minimum around 3–4 m/s	Not a design variable; mitigate via wind shielding or glazing
Ambient temperature, T_{amb}(°C)	22 – 30	Increases strongly with T_{amb}	Decreases with T_{amb}	Not controllable; emphasizes need for thermal loss reduction
Peak irradiance, G_{max}(W/m²)	600 – 1050	Increases with G_{max}	Decreases with G_{max}	Not controllable; requires improved thermal management at high G
Insulation thickness, δ_{ins} (mm)	20 – 100	Slight increase with δ_{ins}	Slight increase with δ_{ins}	$\delta_{ins} \gtrsim 50$ mm (diminishing returns beyond this)
PV–absorber coupling, $U A_{pa}$(W/K)	Low → High (= 100–500 W/K)	Increases moderately with coupling	Increases clearly with coupling	As high as practically achievable (good thermal contact, soldering/bonding)

Physically, the observed reduction in exergy efficiency at higher flow rates arises because the coolant extracts heat more rapidly while simultaneously reducing the useful temperature lift across the collector. Although enhanced cooling improves PV electrical behavior, the corresponding reduction in fluid temperature gain limits the quality of the recovered thermal energy from a second-law perspective. This demonstrates the competing interaction between thermal extraction and thermodynamic usefulness within the PVT system.

6.3.1 Effect of Mass Flow Rate

The influence of the mass flow rate $\dot{m}$on the thermodynamic performance is summarized in Figure 8, which shows the variation of the daily exergy efficiency $\eta_{ex,day}$ with $\dot{m}$.

As seen in Figure 9, the exergy efficiency decreases gradually as the mass flow rate is increased over the investigated range. The best exergy performance is obtained at the lowest tested flow rate, around $\dot{m} = 0.01\ kgs^{-1}$. This behavior can be explained by the irreversibility structure identified in Section 6.2: since ambient heat losses dominate exergy destruction, increasing the flow rate does not significantly mitigate the main loss mechanism, while it redistributes irreversibility within the internal heat transfer chain.

The corresponding variation of the daily entropy generation with $\dot{m}$ exhibits the same trend, confirming that, for the present configuration, operating the system at unnecessarily high flow rates is thermodynamically suboptimal.

ARTICLE IN PRESS

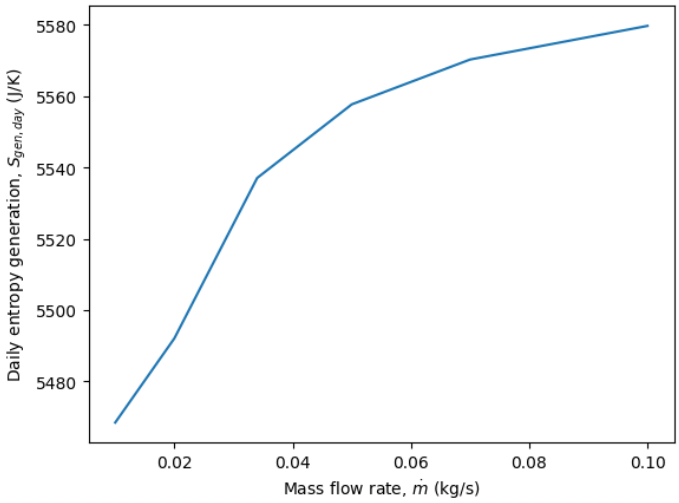

Figure 9. Effect of mass flow rate on daily entropy generation (baseline day)

6.3.2 Effect of Wind Speed and Ambient Temperature

The effect of wind speed on system irreversibility is shown in Figure 10, which presents the daily entropy generation $S_{gen,day}$ as a function of the wind speed v_w.

As illustrated in Figure 10, increasing the wind speed leads to a marked reduction in total entropy generation. This occurs because stronger convective cooling reduces the collector surface temperature and, consequently, the magnitude of finite-temperature-difference heat transfer to the environment. However, the corresponding change in exergy efficiency is comparatively modest, indicating that the beneficial effect of lower surface temperatures is partly offset by enhanced convective heat losses.

A similar sensitivity was observed for ambient temperature: higher ambient temperatures systematically increase entropy generation and reduce exergy efficiency by shifting the entire system to higher operating temperatures and degrading PV electrical performance.

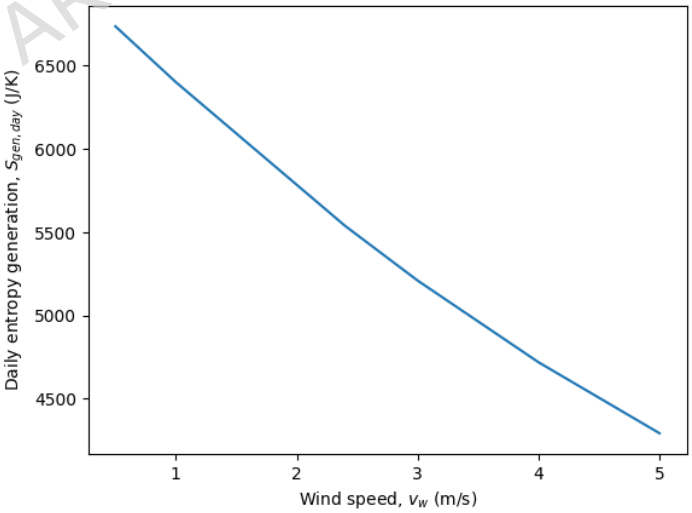

Figure 10. Effect of wind speed on daily entropy generation (baseline day)

ARTICLE IN PRESS

The results further indicate that elevated ambient temperatures reduce the thermodynamic potential for useful heat transfer to the surroundings, thereby influencing both collector cooling behavior and exergy recovery characteristics. This highlights the strong sensitivity of PVT thermodynamic performance to climatic operating conditions in tropical environments.

6.3.3 Effect of Irradiance Level

The impact of solar resource intensity on the thermodynamic performance is illustrated in Figure 10, which shows the variation of the daily exergy efficiency $\eta_{ex,day}$ with the peak irradiance level G_{max}.

As shown in Figure 11, the exergy efficiency decreases monotonically as the irradiance level increases. Although higher irradiance naturally increases absolute energy production, it also leads to higher operating temperatures and, consequently, to a disproportionate increase in ambient-loss irreversibility. As a result, a larger fraction of the available solar exergy is destroyed rather than converted into useful outputs.

The corresponding increase in total entropy generation with irradiance level confirms that stronger solar forcing amplifies irreversibility unless accompanied by improved thermal management.

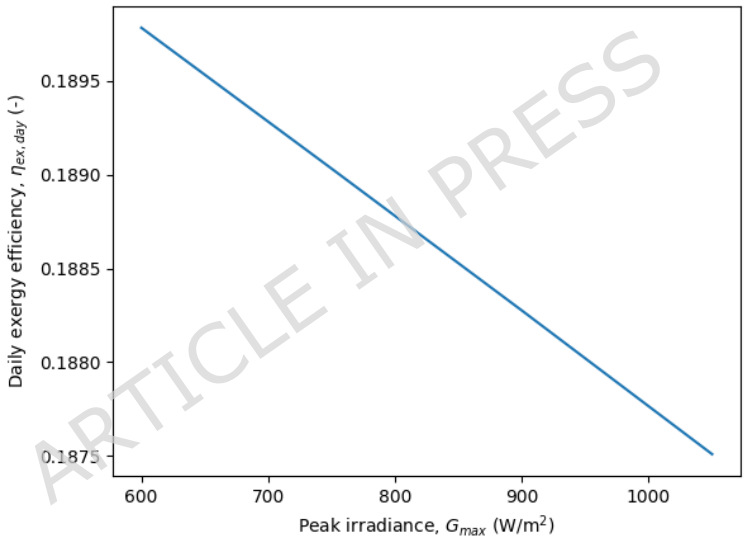

Figure 11. Effect of irradiance level on daily exergy efficiency (baseline day)

6.3.4 Effect of Design Parameters

Among the design parameters, the effects of insulation thickness and PV–absorber thermal coupling were examined. The influence of insulation thickness on the daily exergy efficiency is presented in Figure 12. Increasing the insulation thickness produces a small but systematic improvement in $\eta_{ex,day}$. This reflects the reduction of back-side heat losses and their associated exergy destruction. However, the improvement is modest, indicating that top losses remain the dominant limitation, in agreement with the second-law analysis in Section 6.2.

The effect of PV–absorber coupling strength shows that improving the thermal contact between the PV layer and the absorber enhances exergy efficiency by facilitating heat extraction and limiting PV temperature penalties, even though it redistributes entropy generation within the collector.

ARTICLE IN PRESS

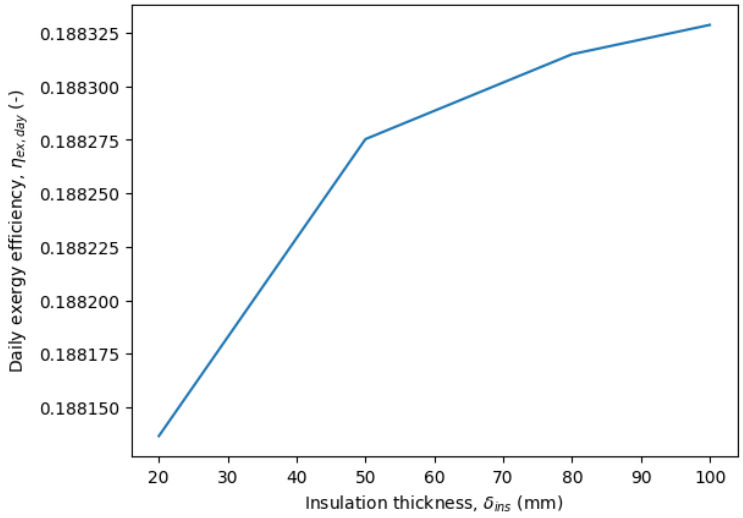

Figure 12. Effect of insulation thickness on daily exergy efficiency (baseline day)

6.4 Optimization and Recommended Operating Region

Based on the parametric results presented in Section 6.3, an optimization-oriented analysis is now performed to identify a rational operating region and extract practical design guidance for tropical PVT deployment. Since the second-law analysis has shown that the system is fundamentally limited by ambient-loss irreversibility, the optimization is formulated in terms of exergy efficiency maximization and entropy generation minimization, rather than energy efficiency alone.

6.4.1 Optimal Flow Rate and Operating Temperature

The effect of mass flow rate on the peak PV operating temperature is shown in Figure 13. It is observed that, within the investigated range, increasing $\dot{m}$produces only a modest reduction in the PV temperature. This indicates that the present system is not primarily constrained by internal heat removal capability, but rather by heat rejection to the environment.

The corresponding influence of $\dot{m}$ on the thermal, electrical, and exergy efficiencies is summarized in Figure 14. While the thermal and electrical efficiencies remain almost constant over the tested range, the exergy efficiency exhibits a slight but systematic decrease as $\dot{m}$i increases. Consequently, the best thermodynamic performance is achieved at the lowest tested mass flow rate, around: $\dot{m} = 0.01\ kg\ s^{-1}$.

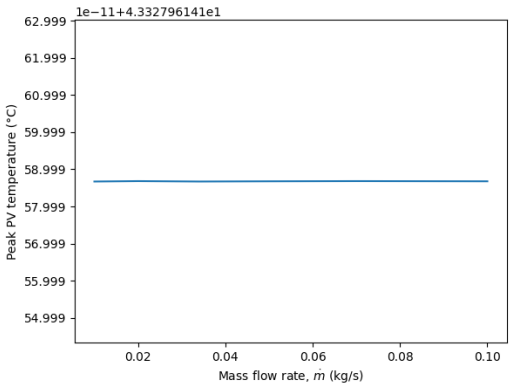

Figure 13. Effect of mass flow rate on peak PV temperature (baseline day)

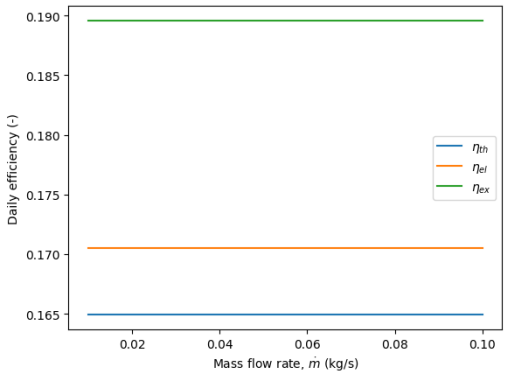

Figure 14. Effect of mass flow rate on thermal, electrical and exergy efficiencies

ARTICLE IN PRESS

This operating point also corresponds to a moderate PV temperature (Figure 13), confirming that aggressive over-cooling is neither necessary nor thermodynamically beneficial in the present configuration.

6.4.2 Energy–Exergy Trade-Off

Figure 14 provides a clear illustration of a central result of this study: the energy-optimal and exergy-optimal operating points do not necessarily coincide. From a first-law perspective, increasing the flow rate does not penalize thermal or electrical efficiency. However, from a second-law perspective, higher flow rates slightly increase the total irreversibility of the system and reduce the fraction of useful work that can be extracted from the same solar input.

This difference arises because energy metrics do not account for where and how irreversibility is produced, whereas the exergy efficiency explicitly penalizes entropy generation, particularly that associated with ambient heat losses. The present results therefore demonstrate that optimizing a PVT system solely on energy efficiency grounds can be thermodynamically misleading.

6.4.3 Design Recommendations for Tropical Deployment

Even under optimized operating conditions, the dominant share of exergy destruction in the system remains associated with heat losses to the ambient environment, while internal heat transfer processes contribute only a minor fraction. This thermodynamic structure leads to three clear and robust design recommendations for PVT systems intended for tropical deployment. First, priority should be given to minimizing top losses through improved glazing, selective coatings, and wind shielding, since these mechanisms dominate exergy destruction. Second, excellent thermal contact between the PV module and the absorber should be ensured, as this enhances heat extraction and limits PV temperature penalties without introducing significant additional irreversibility. Third, moderate mass flow rates are sufficient; oversizing pumps or operating at excessively high flow rates provides little thermodynamic benefit and may even reduce exergy efficiency.

In summary, the optimal design strategy is not to maximize heat removal, but rather to minimize irreversible heat rejection to the environment, in full agreement with the second-law analysis presented in Section 6.2.

ARTICLE IN PRESS

7.0 Conclusions and Practical Recommendations

This study developed a coupled transient thermal–electrical framework for second-law analysis of a water-cooled photovoltaic–thermal (PVT) system operating under tropical climatic conditions. Unlike conventional PVT investigations that primarily emphasize overall thermal or exergy efficiencies, the proposed framework explicitly incorporated Gibbs Tds-based thermodynamic relations to resolve subsystem-level entropy generation and exergy destruction mechanisms governing useful energy degradation. The analysis demonstrated that the baseline system (1.66 m² collector integrated with a 100 L storage tank under Kampala TMY conditions) maintained PV temperatures below approximately 43 °C while delivering about 1.9 kWh of useful thermal energy and 1.95 kWh of electrical energy over a representative operating day.

The second-law analysis revealed that ambient heat rejection constituted the dominant thermodynamic irreversibility mechanism, accounting for approximately 95% of the total exergy destruction, whereas internal heat-transfer processes contributed only a comparatively minor fraction. The results further demonstrated that operating conditions associated with maximum thermal extraction or improved first-law efficiency do not necessarily correspond to

ARTICLE IN PRESS

thermodynamically optimal conditions when entropy generation and exergy destruction are considered simultaneously. In particular, increasing mass flow rate, irradiance level, and ambient temperature reduced exergy efficiency despite relatively small changes in energy efficiency, indicating that energy-based optimization alone may provide misleading design guidance. The thermodynamically favorable operating region for the investigated configuration occurred at low-to-moderate flow rates near $\dot{m} = 0.01\ kg\ s^{-1}$.

From a practical perspective, the findings indicate that thermodynamic optimization of tropical PVT systems should prioritize reduction of irreversible ambient thermal losses through improved insulation, enhanced PV–absorber thermal coupling, selective surface treatment, and reduction of external convection losses rather than simply increasing coolant circulation rates. The study further demonstrates that the principal thermodynamic significance of the proposed configuration lies not merely in incremental electrical enhancement, but in integrated recovery of useful low-temperature thermal energy together with simultaneous PV temperature regulation. Consequently, the proposed framework provides physically diagnostic second-law design guidance for tropical solar-energy applications including domestic hot water production, building-integrated systems, and decentralized renewable-energy deployment.

Declarations

Authors contribution: **Conceptualization, MMM, JIS, SNN, DEU, writing – original draft:** MMM, **Writing – review & editing: All authors**

Competing interests: None

Consent to participate: NA

Consent to publish: NA

Ethical Approval: NA

Funding: No funding received

Data availabity: Data will be made available on request from the authors

ARTICLE IN PRESS

References

Abdulameer, L., Dzhumagulova, N., Algretawee, H., Zhuravleva, L., & Alshammari, M. (2022). Comparison between Hazen-Williams and Darcy-Weisbach equations to calculate head loss through conveyancing treated wastewater in Kerbala city, Iraq. *Eastern-European Journal of Enterprise Technologies*. https://doi.org/10.15587/1729-4061.2022.251385

Abdul-Ganiyu, S., Quansah, D., Ramde, E., Seidu, R., & Adaramola, M. (2021). Study effect of flow rate on flat-plate water-based photovoltaic-thermal (PVT) system performance by analytical technique. *Journal of Cleaner Production*. https://doi.org/10.1016/j.jclepro.2021.128985

Abdullah, A., Misha, S., Tamaldin, N., Rosli, M., & Sachit, F. (2020). Theoretical study and indoor experimental validation of performance of the new photovoltaic thermal solar collector (PVT) based water system. *Case Studies in Thermal Engineering*, 18, 100595. https://doi.org/10.1016/j.csite.2020.100595

Abimanyu, R., Yanuar, Y., Waskito, K., Sari, W., & Ogata, S. (2025). Impact of Reynolds Number on Flow Behavior in Spiral Pipe Profiles: A Review. *Journal of Advanced Research in Fluid Mechanics and Thermal Sciences*. https://doi.org/10.37934/arfmts.129.2.216243

Alami, Y., Baghaz, E., Nasrin, R., Al-Damook, M., Bendaoud, R., Bouragba, T., Melhaoui, M., & Benhmida, M. (2025). Up-to-Date Review on Flat-Plate Solar Hybrid Photovoltaic

ARTICLE IN PRESS

Thermal Systems: Absorber Designs and Fabrication Materials. *International Journal of Energy Research*. https://doi.org/10.1155/er/5547555

Alessandro, M., Aste, N., Claudio, D., & Fabrizio, L. (2021). Photovoltaic-thermal solar-assisted heat pump systems for building applications: Integration and design methods. *Energy and Built Environment*. https://doi.org/10.1016/j.enbenv.2021.07.002

Al-Najjar, H., Mahdi, J., Alsharifi, T., Homod, R., Talebizadehsardari, P., & Keshmiri, A. (2024). Thermodynamic Modeling and Performance Analysis of Photovoltaic-Thermal Collectors Integrated with Phase Change Materials: Comprehensive Energy and Exergy Analysis. *Results in Engineering*. https://doi.org/10.1016/j.rineng.2024.102277

Al-Najjar, H., Mahdi, J., Alsharifi, T., Homod, R., Talebizadehsardari, P., & Keshmiri, A. (2024). Thermodynamic modeling and performance analysis of photovoltaic–thermal collectors integrated with phase change materials: Comprehensive energy and exergy analysis. *Results in Engineering, 22*, 102277. https://doi.org/10.1016/j.rineng.2024.102277

Al-Waeli, A., Kazem, H., Chaichan, M., & Sopian, K. (2020). A review of photovoltaic thermal systems: Achievements and applications. *International Journal of Energy Research*, 45, 1269 - 1308. https://doi.org/10.1002/er.5872

Arenandan, V., Wong, J., Ahmed, A., & Chow, M. (2022). Efficiency enhancement in energy production of photovoltaic modules through green roof installation under tropical climates. *Ain Shams Engineering Journal*. https://doi.org/10.1016/j.asej.2022.101741

Asefi, G., Ma, T., & Wang, R. (2022). Parametric investigation of photovoltaic–thermal systems integrated with porous phase change material. *Applied Thermal Engineering, 201*, 117727. https://doi.org/10.1016/j.applthermaleng.2021.117727

Attia, M. E. H., Kabeel, A. E., Khelifa, A., Abdelgaied, M., Arıcı, M., & Abdel-Aziz, M. M. (2025). Performance enhancement of PVT modules using bi-fluid air/CuO–water-based nanofluid and fins: Energy and exergy analysis. *Clean Technologies and Environmental Policy, 27*, 4541–4559. https://doi.org/10.1007/s10098-025-03149-1

Bakari, R., Minja, R., & Njau, K. (2014). Effect of Glass Thickness on Performance of Flat Plate Solar Collectors for Fruits Drying. *Journal of Energy*, 2014, 1-8. https://doi.org/10.1155/2014/247287

Ballina, J., & Go, Y. (2025). Quantification and Comparative Analysis of Environmental Factors to Large-Scale Solar Plant's Energy Performance via Regression and Linear Correlation Models. *Journal of Energy and Power Technology*. https://doi.org/10.21926/jept.2501001

Bandaru, S., Becerra, V., Khanna, S., Radulovic, J., Hutchinson, D., & Khusainov, R. (2021). A Review of Photovoltaic Thermal (PVT) Technology for Residential Applications: Performance Indicators, Progress, and Opportunities. *Energies*. https://doi.org/10.3390/en14133853

Basuhaib, A., Selvaraj, J., Hasanuzzaman, M., Anjum, T., & Kumar, L. (2024). Experimental investigation the effect of different operating parameters and optimized the water-based PVT system for domestic applications. *Solar Energy*. https://doi.org/10.1016/j.solener.2023.112278

Bejan, A. (2002). Fundamentals of exergy analysis, entropy generation minimization, and the generation of flow architecture. *International Journal of Energy Research*, 26. https://doi.org/10.1002/er.804

Bejan, A. (2013). *Entropy generation minimization: the method of thermodynamic optimization of finite-size systems and finite-time processes*. CRC press.

ARTICLE IN PRESS

Bian, C., Song, J., Jin, X., Jiang, W., Jie, X., & Yang, L. (2025). Thermal management in photovoltaic–thermal systems: Advances, challenges, and cross-domain applications. *Applied Thermal Engineering, 279*, 127791. https://doi.org/10.1016/j.applthermaleng.2025.127791

Bigorajski, J., & Chwieduk, D. (2018). Analysis of a micro photovoltaic/thermal – PV/T system operation in moderate climate. *Renewable Energy*. https://doi.org/10.1016/j.renene.2018.01.116

Cengel, Y. A., & Boles, M. A. (2002). Thermodynamics: an engineering approach. *Sea*, *1000*(8862), 287-93.

Chander, S., Purohit, A., Sharma, A., , A., Nehra, S., & Dhaka, M. (2015). A study on photovoltaic parameters of mono-crystalline silicon solar cell with cell temperature. *Energy Reports*, 1, 104-109. https://doi.org/10.1016/j.egyr.2015.03.004

Chyngyzbekkyzy, Z., & Satybaldyev, A. (2025). Comparative Multicriteria Analysis of Thermophysical and Corrosion Properties of main Types of Heat Transfer fluids for Solar Water Heating Collectors. *Bulletin of Science and Practice*. https://doi.org/10.33619/2414-2948/118/17

Ciprian, B. (2019). The Quest for the Ideal Darcy-Weisbach Friction Factor Equation from the Perspective of a Building Services Engineer. *Ovidius University Annals of Constanta - Series Civil Engineering*, 21, 65 - 73. https://doi.org/10.2478/ouacsce-2019-0008

Costa, S., & Kenisarin, M. (2022). A review of metallic materials for latent heat thermal energy storage: Thermophysical properties, applications, and challenges. *Renewable and Sustainable Energy Reviews*. https://doi.org/10.1016/j.rser.2021.111812

Cotfas, D., Cotfas, P., & Machidon, O. (2018). Study of Temperature Coefficients for Parameters of Photovoltaic Cells. *International Journal of Photoenergy*, 2018, 1-12. https://doi.org/10.1155/2018/5945602

Dancker, J., & Wolter, M. (2021). Improved quasi-steady-state power flow calculation for district heating systems: A coupled Newton-Raphson approach. *Applied Energy*, 295, 116930. https://doi.org/10.1016/j.apenergy.2021.116930

David, A., Lakshya, A., Sahu, M., & Sinha, R. (2021). Stating and Deriving Bernoulli's Theorem as a Special Case of Steady Flow Energy Equation. *Lecture Notes in Mechanical Engineering*. https://doi.org/10.1007/978-981-16-4489-4_20

David, M., Toutant, A., & Bataille, F. (2021). Numerical development of heat transfer correlation in asymmetrically heated turbulent channel flow. *International Journal of Heat and Mass Transfer*, 164, 120599. https://doi.org/10.1016/j.ijheatmasstransfer.2020.120599

Design and Simulation of an Inverter Muhamad, M. M., Kibirige, D., Uzorka, A., & John, U. K. (2022). Drive System with a Display for a Renewable Energy System in the Rural Isolated Communities of Uganda. *Journal of Power and Energy Engineering*, *10*(12), 1-14. https://doi.org/10.4236/jpee.2022.1012001

Diwania, S., Agrawal, S., Siddiqui, A., & Singh, S. (2020). Photovoltaic–thermal (PV/T) technology: a comprehensive review on applications and its advancement. *International Journal of Energy and Environmental Engineering*, 11, 33-54. https://doi.org/10.1007/s40095-019-00327-y

Dubey, S., & Tay, A. (2013). Testing of two different types of photovoltaic–thermal (PVT) modules with heat flow pattern under tropical climatic conditions. *Energy for Sustainable Development*, 17, 1-12. https://doi.org/10.1016/j.esd.2012.09.001

ARTICLE IN PRESS

ARTICLE IN PRESS

Eicker, U., & Dalibard, A. (2011). Photovoltaic–thermal collectors for night radiative cooling of buildings. *Solar Energy*, 85, 1322-1335. https://doi.org/10.1016/j.solener.2011.03.015

Elsabahy, M., Emam, M., Sekiguchi, H., & Ahmed, M. (2024). Performance mapping of silicon-based solar cell for efficient power generation and thermal utilization: Effect of cell encapsulation, temperature coefficient, and reference efficiency. *Applied Energy*. https://doi.org/10.1016/j.apenergy.2023.122385

Evola, G., & Marletta, L. (2014). Exergy and thermoeconomic optimization of a water-cooled glazed hybrid photovoltaic/thermal (PVT) collector. *Solar Energy*, 107, 12-25. https://doi.org/10.1016/j.solener.2014.05.041

Fashina, A., Mundu, M., Akiyode, O., Abdullah, L., Sanni, D., & Ounyesiga, L. (2018). The drivers and barriers of renewable energy applications and development in Uganda: a review. *Clean Technologies*, *1*(1), 9-39.

Francisco, B., Nelson, S., Christoph, R., & Hatef, M. (2024). Cold solar: PVT heat exchanger designs for heat pump integration. *Applied Thermal Engineering*. https://doi.org/10.1016/j.applthermaleng.2024.125020

Giovannetti, F., Föste, S., Ehrmann, N., & Rockendorf, G. (2014). High transmittance, Low Emissivity Glass Covers for Flat Plate Collectors: Applications and Performance. *Energy Procedia*, 30, 106-115. https://doi.org/10.1016/j.egypro.2012.11.014

Guarracino, I., Freeman, J., Ramos, A., Kalogirou, S., Ekins-Daukes, N., & Markides, C. (2019). Systematic testing of hybrid PV-thermal (PVT) solar collectors in steady-state and dynamic outdoor conditions. *Applied Energy*. https://doi.org/10.1016/j.apenergy.2018.12.049

Guarracino, I., Mellor, A., Ekins-Daukes, N., & Markides, C. (2016). Dynamic coupled thermal-and-electrical modelling of sheet-and-tube hybrid photovoltaic/thermal (PVT) collectors. *Applied Thermal Engineering*, 101, 778-795. https://doi.org/10.1016/j.applthermaleng.2016.02.056

Hai, T., El-Rahman, M., Li, S., Malekshah, E., Aybar, H., & El-Shafay, A. (2023). The entropy generation analysis and optimization of a water/silver nanofluid flow inside a photovoltaic thermal collector considering plain, ribbed, and porous-ribbed absorber tubes. *Journal of the Taiwan Institute of Chemical Engineers*. https://doi.org/10.1016/j.jtice.2023.104695

Hellström, B., Adsten, M., Nostell, P., Karlsson, B., & Wäckelgård, E. (2003). The impact of optical and thermal properties on the performance of flat plate solar collectors. *Renewable Energy*, 28, 331-344. https://doi.org/10.1016/s0960-1481(02)00040-x

Herrando, M., Ramos, A., Zabalza, I., & Markides, C. (2019). A comprehensive assessment of alternative absorber-exchanger designs for hybrid PVT-water collectors. *Applied Energy*. https://doi.org/10.1016/j.apenergy.2018.11.024

Hong, W., Li, B., Li, H., Niu, X., Li, Y., & Lan, J. (2022). Recent progress in thermal energy recovery from the decoupled photovoltaic/thermal system equipped with spectral splitters. *Renewable and Sustainable Energy Reviews*. https://doi.org/10.1016/j.rser.2022.112824

Hu, M., Zhao, B., , S., Ao, X., Cao, J., Wang, Q., Riffat, S., Su, Y., & Pei, G. (2022). Applications of radiative sky cooling in solar energy systems: Progress, challenges, and prospects. *Renewable and Sustainable Energy Reviews*. https://doi.org/10.1016/j.rser.2022.112304

Huang, Y., Sun, Q., Li, Y., Sun, C., & Chen, Z. (2023). Damping technique empowered robust energy flow calculation for integrated energy systems. *Applied Energy*. https://doi.org/10.1016/j.apenergy.2023.121168

Incropera, F. P., DeWitt, D. P., Bergman, T. L., & Lavine, A. S. (1996). *Fundamentals of heat and mass transfer* (Vol. 6, p. 116). New York: Wiley.

ARTICLE IN PRESS

Jamshed, W., Eid, M., Aissa, A., Mourad, A., Nisar, K., Shahzad, F., Saleel, C., & Vijayakumar, V. (2021). Partial velocity slip effect on working magneto non-Newtonian nanofluids flow in solar collectors subject to change viscosity and thermal conductivity with temperature. *PLoS ONE*, 16. https://doi.org/10.1371/journal.pone.0259881

Jia, L., Lu, L., Chen, J., & Han, J. (2022). A novel radiative sky cooling-assisted ground-coupled heat exchanger system to improve thermal and energy efficiency for buildings in hot and humid regions. *Applied Energy*. https://doi.org/10.1016/j.apenergy.2022.119422

Jia, Y., Alva, G., & Fang, G. (2019). Development and applications of photovoltaic–thermal systems: A review. *Renewable and Sustainable Energy Reviews*. https://doi.org/10.1016/j.rser.2018.12.030

Joshi, A., Dincer, I., & Reddy, B. (2009). Thermodynamic assessment of photovoltaic systems. *Solar Energy*, 83, 1139-1149. https://doi.org/10.1016/j.solener.2009.01.011

Kalateh, M. R., Kianifar, A., & Sardarabadi, M. (2022). Energy, exergy, and entropy generation analyses of a water-based photovoltaic thermal system equipped with clockwise–counter-clockwise twisted tapes: An indoor experimental study. *Applied Thermal Engineering, 215*, 118906. https://doi.org/10.1016/j.applthermaleng.2022.118906

Kallio, S., & Siroux, M. (2020). Energy Analysis and Exergy Optimization of Photovoltaic-Thermal Collector. *Energies*. https://doi.org/10.20944/preprints202009.0219.v1

Kenfack, A., Nematchoua, M., Simo, E., Mfoundikou, M., Fosso, J., Babikir, M., & Chara-Dackou, V. (2023). Exergetic optimization of some design parameters of the hybrid photovoltaic/thermal collector with bi-fluid air/ternary nanofluid (CuO/MgO/TiO2). *SN Applied Sciences*, 5. https://doi.org/10.1007/s42452-023-05455-z

Khoukhi, M., & Maruyama, S. (2005). Theoretical approach of a flat plate solar collector with clear and low-iron glass covers taking into account the spectral absorption and emission within glass covers layer. *Renewable Energy*, 30, 1177-1194. https://doi.org/10.1016/j.renene.2004.09.014

Khoukhi, M., & Maruyama, S. (2006). Theoretical approach of a flat-plate solar collector taking into account the absorption and emission within glass cover layer. *Solar Energy*, 80, 787-794. https://doi.org/10.1016/j.solener.2005.06.002

Kim, J., & Kim, J. (2012). The Experimental Performance of an Unglazed PVT Collector with Two Different Absorber Types. *International Journal of Photoenergy*, 2012, 1-6. https://doi.org/10.1155/2012/312168

Kotas, T. J. (2012). *The exergy method of thermal plant analysis*. Paragon Publishing.

Kramer, K., Mehnert, S., Munz, G., Helmling, S., & Lämmle, M. (2023). Photovoltaic-Thermal Technology – PVT Collectors, Systems and Applications. *Energy Technology*. https://doi.org/10.1002/ente.202300378

Krishna, Y., Faizal, M., Saidur, R., Ng, K., & Aslfattahi, N. (2020). State-of-the-art heat transfer fluids for parabolic trough collector. *International Journal of Heat and Mass Transfer*. https://doi.org/10.1016/j.ijheatmasstransfer.2020.119541

Kumar, S. (2022). Application of First Law of Thermodynamics to Flow Processes Thermodynamics. *Thermal Engineering Volume 1*. https://doi.org/10.1007/978-3-030-67274-4_4

Lima, G., Flores, J., Faria, L., Da Silva Martins Pitana, K., Saretta, E., Massey, J., & De Oliveira, H. (2025). Darcy Friction Factor Equations for Small-Diameter Pipes in Lateral Irrigation Systems: An Experimental Study. *Journal of the ASABE*. https://doi.org/10.13031/ja.16338

ARTICLE IN PRESS

Liu, L., Shalwan, A., Teng, J., Liu, C., & Li, Z. (2023). The entropy generation analysis of a PVT solar collector with internally needle finned serpentine absorber tube. *Engineering Analysis with Boundary Elements*. https://doi.org/10.1016/j.enganabound.2023.07.018

Maadi, S., Kolahan, A., Passandideh-Fard, M., Sardarabadi, M., & Moloudi, R. (2017). Characterization of PVT systems equipped with nanofluids-based collector from entropy generation. *Energy Conversion and Management*, 150, 515-531. https://doi.org/10.1016/j.enconman.2017.08.039

Malekan, M., Khosravi, A., & Syri, S. (2019). Heat transfer modeling of a parabolic trough solar collector with working fluid of Fe3O4 and CuO/Therminol 66 nanofluids under magnetic field. *Applied Thermal Engineering*. https://doi.org/10.1016/j.applthermaleng.2019.114435

Maoulida, F., Djedjig, R., Kassim, M., & Ganaoui, M. (2022). Numerical Study for the Evaluation of the Effectiveness and Benefits of Using Photovoltaic-Thermal (PV/T) System for Hot Water and Electricity Production under a Tropical African Climate: Case of Comoros. *Energies*. https://doi.org/10.3390/en16010240

Misha, S., Abdullah, A., Tamaldin, N., Rosli, M., & Sachit, F. (2019). Simulation CFD and experimental investigation of PVT water system under natural Malaysian weather conditions. *Energy Reports*. https://doi.org/10.1016/j.egyr.2019.11.162

Mohammad, A., & Al-Shohani, W. (2022). Numerical and experimental investigation for analyzing the temperature influence on the performance of photovoltaic module. *AIMS Energy*. https://doi.org/10.3934/energy.2022047

Moran, M. J., Shapiro, H. N., Boettner, D. D., & Bailey, M. B. (2010). *Fundamentals of engineering thermodynamics*. John Wiley & Sons.

Mundu, M. M., Nnamchi, S. N., & Muhaise, H. (2024). Sustainable Energy transitions in Uganda: Influential determinants of the renewable energy landscape. *IAA Journal of Applied Sciences*, *11*(1), 57–72. https://doi.org/10.59298/iaajas/2024/6.68.40.35

Mundu, M. M., Nnamchi, S. N., & Ukagwu, K. J. (2020). Algorithmized modelling, simulation and validation of clearness index in four regions of Uganda. *Journal of Solar Energy Research*, *5*(2), 432–452. https://doi.org/10.22059/jser.2020.300924.1150

Mundu, M. M., Nnamchi, S. N., Ukagwu, K. J., Peter, B. A., Nnamchi, O. A., & Ssempewo, J. I. (2022). Numerical modelling of wind flow for solar power generation in a case study of the tropical zones. *Modeling Earth Systems and Environment*, *8*(3), 4123–4134. https://doi.org/10.1007/s40808-021-01343-w

Mundu, M. M., Sempewo, J. I., Nnamchi, S. N., & Uti, D. E. (2025a). Solar-Powered desalination technologies for sustainable water security solutions. *International Journal of Energy Research*, *2025*(1). https://doi.org/10.1155/er/3482306

Mundu, M. M., Sempewo, J. I., Nnamchi, S. N., Mahoro, G. B., & Uti, D. E. (2025b). Integration of wind flow effects in theoretical and experimental models for solar power generation. *Scientific Reports*, *15*(1). https://doi.org/10.1038/s41598-025-90680-2

Mundu, M., Nnamchi, S., Sempewo, J., & Uti, D. E. (2024). Simulation modeling for energy systems analysis: A critical review. *Energy Informatics*, *7*(1), 75. https://doi.org/10.1186/s42162-024-00374-8

Mwesigye, A., Yılmaz, İ., & Meyer, J. (2018). Numerical analysis of the thermal and thermodynamic performance of a parabolic trough solar collector using SWCNTs-Therminol®VP-1 nanofluid. *Renewable Energy*, 119, 844-862. https://doi.org/10.1016/j.renene.2017.10.047

ARTICLE IN PRESS

Narkwatchara, P., Ratanatamskul, C., & Chandrachai, A. (2020). Effects of particulate matters and climate condition on photovoltaic system efficiency in tropical climate region. *Energy Reports*, 6, 2577-2586. https://doi.org/10.1016/j.egyr.2020.09.016

Nasrin, R., Alim, M., & Hasanuzzzaman, M. (2016). Assisted convective heat transfer and entropy generation in a solar collector filled with nanofluid. *Journal of Naval Architecture and Marine Engineering*, 13, 135-150. https://doi.org/10.3329/jname.v13i2.27774

Nnamchi, S. N., & Mundu, M. M. (2022a). Development of solar isodose lines: Mercatorian and spatial guides for mapping solar installation areas. *Heliyon*, *8*(10), e11045. https://doi.org/10.1016/j.heliyon.2022.e11045

Nnamchi, S. N., Mundu, M. M., Nnamchi, O. A., Onochie, U., & Jagun, Z. O. (2021). Differential modelling and simulation of solar power potential: a helio-application of biharmonic model. *Modeling Earth Systems and Environment*, *8*(2), 2383–2400. https://doi.org/10.1007/s40808-021-01232-2

Nnamchi, S. N., Mundu, M. M., Ukagwu, K. J., & Oyagbola, I. A. (2022b). Development and adaptation of relative sunshine hours models for the equatorial latitudes: a case study. *Modeling Earth Systems and Environment*, *8*(1), 1191-1201. https://doi.org/10.1007/s40808-021-01147-y

Nnamchi, S. N., Nnamchi, O. A., Sanya, O. D., Mundu, M. M., & Gabriel, V. (2020). Dynamic analysis of performance of photovoltaic generators under moving cloud conditions. *Journal of Solar Energy Research*, *5*(2), 453-468. https://doi.org/10.22059/jser.2020.304561.1158

Omara, A., Mohamed, O., Mohammedali, A., & Ahmed, M. (2024). Effect of ten different physical parameters on solar still productivity: Theoretical modeling. *Environmental Progress & Sustainable Energy*, 43. https://doi.org/10.1002/ep.14416

Osara, J., & Bryant, M. (2024). Methods to Calculate Entropy Generation. *Entropy*, 26. https://doi.org/10.3390/e26030237

Osorio, L., Moreno, M., Rivera, M., Tuninetti, V., Chavarria, G., Duchêne, L., & Wheeler, P. (2024). A metaheuristic-based method for photovoltaic temperature computation under tropical conditions. *Solar Energy*. https://doi.org/10.1016/j.solener.2024.112414

Ozcan, B., & Seval, M. (2022). Temperature-Irradiance Matrix and Determination of Temperature Coefficients of a Monocrystalline PV Module. *Open Journal of Energy Efficiency*. https://doi.org/10.4236/ojee.2022.113008

Pal, R. (2017). Demystification of the Gouy-Stodola theorem of thermodynamics for closed systems. *International Journal of Mechanical Engineering Education*, 45, 142 - 153. https://doi.org/10.1177/0306419016689501

Pal, R. (2018). Entropy Generation and Exergy Destruction in Flow of Multiphase Dispersions of Droplets and Particles in a Polymeric Liquid. *Fluids*, 3, 19. https://doi.org/10.3390/fluids3010019

Pal, R. (2019). Comparison of entropic and exergetic methods of quantification of loss of power due to irreversibilities in real processes using the Gouy–Stodola theorem. *International Journal of Mechanical Engineering Education*, 47, 73 - 96. https://doi.org/10.1177/0306419017749801

Poongavanam, P., Chand, A., Tai, V., Gupta, Y., Kuppusamy, M., Dhanraj, J., Velmurugan, K., Rajagopal, R., Ramachandran, T., Prasad, K., Chand, S., Raj, S., & Mamun, K. (2023). Annual Thermal Management of the Photovoltaic Module to Enhance Electrical Power and Efficiency Using Heat Batteries. *Energies*. https://doi.org/10.3390/en16104049

ARTICLE IN PRESS

Ramírez-Minguela, J., Rangel-Hernandez, V., Alfaro-Ayala, J., Elizalde-Blancas, F., Ruíz-Camacho, B., López-Núñez, O., & Alvarado-Rodríguez, C. (2023). Performance Comparison of Different Flat Plate Solar Collectors by Means of the Entropy Generation Rate Using Computational Fluid Dynamics. *Entropy*, 25. https://doi.org/10.3390/e25040621

Rao, T., Sekhar, R., Arıcı, M., Pochont, N., & Prasad, D. (2024). Experimental investigations on bi-symmetrical web flow water based photovoltaic-thermal (PVT) system: Energy, exergy, and entropy (3-E) analysis. *Solar Energy*. https://doi.org/10.1016/j.solener.2024.112445

Rashidi, S., Yang, L., Khoosh-Ahang, A., Jing, D., & Mahian, O. (2020). Entropy generation analysis of different solar thermal systems. *Environmental Science and Pollution Research*, 27, 20699-20724. https://doi.org/10.1007/s11356-020-08472-2

Saldaña, M., Gallegos, S., Gálvez, E., Castillo, J., Salinas-Rodríguez, E., Cerecedo-Sáenz, E., Hernández-Ávila, J., Navarra, A., & Toro, N. (2024). The Reynolds Number: A Journey from Its Origin to Modern Applications. *Fluids*. https://doi.org/10.3390/fluids9120299

Samykano, M. (2023). Hybrid Photovoltaic Thermal Systems: Present and Future Feasibilities for Industrial and Building Applications. *Buildings*. https://doi.org/10.3390/buildings13081950

Satpute, J., Deshmukh, S., Kale, P., & Patil, R. (2025). Computational study on water-based hybrid photovoltaic thermal absorber configurations. *Scientific Reports, 15*, 82690. https://doi.org/10.1038/s41598-024-82690-3

Shaik, S., Bhardwaj, M., Agarwal, S., Yendaluru, R., , H., & Sharma, K. (2021). Evaluation of Optical Transmissivity of Transparent Materials on the Performance of Solar Flat Plate Collectors. *Journal of Solar Energy Engineering-transactions of The Asme*, 143. https://doi.org/10.1115/1.4050214

Shao, N., , L., Zhou, C., & Zhang, D. (2022). Experimental study on the heat transfer performance of the PVT ventilated roof as heat exchanger for heat pump system. *Renewable Energy*. https://doi.org/10.1016/j.renene.2022.01.084

Skoplaki, E., & Palyvos, J. (2009). On the temperature dependence of photovoltaic module electrical performance: a review of efficiency/ power correlations. *Solar Energy*, 83, 614-624. https://doi.org/10.1016/j.solener.2008.10.008

Soliman, A. (2023). A Numerical Investigation of PVT System Performance with Various Cooling Configurations. *Energies*. https://doi.org/10.3390/en16073052

Sun, V., Asanakham, A., Deethayat, T., & Kiatsiriroat, T. (2021). Evaluation of nominal operating cell temperature (NOCT) of glazed photovoltaic thermal module. *Case Studies in Thermal Engineering*, 28, 101361. https://doi.org/10.1016/j.csite.2021.101361

Takyi, G., & Nyarko, F. (2020). Investigation of the Effect of Temperature Coefficients on Mono-Crystalline Silicon PV Module Installed in Kumasi, Ghana. *Journal of Power and Energy Engineering*. https://doi.org/10.4236/jpee.2020.89003

Tamburrino, A., & Niño, Y. (2025). The Universal Presence of the Reynolds Number. *Fluids*. https://doi.org/10.3390/fluids10050117

Torabi, M., Karimi, N., Torabi, M., Peterson, G., & Simonson, C. (2020). Generation of entropy in micro thermofluidic and thermochemical energy systems-A critical review. *International Journal of Heat and Mass Transfer*. https://doi.org/10.1016/j.ijheatmasstransfer.2020.120471

ARTICLE IN PRESS

Unar, I., Maitlo, G., Ahmed, S., Ali, S., Memon, A., Kandhro, G., & Jatoi, A. (2020). Performance evaluation of solar flat plate collector using different working fluids through computational fluid dynamics. *SN Applied Sciences*, 2. https://doi.org/10.1007/s42452-020-2005-z

Van Zyl, W., Dirker, J., & Meyer, J. (2013). Single-Phase Convective Heat Transfer and Pressure Drop Coefficients in Concentric Annuli. *Heat Transfer Engineering*, 34, 1112 - 1123. https://doi.org/10.1080/01457632.2013.763550

Wang, Y., & Wang, P. (2020). Application of stable flow energy equation in steam turbine and other power machines. *IOP Conference Series: Earth and Environmental Science*, 474. https://doi.org/10.1088/1755-1315/474/5/052087

Wang, Z., Hou, G., Taherian, H., & Song, Y. (2024). Numerical Investigation of Innovative Photovoltaic–Thermal (PVT) Collector Designs for Electrical and Thermal Enhancement. *Energies*. https://doi.org/10.3390/en17102429

Wang, Z., Li, H., Chen, Y., & Zhang, X. (2024). Numerical investigation of innovative photovoltaic–thermal structures. *Energies, 17*(10), 2429. https://doi.org/10.3390/en17102429

Yan, B., Wu, Q., Chi, X., Wu, C., Luo, P., Luo, Y., & Zeng, P. (2022). Numerical and Experimental Investigation of Photovoltaic/Thermal Systems: Parameter Analysis and Determination of Optimum Flow. *Sustainability*. https://doi.org/10.3390/su141610156

Zhao, B., Ao, X., Chen, N., Xuan, Q., Hu, M., & Pei, G. (2020). A spectrally selective surface structure for combined photothermic conversion and radiative sky cooling. *Frontiers in Energy*, 14, 882 - 888. https://doi.org/10.1007/s11708-020-0694-z

Zm, A., Sinuraya, E., & Winardi, B. (2025). The Effect of Temperature and Weather Conditions on the Performance of Photovoltaic Modules in Tropical Indonesia. *West Science Information System and Technology*. https://doi.org/10.58812/wsist.v3i01.1870

ARTICLE IN PRESS

ARTICLE IN PRESS

Thermodynamic Design and Energy–Exergy Analysis of a Water-Cooled Photovoltaic–Thermal Systems under Tropical Conditions

M. M. Mundu[1*], J. I. Ssempewo[2], S. N. Nnamchi[3] and Daniel Ejim Uti[4*]

1. Department of Electrical, Telecommunication and Computer Engineering, Kampala International University, P. O. Box 20000, Kampala, Uganda, mundu.mustafa@kiu.ac.ug, ORCID; https://orcid.org/0000-0003-1345-9999.
2. Department of Civil and Environmental Engineering, College of Engineering, Design Art and Technology, Makerere University, P.O. Box 7062, Kampala, Uganda, jotham.sempewo@mak.ac.ug, ORCID; https://orcid.org/0000-0002-9897-211x.
3. Department of Mechanical and Industrial Engineering, Faculty of Science and Technology, Mbarara University of Science and Technology, snnamchi@must.ac.ug, ORCID; https://orcid.org/0000-0002-6368-2913
4. Daniel Ejim Uti (PhD). Department of Research and Publications, Kampala International University, P.O. Box 20000, Kampala, Uganda. Email: daniel.ejimuti@kiu.ac.ug

***Corresponding authors:** Mundu, M. M (PhD). Department of Electrical, Telecommunication and Computer Engineering, Kampala International University, P.O. Box 20000, Kampala, Uganda, mundu.mustafa@kiu.ac.ug.

Daniel Ejim Uti (PhD). Department of Research and Publications, Kampala International University, P. O. Box 20000, Kampala, Uganda. Email: dan4uti@gmail.com, daniel.ejimuti@kiu.ac.ug

Abstract

Photovoltaic–thermal (PVT) systems provide a promising approach for simultaneous electrical and thermal energy generation under high-irradiance tropical conditions. However, most existing studies primarily focus on first-law energy performance or global exergy indicators without detailed thermodynamic irreversibility diagnostics. This study presents a second-law thermodynamic analysis of a closed-loop water-cooled PVT system coupled to a well-mixed thermal storage tank under tropical climatic conditions. A coupled transient thermal–electrical numerical framework incorporating explicit Gibbs Tds thermodynamic relations is developed to evaluate entropy generation, exergy destruction, and subsystem-level thermodynamic irreversibilities within the PVT system. The model was applied to a representative tropical day using Typical Meteorological Year data for Kampala, Uganda. Under baseline operating conditions for a 1.66 m² collector integrated with a 100 L storage tank, the system maintained PV temperatures below approximately 43 °C while delivering about 1.9 kWh_{th} of useful thermal energy and 1.95 kWh_{el} of electrical energy. The second-law analysis further revealed that ambient heat rejection accounted for nearly 95% of the total exergy destruction, identifying it as the dominant thermodynamic irreversibility mechanism. Parametric analysis showed that increasing mass flow rate, solar irradiance, and ambient temperature reduced exergy efficiency despite relatively stable first-law energy efficiencies, confirming that energy-optimal and exergy-optimal operating conditions do not necessarily coincide. The thermodynamically favorable operating region was identified at low-to-moderate flow rates near 0.01 kg s^{-1} for the investigated configuration. Unlike many conventional PVT studies that primarily report overall energy or exergy efficiencies, the present work provides a mechanism-resolved second-law interpretation by explicitly linking entropy generation and exergy destruction to the governing thermodynamic processes within the collector and storage subsystems under tropical operating conditions. The results further demonstrate that the principal advantage of the proposed configuration lies in enhanced overall solar-energy utilization through simultaneous electrical and useful low-

ARTICLE IN PRESS

temperature thermal energy recovery rather than electrical enhancement alone. The study therefore provides second-law-based thermodynamic design guidance for optimization of tropical PVT systems, particularly regarding reduction of ambient thermal losses and improvement of PV–absorber thermal coupling.

Keywords: PVT systems; Exergy analysis; Entropy generation; Tds formulation; Second-law efficiency; Tropical climate; Thermodynamic optimization; Solar energy systems

1.0 Introduction

1.1 Background and Motivation

Photovoltaic (PV) technology is widely recognized as a major pillar of the global transition toward low-carbon energy systems. However, PV module efficiency decreases significantly with increasing cell temperature, typically by about 0.4–0.5% per °C above standard test conditions for crystalline silicon modules. Under tropical climatic conditions, high solar irradiance combined with elevated ambient temperature causes PV modules to operate substantially above nominal temperatures, resulting in considerable electrical performance degradation. Experimental and numerical studies in tropical regions have confirmed that elevated operating temperatures reduce PV electrical output, while cooling strategies such as phase change materials, green roofs, and active thermal management can mitigate thermal losses and improve system efficiency (Zm et al., 2025; Poongavanam et al., 2023; Arenandan et al., 2022; Dubey & Tay, 2013; Bian et al., 2025; Fashina et al., 2018). Additional environmental factors including humidity, dust accumulation, and particulate matter further degrade PV performance in tropical environments (Zm et al., 2025; Narkwatchara et al., 2020; Ballina & Go, 2025). Consequently, effective thermal management and site-specific operational strategies are essential for sustaining PV performance under high-temperature operating conditions.

In tropical regions, elevated solar irradiance and ambient temperature not only intensify PV thermal losses but also create substantial opportunities for low-grade thermal energy recovery. Consequently, photovoltaic–thermal (PVT) systems have attracted increasing attention because they simultaneously generate electrical and useful thermal energy from the same collector aperture area while reducing PV operating temperature. Such integrated energy utilization is particularly attractive for domestic hot water production, low-temperature thermal applications, building-integrated renewable-energy systems, and decentralized energy deployment in hot-climate environments.

In conventional PV modules, only a limited fraction of the incident solar radiation is converted into electricity, while the remaining energy is dissipated as heat, increasing cell temperature and reducing electrical efficiency. PVT systems address this limitation by integrating a thermal collector with the PV module to extract waste heat using a circulating working fluid, thereby simultaneously enhancing electrical performance and recovering useful thermal energy. Recent advances include spectral-splitting PVT configurations, thermally enhanced collectors, and PVT–heat-pump integrations for improved overall solar-energy utilization (Hong et al., 2022; Alessandro et al., 2021). Various cooling approaches involving air, water, nanofluids, and phase change materials have also been investigated to improve thermal extraction and combined system efficiency (Al-Waeli et al., 2020; Diwania et al., 2020; Bandaru et al., 2021; Muhamad et al., 2022; Kalateh et al., 2022; Al-Najjar et al., 2024; Bian et al., 2025). In addition, flow-channel modifications, enhanced absorber configurations, and integration with thermal storage systems have demonstrated further potential for improving PVT thermodynamic performance (Diwania et

ARTICLE IN PRESS

al., 2020; Jia et al., 2019; Asefi et al., 2022; Wang et al., 2024; Attia et al., 2025). Despite challenges associated with thermal losses, system complexity, and optimization trade-offs, PVT systems remain promising technologies for enhanced solar-energy utilization through simultaneous electricity generation and useful heat recovery (Hong et al., 2022; Bandaru et al., 2021; Samykano, 2023).

The fundamental energy flow in a PVT system is illustrated schematically in Figure 1, where the incident solar radiation is partitioned into three main components: electrical power output, useful thermal energy transferred to the working fluid, and unavoidable thermal losses to the environment.

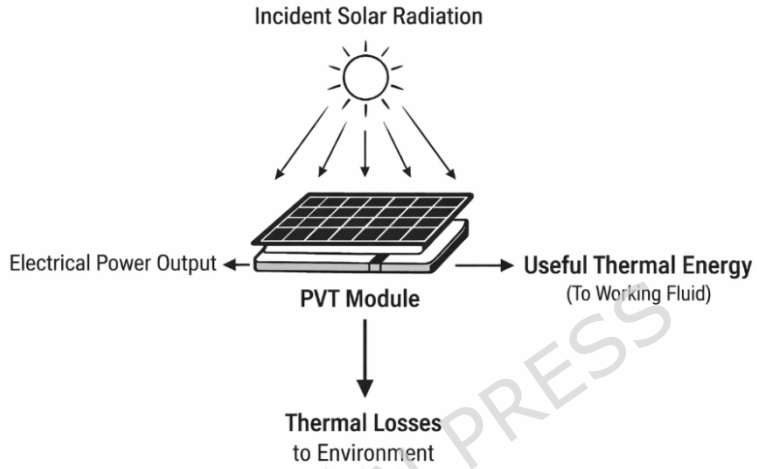

Figure 1 Conceptual energy flow diagram of the PVT system

1.2 Problem Statement and Research Gap

Photovoltaic–thermal systems have been widely investigated for simultaneous electrical and thermal energy generation; however, most existing studies remain dominated by first-law performance indicators such as thermal efficiency, electrical efficiency, and overall energy recovery, which quantify energy quantities without adequately addressing energy quality or thermodynamic irreversibility. Even in studies incorporating exergy analysis, the evaluation is commonly limited to global exergy efficiencies or generalized energy–exergy trade-offs without detailed identification of the irreversible thermodynamic mechanisms governing system degradation. Consequently, subsystem-level entropy generation associated with finite-temperature heat transfer, ambient thermal rejection, and fluid-flow dissipation remains insufficiently resolved in many existing PVT modeling frameworks (Joshi et al., 2009; Evola & Marletta, 2014; Kallio & Siroux, 2020; Kalateh et al., 2022; Rao et al., 2024; Al-Najjar et al., 2024). As a result, energy-based optimization alone is often insufficient for identifying true thermodynamic performance limits or guiding rational system design.

Second-law thermodynamics indicates that irreversibilities in PVT systems primarily originate from heat transfer across finite temperature differences, thermal losses to the ambient, and viscous dissipation within fluid channels (Maadi et al., 2017; Mundu et al., 2020; Liu et al., 2023; Hai et al., 2023; Ramírez-Minguela et al., 2023). Accordingly, recent studies emphasize that entropy generation analysis is essential for meaningful thermodynamic optimization of solar thermal and micro-thermofluidic systems (Torabi et al., 2020; Rashidi et al., 2020; Ramírez-Minguela et al.,

ARTICLE IN PRESS

2023). Although detailed CFD-based investigations have decomposed entropy generation into thermal and viscous contributions, such approaches are computationally intensive and rarely incorporated into design-oriented transient PVT frameworks (Maadi et al., 2017; Liu et al., 2023; Hai et al., 2023; Mundu et al., 2024).

Furthermore, relatively few studies have developed transient thermodynamic PVT models capable of simultaneously coupling thermal behavior, electrical performance, entropy generation, and exergy destruction under realistic tropical operating conditions. Existing analyses frequently rely on steady-state assumptions or simplified exergy formulations that provide limited diagnostic insight into the physical sources of irreversibility within collector and storage subsystems. More importantly, despite their fundamental thermodynamic significance, Gibbs Tdsrelations are seldom explicitly integrated into transient numerical PVT simulations. Instead, entropy generation is often treated using lumped or non-diagnostic formulations without direct linkage to the governing thermodynamic processes (Rashidi et al., 2020; Ramírez-Minguela et al., 2023; Mundu et al., 2022; Torabi et al., 2020; Osara & Bryant, 2024; Nnamchi et al., 2021). Consequently, many existing exergy-based studies remain focused primarily on global performance indicators and inlet-temperature optimization, providing limited guidance regarding collector design, thermal coupling, and thermodynamically optimal operating conditions under tropical high-irradiance environments (Kallio & Siroux, 2020; Al-Najjar et al., 2024; Rao et al., 2024; Nnamchi et al., 2022a; Nnamchi et al., 2022b).

In addition, many existing investigations implicitly treat thermal extraction mainly as a mechanism for improving PV electrical efficiency, with comparatively limited emphasis on the broader thermodynamic significance of simultaneous thermal energy recovery. Under tropical climatic conditions, however, useful recovery of low-grade thermal energy can represent a substantial component of the total solar-energy utilization potential of PVT systems. Therefore, there remains a need for a rigorous second-law-based framework capable of simultaneously evaluating electrical enhancement, thermal energy recovery, entropy generation, and exergy destruction in order to identify dominant irreversibility mechanisms and thermodynamically favorable operating conditions.

Accordingly, the present study develops a coupled transient thermal–electrical PVT framework that explicitly integrates Gibbs Tds thermodynamic relations, subsystem-level entropy generation diagnostics, and exergy destruction analysis under tropical climatic conditions. Unlike many conventional PVT investigations that primarily emphasize overall thermal or exergy efficiencies, the proposed framework provides a physically diagnostic second-law interpretation capable of explicitly linking entropy generation and exergy destruction to the governing irreversible thermodynamic processes within the collector and storage subsystems.

1.3 Aim and Objectives

The aim of this study is to develop a comprehensive first- and second-law-based numerical model of a water-cooled PVT system coupled to a closed-loop, well-mixed thermal storage tank, and to use this framework to evaluate and optimize its thermodynamic performance under tropical operating conditions. Specifically, the objectives are to (i) develop a coupled thermal–electrical model of the PVT collector and storage tank based on energy conservation principles, (ii) formulate entropy balances and entropy generation terms explicitly using the Gibbs (Tds) thermodynamic relations, (iii) evaluate exergy flows and exergy destruction rates in the system components through application of the Gouy–Stodola theorem, (iv) perform a parametric analysis to quantify the effects of key design and operating parameters, including mass flow rate, ambient

temperature, and solar irradiance, on energy efficiency, exergy efficiency, and entropy generation, and (v) identify thermodynamically optimal operating regions that maximize useful energy recovery while minimizing irreversible losses.

1.4 Contributions of the Present Study

The scientific contributions and novel aspects of the present study are as follows: (i) the development of a coupled transient thermal–electrical numerical framework for a closed-loop water-cooled PVT system under tropical climatic conditions, (ii) the explicit integration of Gibbs Tds thermodynamic relations into the entropy generation formulation of the PVT collector and storage system, (iii) the implementation of a mechanism-resolved second-law analysis capable of distinguishing entropy generation associated with finite-temperature heat transfer, ambient thermal rejection, and fluid friction, (iv) a detailed subsystem-level exergy destruction mapping based on the Gouy–Stodola theorem, and (v) a second-law-based thermodynamic optimization framework demonstrating that energy-optimal and exergy-optimal operating conditions do not necessarily coincide under tropical operating environments.

2.0 System Description and Design Configuration

2.1 System Architecture

The system considered in this study is a closed-loop, water-cooled PVT system coupled to a well-mixed thermal storage tank. The overall configuration consists of four main subsystems: (i) the PVT collector, (ii) the working fluid circulation loop, (iii) the storage tank, and (iv) the electrical load/inverter (Figure 2).

ARTICLE IN PRESS

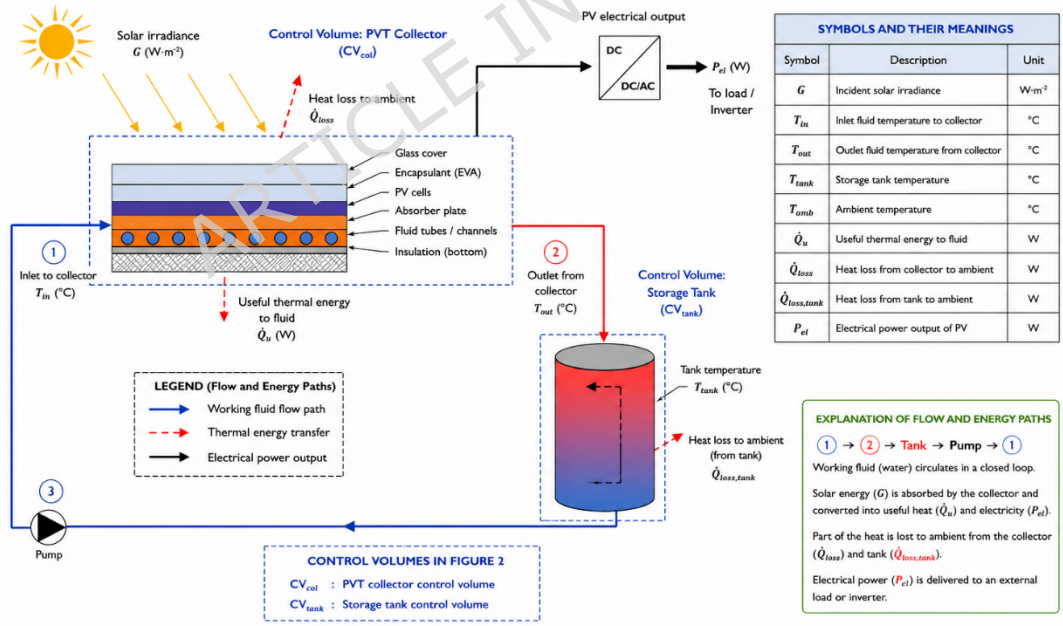

Figure 2. Schematic representation of the closed-loop water-cooled PVT system showing the collector, working-fluid circulation loop, storage tank coupling, thermal energy transfer paths, electrical output, and principal thermodynamic control volumes used in the analysis.

The conceptual energy flow paths and the main system components are illustrated in Figure 2, which also indicates the control volumes used later for the thermodynamic analysis. The notation

ARTICLE IN PRESS

adopted in Figure 2 is maintained consistently throughout the governing equations, thermodynamic formulations, and parameter tables presented in subsequent sections. The PVT collector is a flat-plate type and is composed, from top to bottom, of a glass cover, photovoltaic cells, a backsheet or bonding layer, a metallic absorber plate, and fluid channels or tubes attached to the absorber. Solar radiation G is incident on the PV surface, where a fraction is converted into electricity, while the remaining part is transformed into heat and conducted to the absorber. The circulating water removes this heat and transports it to the storage tank.

The hydraulic loop comprises a circulation pump, connecting pipes, and the storage tank. The water leaving the tank at temperature T_{tank} enters the PVT collector at T_{in}, absorbs heat, and exits the collector at T_{out} before returning to the tank. The storage tank is modeled as a well-mixed control volume, implying a spatially uniform tank temperature. The electrical output of the PV module is delivered to an external load or inverter.

2.2 Design Assumptions and Operating Modes

To obtain a tractable and robust numerical model, the following assumptions are adopted:

1. Heat transfer in the PVT collector is modeled using a one-dimensional (1D) thermal resistance network in the direction normal to the collector plane.
2. The system can be simulated in steady-state or transient mode; in the present formulation, the tank introduces time dependence, while the collector is treated in quasi-steady state at each time step.
3. The storage tank is assumed to be well-mixed, such that its temperature $T_{tank}(t)$ is spatially uniform.
4. Thermophysical properties of the working fluid and solid materials are either taken as constant or evaluated at mean operating temperature.
5. Heat losses from the collector to the ambient are represented by a lumped overall heat loss coefficient U_L.
6. Heat losses from the tank to the ambient are represented by a lumped coefficient $U_t A_t$.
7. Pressure losses in the fluid loop may be included to evaluate entropy generation due to friction, but they do not significantly affect the energy balance.

These assumptions were adopted to establish a computationally tractable transient thermodynamic framework while preserving the dominant heat transfer, thermal coupling, and irreversible loss mechanisms governing the operation of the investigated PVT system under tropical climatic conditions.

The system operates in a closed-loop recirculation mode, where the tank temperature determines the collector inlet temperature in Equation (1)

$$T_{in}(t) = T_{tank}(t) \tag{1}$$

where $T_{in}(t)$ is the inlet fluid temperature to the PVT collector and $T_{tank}(t)$ is the instantaneous temperature of the well-mixed storage tank. This relation provides the thermal coupling between the collector and the storage subsystem.

2.3 Geometric Design Parameters

The main geometric and design parameters of the PVT collector and storage tank are summarized in Table 1. These parameters define both the optical–thermal behavior of the collector and the thermal inertia of the storage system. The geometric configuration shown schematically in Figure 2 is used as the basis for the numerical model developed in Section 3.

ARTICLE IN PRESS

2.4 Working Fluid and Material Properties

The working fluid employed in the cooling loop is liquid water, selected because of its high specific heat capacity, relatively high thermal conductivity, low cost, wide availability, and suitability for low-temperature thermal energy applications. Water also exhibits favorable thermophysical behavior for heat extraction under moderate operating temperatures, making it a widely adopted benchmark fluid in photovoltaic–thermal systems. Furthermore, its relatively low viscosity contributes to reduced pumping requirements and lower hydraulic irreversibility during circulation, which is important for second-law thermodynamic assessment.

The thermophysical properties of water density ρ, specific heat capacity c_p, and thermal conductivity k are evaluated at the mean fluid temperature unless otherwise stated. The main solid materials and their properties are also listed in Table 1. These properties are required for the calculation of heat transfer rates, PV electrical efficiency, and overall system losses in the mathematical model presented in Section 3.

Table 1. Main design parameters, material properties, and PV module specifications used in the simulation (baseline case)

Table 1(a) System geometry and operating conditions (single-module PVT, DHW)

Parameter	Symbol	Baseline value	Unit
1. Collector gross area (single module)	A_c	1.66	m^2
2. Module dimensions (L × W × H)	–	1675 × 992 × 35	mm
3. Tilt angle (Kampala near-equator baseline)	β	10	°
4. Working fluid	–	Water	–
5. Tank volume (well-mixed)	V_{tank}	100	L
6. Tank volume	V_{tank}	0.10	m^3
7. Tank initial temperature	$T_{tank,0}$	26	$°C$
8. Ambient temperature (baseline daytime)	T_{amb}	26	$°C$
9. Wind speed (baseline)	v_w	2.4	ms^{-1}
10. Mass flow rate (closed loop)	$\dot{m}$	0.034	kgs^{-1}

Table 1(a) summarizes the geometry and operating conditions of the reference single-module PVT system modeled for domestic hot water (DHW) production in Kampala. The collector gross area (1.66 m²) and module dimensions correspond to a standard residential PV module footprint, in line with many experimental and numerical PVT studies that use single flat-plate modules of roughly $1.5 - 1.7\ m\ \times\ 1.0\ m$ (Wang et al., 2024; Yan et al., 2022; Maoulida et al., 2022). The tilt angle of 10° represents a near-equatorial installation, comparable to other tropical and subtropical PVT investigations in Ghana, Malaysia, and Comoros, where low tilt angles are adopted to reflect local latitude and maximize annual irradiation on the collector surface (Abdul-Ganiyu et al., 2021; Basuhaib et al., 2024; Misha et al., 2019; Maoulida et al., 2022; Mundu et al., 2025a; Mundu et al., 2025b).

The system is configured as a closed-loop water-based PVT for DHW, with a well-mixed 100 L storage tank ($0.10\ m^3$). Similar storage volumes (100–200 L) are widely used in residential PVT DHW simulations and field tests, providing a realistic match to typical household hot water

ARTICLE IN PRESS

demand (Bigorajski & Chwieduk, 2018; Yan et al., 2022; Maoulida et al., 2022). The baseline ambient temperature is set to 26 °C, consistent with typical daytime conditions in tropical locations where reported ambient temperatures during PVT testing range from about 25–30 °C (Rao et al., 2024; Basuhaib et al., 2024; Wang et al., 2024; Misha et al., 2019; Kenfack et al., 2023; Maoulida et al., 2022). The baseline wind speed of 2.4 ms^{-1} is also representative of moderate natural convection conditions used in PVT performance analyses and NOCT/thermal characterizations, where values between about $2-3\ ms^{-1}$ are commonly assumed or measured (Wang et al., 2024; Kenfack et al., 2023; Kramer et al., 2023; Sun et al., 2021).

The closed-loop mass flow rate of 0.034 kgs^{-1} lies within the lower range of water flow rates investigated in tropical PVT experiments and optimization studies (typically $0.025-0.083\ kgs^{-1}$ for single modules), where such values have been shown to provide effective cooling without excessive pumping power or diminishing returns in electrical/thermal performance (Abdul-Ganiyu et al., 2021; Basuhaib et al., 2024; Misha et al., 2019; Abdullah et al., 2020; Soliman, 2023). This choice therefore represents a realistic baseline operating point for subsequent parametric and second-law analyses under Kampala-type tropical conditions (for all simulations presented in Section 6).

Table 1(b) PVT collector construction (sheet-and-tube absorber)

Parameter	Symbol	Baseline value	Unit
1. Glass cover thickness (tempered)	δ_g	3.2	mm
2. Absorber plate material	–	Copper	–
3. Absorber plate thickness	δ_{abs}	0.5	mm
4. Tube inner diameter	D_i	8	mm
5. Tube outer diameter	D_o	10	mm
6. Number of parallel tubes	N_t	10	–
7. Tube spacing (center-to-center)	s_t	0.10	m
8. Back insulation thickness	δ_{ins}	50	mm

ARTICLE IN PRESS

The PVT collector construction in Table 1(b) reflects a conventional sheet-and-tube flat-plate design, widely used in commercial and research PVT systems due to its proven thermal performance and manufacturability (Herrando et al., 2019; Guarracino et al., 2016; Kim & Kim, 2012). The 3.2 mm tempered glass cover thickness is typical for durability and optical transmittance balance, protecting the PV cells while minimizing solar radiation losses (Guarracino et al., 2019; Kim & Kim, 2012). The copper absorber plate with a thickness of 0.5 mm offers excellent thermal conductivity, enhancing heat transfer from the PV cells to the fluid, which is consistent with common practice in high-performance PVT collectors (Herrando et al., 2019; Alami et al., 2025; Kim & Kim, 2012). Its high thermal conductivity also improves thermal coupling between the absorber and working fluid, and contributes to reduced temperature gradients and entropy generation within the collector. The tube dimensions (8 mm inner diameter, 10 mm outer diameter) and spacing (0.10 m center-to-center) align with standard sheet-and-tube configurations designed to optimize fluid flow and heat extraction without excessive pressure drop (Herrando et al., 2019; Guarracino et al., 2016; Francisco et al., 2024). The use of 10 parallel tubes ensures sufficient coolant coverage across the absorber area, balancing hydraulic and thermal performance (Guarracino et al., 2016; Francisco et al., 2024). Finally, the 50 mm back insulation

ARTICLE IN PRESS

thickness is chosen to minimize rear heat losses, making top losses dominant as typical for flat-plate collectors aiming to maximize thermal efficiency under steady-state conditions (Alami et al., 2025; Guarracino et al., 2019). Moreover, these parameters are consistent with those reported in detailed numerical and experimental studies of sheet-and-tube PVT collectors, which emphasize copper absorbers, tempered glass covers around 3 mm thick, and back insulation thicknesses between 40–60 mm to optimize thermal performance while maintaining structural integrity (Herrando et al., 2019; Guarracino et al., 2016; Alami et al., 2025; Nnamchi et al., 2020; Guarracino et al., 2019; Kim & Kim, 2012).

Table 1(c) Optical properties

Parameter	Symbol	Baseline value	Unit
1. Glass transmittance	τ_g	0.90	–
2. Effective absorptance (PV/absorber)	α_{eff}	0.90	–
3. Effective emissivity (outer surface)	ε_{eff}	0.88	–

Table 1(c) summarizes the key optical properties that control both solar energy capture and radiative heat exchange with the surroundings. The glass transmittance of 0.90 represents high-quality low-iron glazing, consistent with commercially available covers that transmit around 90% of incident solar radiation and are widely used in flat-plate collectors for enhanced thermal performance (Giovannetti et al., 2014; Shaik et al., 2021; Bakari et al., 2014). Tempered low-iron glass was selected because of its high solar transmittance, mechanical durability, and favorable optical performance under outdoor tropical operating conditions. The effective absorptance of the combined PV/absorber surface is also set to 0.90, reflecting a well-coupled interface with high solar absorptivity, in line with values typically targeted for efficient solar absorbers (Hellström et al., 2003). The effective emissivity of the outer surface, $\varepsilon_{eff} = 0.88$, characterizes its long-wave infrared behavior and is comparable to standard clear or low-iron glass, which typically exhibits mid-infrared emissivity around 0.8–0.85 (Giovannetti et al., 2014; Khoukhi & Maruyama, 2006; Khoukhi & Maruyama, 2005). This parameter is essential for accurately predicting radiative heat losses, especially at elevated operating temperatures where long-wave radiation can dominate over convection. Thus, these baseline values are representative of conventional, high-quality flat-plate solar collector glazing and provide a realistic basis for performance modeling.

Table 1(d) Material and fluid properties (evaluated near 25–60°C)

Parameter	Symbol	Baseline value	Unit
1. Water density	ρ	997	kg/m³
2. Water specific heat	c_p	4180	J/kg·K
3. Water thermal conductivity	k_f	0.60	W/m·K
4. Water dynamic viscosity	μ	0.89×10^{-3}	Pa·s
5. Copper conductivity	k_{cu}	385	W/m·K
6. Glass conductivity	k_g	1.0	W/m·K
7. Insulation conductivity	k_{ins}	0.040	W/m·K

ARTICLE IN PRESS

Table 1(d) reports the thermophysical properties of the working fluid and structural materials adopted in the model over the representative operating range of 25–60 °C. Water is selected as the heat transfer fluid because of its high specific heat capacity, relatively high thermal conductivity, low viscosity, and low cost, which make it a standard choice and performance benchmark for solar thermal and flat-plate collector systems (Unar et al., 2020; Jamshed et al., 2021; Chyngyzbekkyzy & Satybaldyev, 2025). The listed water density, specific heat, thermal conductivity, and dynamic viscosity are consistent with reference values commonly used in modeling and CFD studies of solar collectors near ambient and moderate operating temperatures (Unar et al., 2020; Jamshed et al., 2021). The thermal conductivities of copper, glass, and insulation define the main conductive heat transfer pathways in the collector, with copper providing highly conductive channels for heat removal, glass acting as a moderate-conductivity cover, and the low-conductivity insulation minimizing heat losses to the surroundings (Costa & Kenisarin, 2022; Unar et al., 2020). The insulation layer was selected primarily to minimize rear conductive heat losses, thereby improving thermal energy retention and reducing irreversible exergy losses to the surroundings. These properties form the basis for the thermal resistance network described in Section 3.3 and are necessary for accurate prediction of fluid temperatures, collector efficiency, and overall system performance.

Table 1(e) PV electrical parameters c-Si modules

Parameter	Symbol	Baseline value	Unit
Reference PV efficiency (STC baseline)	η_{ref}	0.18	–
Reference temperature	T_{ref}	25	°C
Power temperature coefficient	β	−0.0037	1/°C

Table 1(e) specifies the PV electrical parameters used to couple the thermal and electrical sub-models. The reference efficiency $\eta_{ref} = 0.18$ at STC (1000 W/m², 25 °C, AM1.5) is representative of commercial crystalline silicon modules and lies within the typical 15–22 % range reported for modern c-Si technologies (Skoplaki & Palyvos, 2009; Elsabahy et al., 2024; Cotfas et al., 2018). Crystalline silicon PV technology was selected because of its widespread commercial deployment, well-characterized thermal behavior, established temperature-dependent electrical performance relationships, and suitability for coupled thermodynamic analysis under tropical operating conditions. The reference temperature $T_{ref} = 25\,°C$ corresponds to the standard test condition used for rating and translating PV performance (Ozcan & Seval, 2022; Skoplaki & Palyvos, 2009). The power temperature coefficient $\beta = -0.0037\,°C^{-1}$ (−0.37 %/°C) falls within the commonly reported interval of roughly −0.3 to −0.5 %/°C for crystalline silicon cells and modules, reflecting the well-known decrease of maximum power and efficiency with increasing cell temperature (Skoplaki & Palyvos, 2009; Takyi & Nyarko, 2020; Chander et al., 2015; Mohammad & Al-Shohani, 2022). Therefore, η_{ref} and β define the linear sensitivity of electrical output to operating temperature and thus provide the key linkage between the thermal model and the electrical performance formulation in Section 3.2, ensuring that simulated power output remains consistent with realistic, datasheet-based PV behavior across the expected operating temperature range.

Thus, the selected materials and component configurations were intentionally chosen to represent a realistic and thermodynamically representative water-cooled flat-plate PVT system suitable for tropical climatic environments and low-temperature thermal energy applications.

ARTICLE IN PRESS

3.0 Mathematical and Thermodynamic Modeling

The overall numerical implementation procedure adopted in the present study consists of the following sequential stages: (i) specification of the meteorological and operating boundary conditions, (ii) solution of the coupled thermal–electrical energy balances for the PVT collector and storage tank, (iii) evaluation of the PV temperature and useful thermal energy transfer, (iv) computation of entropy generation and subsystem exergy destruction using the Gibbs Tds formulation, and (v) thermodynamic performance assessment through parametric and second-law analyses. This structured workflow ensures consistent coupling between the thermal, electrical, and thermodynamic components of the model.

In the present study, the reported thermal, electrical, entropy-generation, and exergy-related parameters were obtained numerically through the developed thermodynamic modeling framework using the governing conservation equations, thermophysical property relations, and meteorological boundary conditions described in the manuscript. The simulation procedure was implemented under transient operating conditions representative of tropical climatic environments.

3.1 Governing Conservation Equations

The thermodynamic model is developed by applying the conservation laws to the two principal control volumes shown in Figure 2: (i) the PVT collector control volume, and (ii) the storage tank control volume. The geometric parameters and material properties required by the model are provided in Table 1.

3.1.1 Energy Balance (Control Volume Form)

(a) General steady-flow energy equation

For a control volume operating under quasi-steady conditions (valid for the collector at each time step), the steady-flow energy equation is written as in Equation (2). This equation accounts for internal energy changes as well as kinetic and potential energy variations in the fluid flow (David et al., 2021; Kumar, 2022). It provides a comprehensive framework to model energy conversion and transport in engineering applications involving fluid flow with heat and work interactions (Wang & Wang, 2020; Kumar, 2022).

$$\dot{Q} - \dot{W} + \sum \dot{m}\left(h + \frac{V^2}{2} + gz\right)_{in} = \sum \dot{m}\left(h + \frac{V^2}{2} + gz\right)_{out} \quad (2)$$

where $\dot{Q}_{cv}$ is the heat transfer rate to the control volume (W), $\dot{W}$ is the work transfer rate from the control volume (W), $\dot{m}$ is the mass flow rate (kgs^{-1}), h is the specific enthalpy (Jkg^{-1}), V is the flow velocity (ms^{-1}), g is the gravitational acceleration (ms^{-2}), and z is the elevation (m), while the subscripts "in" and "out" denote inlet and outlet states, respectively. Extensions of this equation also support dynamic modeling of integrated energy systems by coupling thermal and hydraulic behaviors (Dancker & Wolter, 2021; Huang et al., 2023).

For the PVT collector, kinetic and potential energy changes are negligible, and shaft work across the collector is zero. Hence, Equation (2) reduces to Equation (3):

$$\dot{Q}_{cv} = \dot{m}(h_{out} - h_{in}) \quad (3)$$

where h_{in} and h_{out} are the specific enthalpies of the fluid at the collector inlet and outlet, respectively.

(b) Useful heat gain to the working fluid

For liquid water, the enthalpy difference is approximated by Equation (4):

$$h_{out} - h_{in} = c_p(T_{out} - T_{in}) \quad (4)$$

ARTICLE IN PRESS

where c_p is the specific heat capacity of the working fluid at constant pressure ($J\ kg^{-1}K^{-1}$), and T_{in} and T_{out} are the inlet and outlet fluid temperatures, respectively (K).
Accordingly, the useful thermal gain of the collector becomes(Equation (5)):

$$\dot{Q}_u = \dot{m} c_p (T_{out} - T_{in}) \quad (5)$$

(c) Solar energy partition in the PVT collector
The absorbed solar power by the collector is defined by Equation (6)

$$\dot{Q}_{abs} = (\tau\alpha) A_c G \quad (6)$$

where τ is the effective transmittance of the cover, α is the effective absorptance of the absorber-PV surface, A_c is the collector aperture area (m^2), and G is the global solar irradiance incident on the collector plane (Wm^{-2}). The product $(\tau\alpha)$ represents the overall optical efficiency of the collector.
The absorbed energy is partitioned into electrical output, useful thermal gain, and thermal losses to the ambient (Equation (7)):

$$\dot{Q}_{abs} = P_{el} + \dot{Q}_u + \dot{Q}_{loss} \quad (7)$$

where $\dot{Q}_{abs}$ is the absorbed solar power (W), P_{el} is the electrical power output of the PV module (W), $\dot{Q}_u$ is the useful thermal power transferred to the working fluid (W), and $\dot{Q}_{loss}$ is the total thermal loss to the surroundings (W).

The lumped thermal loss term is modeled as (Equation (8)):

$$\dot{Q}_{loss} = U_L A_c (T_{pvt} - T_{amb}) \quad (8)$$

where T_{pvt} represents a characteristic collector temperature (e.g., PV cell or absorber mean temperature, depending on the implemented resistance network) and U_L is the overall heat loss coefficient of the collector ($Wm^{-2}K^{-1}$). The overall heat loss coefficient U_L accounts for the combined effects of convective, radiative, and conductive heat losses from the collector to the environment.

(d) Storage tank energy balance (well-mixed)
The tank is modeled as a well-mixed thermal capacitance with uniform temperature $T_{tank}(t)$. The transient tank energy balance is (Equation (9)):

$$m_t c_p \frac{dT_{tank}}{dt} = \dot{m} c_p (T_{out} - T_{tank}) - U_t A_t (T_{tank} - T_{amb}) \quad (9)$$

where $m_t = \rho V_t$ and ρ and c_p are evaluated at the mean tank temperature.

3.1.2 Mass and Momentum

(a) Mass conservation
Since the system operates in a closed loop with incompressible water, the mass flow rate is constant along the loop (Equation (10)):

$$\dot{m}_{in} = \dot{m}_{out} = \dot{m} \quad (10)$$

(b) Pressure drop model

ARTICLE IN PRESS

Pressure losses in the collector tubes (and optionally pipes) are modeled to enable frictional entropy generation terms later in the second-law analysis. The Darcy–Weisbach equation is applied (Equation (11)). This equation is widely used due to its broad applicability in pressurized pipe flow and forms a basis for calculating head loss in engineering systems (De Almeida Minhoni et al., 2020; Abdulameer et al., 2022).

$$\Delta P = f\frac{L}{D_h}\frac{\rho v^2}{2} + \sum K\frac{\rho v^2}{2} \tag{11}$$

where f is the friction factor, L is the flow length, D_h is the hydraulic diameter, v is the mean velocity, and K represents minor loss coefficients. Experimental studies confirm that Darcy–Weisbach accurately predicts head loss in various pipe materials and flow regimes, including turbulent flows in small-diameter pipes common in irrigation systems (Lima et al., 2025; Ciprian, 2019).

The mean velocity is expressed as (Equation (12)):

$$v = \frac{\dot{m}}{\rho A_f} \tag{12}$$

with A_f being the flow cross-sectional area.

For laminar flow ($Re < 2300$):

$$f = \frac{64}{Re} \tag{13}$$

For turbulent flow, f may be computed using a standard explicit correlation (e.g., Blasius for smooth tubes) for appropriate Reynolds number ranges (Equation (14)):

$$f = 0.3164\, Re^{-0.25} \tag{14}$$

The Reynolds number is (Equation (15)):

$$Re = \frac{\rho v D_h}{\mu} \tag{15}$$

The pressure drop formulation in Equations (11) – (15) is used in Section 3.4 to quantify frictional irreversibility through entropy generation and exergy destruction.

ARTICLE IN PRESS

3.1.3 Boundary Conditions

The model requires time-dependent environmental inputs and specified operating conditions.

(a) Meteorological boundary conditions

At each simulation time step (Equation (16)):

$$G = G(t),\ T_{amb} = T_{amb}(t) \tag{16}$$

If wind speed is used to evaluate convective losses (Equation (17)):

$$v_w = v_w(t) \tag{17}$$

(b) Hydraulic boundary conditions

The mass flow rate is specified (constant or time-dependent) (Equation (18)):

$$\dot{m} = \dot{m}(t) \tag{18}$$

(c) Thermal coupling condition (tank–collector)

For the closed-loop well-mixed tank configuration in Figure 2, the collector inlet temperature equals the tank temperature (Equation (18)):

ARTICLE IN PRESS

$$T_{in}(t) = T_{tank}(t) \tag{19}$$

(d) Initial condition for transient simulation
For simulations including the tank transient (Equation (20)):

$$T_{tank}(t = 0) = T_{tank,0} \tag{20}$$

Equations (2) – (20) define the conservation-law foundation of the model. In the next subsection, the electrical behavior of the PV layer is introduced and coupled to the thermal model through the temperature-dependent electrical efficiency relation.

3.2 PV Electrical Model

The electrical behavior of the photovoltaic layer is strongly dependent on the cell operating temperature, which is governed by the thermal balance of the PVT collector described in Section 3.1. In this study, the PV electrical model is therefore fully coupled to the thermal model through the PV cell temperature T_{pv}, as indicated schematically in Figure 2.

3.2.1 PV Temperature Model

The PV cell temperature is not an independent variable but results from the heat transfer processes within the PVT collector. It is determined from the collector thermal balance through the thermal resistance network between the PV cells, absorber, working fluid, and ambient environment.
In lumped-parameter form, the energy balance on the PV layer can be expressed as (Equation (21)):

$$(\tau\alpha)A_c G = P_{el} + \dot{Q}_{pv\to f} + \dot{Q}_{pv\to amb} \tag{21}$$

Where $\dot{Q}_{pv\to f}$ is the heat transferred from the PV layer to the absorber/fluid and $\dot{Q}_{pv\to amb}$ is the heat lost from the PV layer to the ambient.
Using a thermal resistance representation, these heat transfer terms are written as (Equation (22)):

$$\dot{Q}_{pv\to f} = \frac{T_{pv} - T_f}{R_{pv-f}} \tag{22}$$

And (Equation (23))

$$\dot{Q}_{pv\to amb} = \frac{T_{pv} - T_{amb}}{R_{pv-amb}} \tag{23}$$

where T_f is a representative mean fluid temperature (e.g., $T_f \approx (T_{in} + T_{out})/2$), and R_{pv-f} and R_{pv-amb} are equivalent thermal resistances, constructed from the material layers and convection/radiation coefficients.
Substituting Equations (22) and (23) into Equation (21) yields Equation (24):

ARTICLE IN PRESS

$$(\tau\alpha)A_cG = P_{el} + \frac{T_{pv} - T_f}{R_{pv-f}} + \frac{T_{pv} - T_{amb}}{R_{pv-amb}} \quad (24)$$

Equation (24) is solved simultaneously with the collector energy equations (Section 3.1) to obtain the PV cell temperature T_{pv} at each time step.
For numerical implementation, the mean fluid temperature is approximated as:

$$T_f = \frac{T_{in} + T_{out}}{2} \quad (25)$$

3.2.2 Electrical Power and Efficiency Relations

The electrical efficiency of the PV module decreases approximately linearly with increasing cell temperature. This effect is modeled using the standard temperature-corrected efficiency relation (Equation (26)):

$$\eta_{el}(T_{pv}) = \eta_{ref}[1-\beta(T_{pv}-T_{ref})] \quad (26)$$

Where η_{ref} is the reference efficiency at temperature T_{ref} (usually 298.15 K) and β is the temperature coefficient of the PV module.
The instantaneous electrical power output of the PVT collector is then given by (Equation (27)):

$$P_{el} = \eta_{el}(T_{pv})A_cG \quad (27)$$

Substituting Equation (26) into Equation (27) yields Equation (28)

$$P_{el} = \eta_{ref}[1-\beta(T_{pv}-T_{ref})]A_cG \quad (28)$$

Equations (26) – (28) establish the direct coupling between the thermal and electrical performances of the PVT collector: any reduction in T_{pv} achieved through enhanced heat extraction by the working fluid (Equation. (5)) leads to an increase in electrical efficiency and power output.
The electrical model given by Equations (21) – (28) is fully coupled to the thermal balances presented in Section 3.1 through the PV cell temperature T_{pv}. In the next subsection, the detailed heat transfer mechanisms within the PVT collector and the associated loss terms are formulated.

3.3 Heat Transfer Sub-Models

The thermal behavior of the PVT collector is governed by a combination of optical absorption, conduction through solid layers, convection to the ambient air, radiation exchange with the surroundings, and convection to the circulating working fluid. These mechanisms are represented using a lumped thermal resistance network consistent with the schematic shown in Figure 2 and the energy balances formulated in Sections 3.1 and 3.2.
In the present study, the heat transfer relations are introduced primarily to establish the coupled thermal interactions governing PV temperature regulation, useful heat extraction, and entropy generation within the PVT collector. Accordingly, emphasis is placed on the thermodynamic implications of these mechanisms rather than on detailed derivational treatment of standard heat transfer correlations.

ARTICLE IN PRESS

3.3.1 Solar Absorption and Optical Losses

The solar radiation incident on the collector surface is partially transmitted through the glass cover and absorbed by the PV cells and the absorber. The effective absorbed solar power is expressed as (Equation (29)):

$$\dot{Q}_{abs} = (\tau\alpha)_{eff} A_c G \tag{29}$$

where $(\tau\alpha)_{eff}$ is the effective transmittance–absorptance product of the glass–PV–absorber assembly.

The optical losses are therefore (Equation (30)):

$$\dot{Q}_{opt,loss} = A_c G\left[1 - (\tau\alpha)_{eff}\right] \tag{30}$$

Only the absorbed part given by Equation (29) contributes to electrical generation and thermal heating in the PVT collector, as already used in Equation (6).

3.3.2 Convection to the Ambient (Wind Correlation)

Convective heat loss from the top surface of the PVT collector to the ambient air is modeled as (Equation (31)):

$$\dot{Q}_{conv,amb} = h_{c,amb} A_c \left(T_{pvt} - T_{amb}\right) \tag{31}$$

The convective heat transfer coefficient is correlated to wind speed using a widely adopted empirical relation (Equation (32)):

$$h_{c,amb} = 5.7 + 3.8\, v_w \tag{32}$$

where v_w is the wind speed in m/s and $h_{c,amb}$ is in W/m²·K.

3.3.3 Radiation Losses

Radiative heat exchange between the PVT surface (or glass cover) and the sky is expressed as (Equation (33)):

$$\dot{Q}_{rad,amb} = \varepsilon_{eff} \sigma A_c \left(T_{pvt}^4 - T_{sky}^4\right) \tag{33}$$

Where ε_{eff} is the effective emissivity of the top surface and σ is the Stefan–Boltzmann constant. This formulation captures long-wave radiative cooling effects that can significantly influence PVT system performance, especially at night or under clear-sky conditions (Eicker & Dalibard, 2011; Zhao et al., 2020). Radiative cooling also plays a role in reducing building energy consumption when integrated into ventilated PVT roofs or ground-coupled heat exchangers, improving thermal efficiency through passive heat rejection to the sky (Shao et al., 2022; Jia et al., 2022). Thus, radiative heat exchange with the sky is a critical factor in optimizing PVT system thermal management and enhancing renewable energy utilization (Hu et al., 2022).

The effective sky temperature is approximated by (Equation (34)):

ARTICLE IN PRESS

$$T_{sky} = 0.0552\, T_{amb}^{1.5} \tag{34}$$

with all temperatures in Kelvin.

3.3.4 Convection to the Fluid (Internal Heat Transfer Coefficient)

The heat transferred from the absorber to the working fluid is modeled as (Equation (35)):

$$\dot{Q}_f = h_f A_f \left(T_{abs} - T_f\right) \tag{35}$$

Where h_f is the internal convective heat transfer coefficient, A_f is the effective heat transfer area, T_{abs} is the absorber temperature and T_f is the mean fluid temperature given by Equation (25). The internal convective heat transfer coefficient is evaluated using standard dimensionless heat transfer correlations based on Reynolds, Prandtl, and Nusselt numbers for laminar and turbulent internal flow conditions (David et al., 2021; Van Zyl et al., 2013):

$$h_f = \frac{Nu\, k_f}{D_h} \tag{36}$$

where Nu is the Nusselt number and D_h is the hydraulic diameter of the flow channel (m).
The Reynolds number is (Saldaña et al., 2024; Tamburrino & Niño, 2025; Abimanyu et al., 2025):

$$Re = \frac{\rho v D_h}{\mu} \tag{37}$$

where μ is the dynamic viscosity of the working fluid (Pas).
For laminar flow ($Re < 2300$):

$$Nu = 4.36 \tag{38}$$

For turbulent flow ($Re > 3000$) (Dittus–Boelter correlation):

$$Nu = 0.023 Re^{0.8} Pr^{0.4} \tag{39}$$

where the Prandtl number is:

$$Pr = \frac{c_p \mu}{k_f} \tag{40}$$

3.3.5 Overall Heat Loss Coefficient

The total heat loss from the collector to the ambient is the sum of convective and radiative losses (Equation (41))::

$$\dot{Q}_{loss} = \dot{Q}_{conv,amb} + \dot{Q}_{rad,amb} \tag{41}$$

This total loss is represented in lumped form by (Equation (42)):

$$\dot{Q}_{loss} = U_L A_c \left(T_{pvt} - T_{amb}\right) \tag{42}$$

ARTICLE IN PRESS

Thus, the overall heat loss coefficient is (Equation (43)):

$$U_L = h_{c,amb} + h_{r,amb} \tag{43}$$

where the equivalent radiative heat transfer coefficient is (Equation (44)):

$$h_{r,amb} = \varepsilon_{eff}\sigma\left(T_{pvt} + T_{sky}\right)\left(T_{pvt}^2 + T_{sky}^2\right) \tag{44}$$

3.3.6 Thermal resistance network formulation

The conduction and convection processes between the PV layer, absorber, fluid, and ambient are represented by an equivalent thermal resistance network. The dominant resistances include (Equation (45)):

$$R_{pv-f} = R_{cond,layers} + \frac{1}{h_f A_f} \tag{45}$$

And (Equation (46)):

$$R_{pv-amb} = \frac{1}{(h_{c,amb} + h_{r,amb})A_c} \tag{46}$$

These resistances are used directly in the PV temperature equation (Equation (24)) and in the global energy balance relations in Section 3.1.

The heat transfer sub-models defined by Equations (29) – (46) close the thermal description of the PVT collector and provide the temperature fields required for the electrical model (Section 3.2) and the second-law analysis developed in the next section.

ARTICLE IN PRESS

3.4 Entropy Generation and Tds-Based Thermodynamic Formulation

The second-law analysis of the PVT system is developed using the fundamental Gibbs relations, also known as the Tds equations. These relations provide the link between entropy variations and changes in internal energy, enthalpy, pressure, and temperature, and form the theoretical basis for the rigorous quantification of irreversibilities in the system components shown in Figure 2.

Unlike conventional PVT analyses that treat entropy generation using simplified global exergy balances, the present formulation directly employs the Gibbs Tds relations to resolve subsystem-level irreversible processes associated with coupled thermal transport, ambient heat rejection, and fluid-flow dissipation. This enables a more physically diagnostic interpretation of thermodynamic losses within the PVT system.

3.4.1 Tds Equations (Gibbs Relations)

For a simple compressible system, the fundamental thermodynamic relations are written as (Equation (47)):

$$T\,dS = dU + P\,dV \tag{47}$$

where T is the absolute temperature (K), S is the entropy (JK^{-1}), U is the internal energy (J), P is the pressure (Pa), and V is the volume (m^3). This form is especially convenient when ($U = U(S,V$)) and underpins entropy balances and entropy generation expressions in second-law analysis of closed or simple PVT systems (Moran et al., 2010; Bejan, 2013).

ARTICLE IN PRESS

And (Equation (48)):

$$T\,dS = dH - V\,dP \tag{48}$$

where H is the enthalpy (J), suitable when ($H = H(S,P)$), as in many flow and control-volume applications (Moran et al., 2010, 2014; Bejan, 2013), while all other symbols have their usual thermodynamic meanings. The Tds underpin entropy balance, entropy generation, and exergy analysis, and are treated as central tools for second-law and optimization-based design in both Moran et al. (2010) and Bejan's (2013) thermodynamics frameworks.

Equations (47) and (48) are equivalent forms of the Gibbs fundamental relation and are used in this work to derive the entropy balance and entropy generation terms for the solid and fluid control volumes.

For an incompressible liquid such as water, the differential entropy change can be approximated as (Equation (49)):

$$ds = c_p \frac{dT}{T} \tag{49}$$

which is consistent with the enthalpy relation $dh = c_p dT$ and is used in the subsequent formulations for the working fluid.

3.4.2 Entropy Balance for System Components

The general entropy balance for a control volume is in Equation (50) (Çengel & Boles, 2002; Nasrin et al., 2016; Malekan et al., 2019; Mwesigye et al., 2018; Krishna et al., 2020; Kalateh et al., 2022; Al-Najjar et al., 2024; Rao et al., 2024):

$$\frac{dS_{cv}}{dt} = \sum \dot{m}_{in} s_{in} - \sum \dot{m}_{out} s_{out} + \sum_k \frac{\dot{Q}_k}{T_k} + \dot{S}_{gen} \tag{50}$$

where S_{cv} is the total entropy within the control volume ($J\,K^{-1}$), s is specific entropy ($Jkg^{-1}\,K^{-1}$), T_k is the boundary temperature at which heat transfer $\dot{Q}_k$ occurs (K), and $\dot{S}_{gen}$ is the entropy generation rate due to irreversibilities (WK^{-1}).

Under quasi-steady conditions for the PVT collector control volume, Equation (51) reduces to:

$$\dot{S}_{gen,cv} = \dot{m}(s_{out} - s_{in}) - \sum_k \frac{\dot{Q}_k}{T_k} \tag{51}$$

(a) Fluid control volume (inside collector tubes)

For the working fluid flowing through the collector (Equation (52)):

$$\dot{S}_{gen,f} = \dot{m}(s_{out} - s_{in}) - \frac{\dot{Q}_u}{T_b} \tag{52}$$

where T_b is a representative boundary temperature at which heat is transferred from the solid to the fluid (e.g., absorber mean temperature).

ARTICLE IN PRESS

Using Equation (49), the entropy change of the fluid becomes:

$$s_{out} - s_{in} = c_p \ln\left(\frac{T_{out}}{T_{in}}\right) \tag{53}$$

Substituting Equation (53) into Equation (52) yields Equation (54),

$$\dot{S}_{gen,f} = \dot{m}\, c_p \ln\left(\frac{T_{out}}{T_{in}}\right) - \frac{\dot{Q}_u}{T_b} \tag{54}$$

(b) Solid control volume (PV + absorber assembly)
For the solid part of the PVT collector, operating under steady conditions (Equation (55)):

$$\dot{S}_{gen,s} = \frac{\dot{Q}_{abs}}{T_{sun}} - \frac{\dot{Q}_{pv\to f}}{T_b} - \frac{\dot{Q}_{loss}}{T_{amb}} \tag{55}$$

where T_{sun} is the effective blackbody temperature of the sun and the terms represent entropy inflow with radiation, entropy outflow to the fluid, and entropy rejected to the ambient, respectively.

3.4.3 Sources of Entropy Generation

In the present system, entropy generation arises from three main physical mechanisms:

(a) Heat transfer across finite temperature differences
This contribution is inherently captured in Equations (54) and (55). In compact form, the contribution associated with finite-temperature heat transfer within the PVT collector can be expressed as (Çengel & Boles, 2002; Nasrin et al., 2016; Malekan et al., 2019; Mwesigye et al., 2018; Krishna et al., 2020; Wang et al., 2024; Satpute et al., 2025) in Equation (56)

$$\dot{S}_{\Delta T} = \dot{m}\, c_p \ln\left(\frac{T_{out}}{T_{in}}\right) - \frac{\dot{Q}_u}{T_b} + \frac{\dot{Q}_{loss}}{T_{amb}} - \frac{\dot{Q}_{abs}}{T_{sun}} \tag{56}$$

This expression explicitly accounts for entropy changes associated with sensible heating of the working fluid, useful heat transfer at the absorber–fluid interface, thermal losses to the ambient, and the exergy content of the absorbed solar radiation, thereby providing a direct second-law measure of thermal irreversibility within the collector.

(b) Viscous friction (pressure drop in tubes)
Using the second Gibbs relation (Equation (48)) for the flowing liquid, the entropy generation associated with pressure drop is approximated by (Equation (57)):

$$\dot{S}_{fr} = \frac{\dot{m}}{\rho}\frac{\Delta P}{T_f} \tag{57}$$

where ΔP is given by Equation (11) and T_f is the mean fluid temperature.

ARTICLE IN PRESS

(c) Thermal losses to the ambient

The entropy generation associated with heat rejection to the ambient is (Equation (58)):

$$\dot{S}_{loss} = \dot{Q}_{loss}\left(\frac{1}{T_{amb}} - \frac{1}{T_{pvt}}\right) \tag{58}$$

3.4.4 Total Entropy Generation Rate (System Level)

The total entropy generation rate of the PVT system is obtained by summing all contributions (Bejan, 2013; Kalateh et al., 2022):

$$\dot{S}_{gen,tot} = \dot{S}_{\Delta T} + \dot{S}_{fr} \tag{59}$$

where $\dot{S}_{\Delta T}$ is the entropy generation rate due to heat transfer across finite temperature differences, and $\dot{S}_{fr}$ is the entropy generation rate due to fluid friction (viscous dissipation). This expression separates thermal irreversibility from hydraulic irreversibility within the PVT system (Equation (60)).

or, equivalently, by summing the component-wise terms:

$$\dot{S}_{gen,tot} = \dot{S}_{gen,f} + \dot{S}_{gen,s} + \dot{S}_{fr} \tag{60}$$

Equations (59) and (60) provide the basis for identifying the dominant irreversibility mechanisms in the system and for the subsequent exergy destruction analysis presented in Section 3.5.

Once the total entropy generation rate is known from Equations (59) – (60), the corresponding exergy destruction can be evaluated using the Gouy–Stodola theorem, as formulated in the next section.

Unlike conventional first-law-based PVT analyses that primarily quantify energy quantities, the present formulation enables direct identification of the dominant irreversibility mechanisms governing thermodynamic performance degradation. This provides a physically meaningful basis for interpreting how thermal coupling, ambient heat rejection, and fluid transport processes influence overall system optimization under tropical operating conditions.

3.5 Exergy Analysis

The exergy analysis provides a second-law measure of the quality of energy flows and quantifies the thermodynamic losses associated with irreversibilities. In this study, the exergy framework is built directly upon the entropy generation model developed in Section 3.4 and the energy balances presented in Sections 3.1–3.3.

The exergy framework is employed not merely to quantify energy conversion performance, but to evaluate the thermodynamic quality of the recovered electrical and thermal energy streams and to identify the irreversible losses limiting useful energy utilization within the PVT system.

All exergy quantities are evaluated relative to the reference (dead) state defined by the ambient conditions (Equation (61)):

$$T_0 = T_{amb},\ P_0 = P_{amb} \tag{61}$$

3.5.1 Flow Exergy of the Working Fluid

ARTICLE IN PRESS

The specific flow exergy of a stream is defined as (Moran et al., 2010, 2014; Bejan, 2013; Kalateh et al., 2022):

$$ex = (h - h_0) - T_0(s - s_0) \tag{62}$$

where ex is the specific flow exergy (Jkg^{-1}), the subscript 0 denotes properties evaluated at the environmental (dead-state) conditions, and T_0 is the ambient reference temperature (K). This expression represents the maximum useful work obtainable as the fluid is brought reversibly to the environmental state.
Accordingly, the exergy rate associated with the working fluid flowing through the PVT collector is (Bejan, 2013; Kalateh et al., 2022):

$$\dot{E}x_f = \dot{m}[(h_{out} - h_{in}) - T_0(s_{out} - s_{in})] \tag{63}$$

where $\dot{E}_{x,f}$ is the rate of flow exergy gain of the working fluid (W).
For liquid water with constant properties, using (Çengel & Boles, 2002; Moran et al., 2010):

$$h_{out} - h_{in} = c_p(T_{out} - T_{in}) \tag{64}$$

This approximation is valid for incompressible liquids over the investigated temperature range, for which variations of c_p are negligible (Moran et al., 2010, Bejan, 2013).

$$s_{out} - s_{in} = c_p \ln\left(\frac{T_{out}}{T_{in}}\right) \tag{65}$$

Equation (63) becomes:

$$\dot{E}x_{th} = \dot{m}c_p\left[(T_{out} - T_{in}) - T_0 \ln\left(\frac{T_{out}}{T_{in}}\right)\right] \tag{66}$$

Equation (66) represents the useful thermal exergy gain of the working fluid.

3.5.2 Solar Radiation Exergy Input

The exergy associated with the incident solar radiation is evaluated using the Petela–Landsberg exergy of solar radiation formulation (Bejan, 2016; Çengel & Boles, 2019; Duffie & Beckman, 2013):

$$\dot{E}x_{solar} = A_c G\left[1 - \frac{4}{3}\left(\frac{T_0}{T_{sun}}\right) + \frac{1}{3}\left(\frac{T_0}{T_{sun}}\right)^4\right] \tag{67}$$

where T_{sun} is the effective temperature of the sun, taken as $T_{sun} = 5777$ K and $T_0 = 298\ K$

3.5.3 Exergy Destruction (Gouy–Stodola Theorem)

ARTICLE IN PRESS

The exergy destruction rate associated with irreversibilities in the system is directly related to the total entropy generation rate obtained in Section 3.4, it is given by Equation (68) by Gouy–Stodola theorem as in (Bejan, 2002; Kotas, 2012; Pal, 2017, Pal, 2018; Pal, 2019).

$$\dot{E}x_{dest} = T_0 \, \dot{S}_{gen,tot} \tag{68}$$

where $\dot{S}_{gen,tot}$ is given by Equations (59) – (60).
Equation (68) provides the quantitative measure of lost work potential due to heat transfer across finite temperature differences, thermal losses, and viscous friction in the PVT system.

3.5.4 Exergy Efficiency Definitions

(a) Electrical exergy output

Since electrical power is a fully convertible (high-grade) form of energy, its exergy is equal to the electrical power itself:

$$\dot{E}x_{el} = P_{el} \tag{69}$$

where $\dot{E}_{x,el}$ is the exergy rate associated with the electrical output (W).

(b) Thermal exergy efficiency

The thermal exergy efficiency is defined as the ratio of useful thermal exergy gain of the fluid to the solar exergy input (Equation (70)):

$$\eta_{ex,th} = \frac{\dot{E}x_{th}}{\dot{E}x_{solar}} \tag{70}$$

where $\dot{E}x_{th}$ is given by Equation (66).

(c) Electrical exergy efficiency

The electrical exergy efficiency is defined as (Equation (71)):

$$\eta_{ex,el} = \frac{P_{el}}{\dot{E}x_{solar}} \tag{71}$$

where $\eta_{ex,el}$ is the electrical exergy efficiency.

(d) Overall exergy efficiency

The overall exergy efficiency of the PVT system is defined as (Equation (72)):

$$\eta_{ex,tot} = \frac{P_{el} + \dot{E}x_{th}}{\dot{E}x_{solar}} \tag{72}$$

where $\eta_{ex,tot}$ is the total exergy efficiency of the PVT system. This definition accounts simultaneously for the useful electrical and thermal exergy outputs relative to the exergy content of the incident solar radiation.

ARTICLE IN PRESS

Consistency relation
From the exergy balance of the system (Equation (73)):

$$\dot{E}x_{solar} = P_{el} + \dot{E}x_{th} + \dot{E}x_{dest} \tag{73}$$

which provides a useful check on numerical accuracy and thermodynamic consistency.

Table 2. Summary of governing thermodynamic relations and their primary outputs used in the numerical model.

Category	Equation No.	Relation	Primary Output
Useful heat gain	(5)	$\dot{Q}_u = \dot{m}c_p(T_{out} - T_{in})$	Thermal power
PV temperature	(24)	Energy balance on PV layer	T_{pv}
Electrical power	(28)	$P_{el} = \eta_{ref}[1 - \beta(T_{pv} - T_{ref})]A_c G$	Electrical power
Tank temperature	(9)	Tank energy balance	$T_{tank}(t)$
Fluid entropy change	(53)	$s_{out} - s_{in} = c_p \ln(T_{out}/T_{in})$	Entropy rise
Fluid entropy generation	(54)	Entropy balance (fluid CV)	$\dot{S}_{gen,f}$
Friction entropy	(57)	$\dot{S}_{fr} = \dot{m}\Delta P/(\rho T_f)$	Friction irreversibility
Total entropy gen.	(60)	Sum of contributions	$\dot{S}_{gen,tot}$
Thermal exergy gain	(66)	Flow exergy rise	$\dot{E}x_{th}$
Solar exergy input	(67)	Petela equation	$\dot{E}x_{solar}$
Exergy destruction	(68)	$T_0 \dot{S}_{gen,tot}$	$\dot{E}x_{dest}$
Overall exergy efficiency	(72)	$(P_{el} + \dot{E}x_{th})/\dot{E}x_{solar}$	$\eta_{ex,tot}$

ARTICLE IN PRESS

With the formulations presented in Sections 3.1–3.5, the complete coupled energy–entropy–exergy model of the PVT system is fully defined. The next section describes the numerical solution procedure used to solve the governing equations and perform the parametric simulations

4.0 Numerical Simulation Procedure

The coupled thermal–electrical and thermodynamic equations developed in the present study were solved numerically under transient operating conditions using time-dependent meteorological inputs representative of Kampala, Uganda. At each simulation time step, the collector energy balances, PV electrical performance relations, storage tank energy equation, entropy generation expressions, and exergy balance equations were solved sequentially to obtain the instantaneous thermodynamic state of the system. The collector inlet temperature was continuously updated from the well-mixed storage tank temperature, thereby maintaining dynamic thermal coupling between the collector and storage subsystems throughout the simulation period. The numerical implementation was used to evaluate temperature evolution, useful thermal energy recovery, electrical output, entropy generation, exergy destruction, and overall thermodynamic performance under varying operating conditions.

ARTICLE IN PRESS

Thermophysical properties, operating parameters, and environmental boundary conditions employed in the simulations were obtained from standard literature correlations, established photovoltaic–thermal modeling practices, and representative meteorological conditions for Kampala, Uganda. The developed numerical framework was subsequently used to evaluate collector temperatures, electrical efficiency, useful thermal energy recovery, entropy generation, and exergy destruction throughout the analysis.

The coupled energy–entropy–exergy model (Sections 3.1–3.5) is solved numerically to obtain transient and steady-state performance metrics of the closed-loop, water-cooled PVT system with well-mixed storage tank shown in Figure 2. This section details the solution strategy, algorithm, inputs, convergence criteria, and validation plan.

4.1 Solution Approach

The model is implemented in a time-marching framework using a lumped parameter solver that advances the tank temperature in time while solving the collector thermal–electrical balance quasi-steadily at each time step.

At each time step t_n:

1. Read meteorological inputs $G(t_n)$,$T_{amb}(t_n)$,$v_w(t_n)$ (Equations 16–17).
2. Solve the thermal–electrical balance (Equations 5, 24, 28) to update T_{pv},T_{out}, and P_{el}.
3. Update entropy generation terms (Equations 54, 57–60).
4. Evaluate exergy flows (Equations 66, 67, 68).
5. Integrate the storage tank energy balance (Equation 9) to find $T_{tank}(t_{n+1})$.

This transient time-marching approach captures dynamic behavior while maintaining computational efficiency because the PVT collector itself is treated as quasi–steady state relative to the slower tank dynamics. Similar lumped-parameter transient approaches are widely adopted in PVT simulation studies due to acceptable accuracy and reduced computational cost compared to full CFD/2-D models.

4.2 Algorithm and Flowchart

The numerical procedure follows an iterative solution within each time step until convergence of key state variables:

Algorithm 4.1 (per time step)

1. Initialize: Set $T_{tank}(t_0) = T_{tank,0}$ (Equation 20).
2. Loop over time: for $t_n = t_0$ to t_{end} with Δt:
   2.1 Assign boundary conditions $G(t_n)$,$T_{amb}(t_n)$,$v_w(t_n)$.
   2.2 Set $T_{in} = T_{tank}(t_n)$ (Equation 19).
   2.3 Guess initial T_{pv} and T_{out}.
   2.4 Inner iteration:
      a. Solve thermal network (Equation 24) for T_{pv}.
      b. Update electrical output P_{el} (Equation 28).
      c. Solve fluid energy balance for T_{out} (Equation 5).
      d. Check inner convergence: $\left|T_{pv}^{k+1} - T_{pv}^{k}\right| < \epsilon_T$, $|T_{out}^{k+1} - T_{out}^{k}| < \epsilon_T$.
   2.5 Compute entropy generation $\dot{S}_{gen,tot}$ (Equation 59–60) and exergy terms (Equations 66 – 68).
   2.6 Advance tank temperature using tank ODE (Equation 9).
   2.7 Store results.

ARTICLE IN PRESS

Convergence criteria for inner iteration are typically set to $\epsilon_T = 10^{-4}$ K and energy balance residuals < 1 W.

4.3 Model Inputs and Datasets

The transient simulation is driven by time-resolved meteorological boundary conditions and a fixed set of system parameters. The required environmental inputs are global solar irradiance $G(t)$, ambient temperature $T_{amb}(t)$, and wind speed $v_w(t)$, while all geometric, thermal, and electrical properties of the collector and storage system are prescribed from the baseline configuration in Table 1.

A Typical Meteorological Year (TMY) dataset representative of the Kampala region is used to impose realistic tropical boundary conditions, obtained from standard satellite-based reanalysis or regional meteorological sources. All optical, thermal, and electrical properties, as well as tank and fluid parameters, are treated as fixed inputs. Owing to the one-dimensional lumped-parameter formulation, no spatial discretization is required, resulting in a computationally efficient framework consistent with most transient PVT models in the literature.

The numerical simulation was conducted over a representative diurnal operating period extracted from the Kampala TMY dataset. Therefore, the "test duration" in the present study refers to the simulated daily operating period rather than an experimental measurement campaign. Time-resolved meteorological inputs, including solar irradiance, ambient temperature, and wind speed, were applied at each simulation time step. Time-step independence was assessed using 3600 s, 1800 s, and 900 s intervals, and a 900 s time step was adopted for the final simulations because it provided stable results with acceptable computational efficiency.

4.4 Numerical Convergence and Independence Tests

Because the model is lumped-parameter, mesh independence is not applicable. Numerical robustness is ensured through time-step independence testing and strict convergence of the inner iterative solution of the coupled collector equations.

Time-step independence is verified by repeating simulations with decreasing time steps until the predicted tank temperature, electrical power, useful thermal output, and exergy efficiency change by less than 1%. Time steps of 3600 s, 1800 s, and 900 s were tested, and 900 s was adopted as a compromise between accuracy and computational cost.

At each time step, the nonlinear algebraic equations governing the thermal coupling between the PV layer, absorber, and working fluid are solved iteratively. Convergence is declared when

$$\left|T_{pv}^{k+1} - T_{pv}^{k}\right| < \varepsilon_T,\ \left|T_{out}^{k+1} - T_{out}^{k}\right| < \varepsilon_T \tag{73.1}$$

with ε_T in the range $10^{-4} - 10^{-3}\ K$.

4.5 Model Verification and Validation

Model credibility is established through internal verification and literature-based validation. Verification is ensured by strict adherence to energy, entropy, and exergy balance relations, with closure confirmed between absorbed solar energy, electrical output, useful thermal gain, and losses, and consistency enforced with the Gibbs (Tds) relations and the Gouy–Stodola theorem. Numerical robustness is further supported by the convergence and time-step independence tests described in Section 4.4.

ARTICLE IN PRESS

Validation is conducted through comparison of predicted transient PV temperature, outlet fluid temperature, useful thermal output, and electrical power with reference results reported in the literature for water-cooled PVT systems modeled using lumped-parameter or experimentally calibrated approaches. Agreement within commonly reported error margins, such as RMSE values below approximately 5% for temperatures and thermal outputs, is considered acceptable for system-level assessment. In the absence of experimental data under identical tropical conditions, the model is validated against high-quality numerical results from published PVT energy and exergy studies, which is appropriate for evaluating thermodynamic trends, irreversibility distributions, and optimization behavior.

ARTICLE IN PRESS

ARTICLE IN PRESS

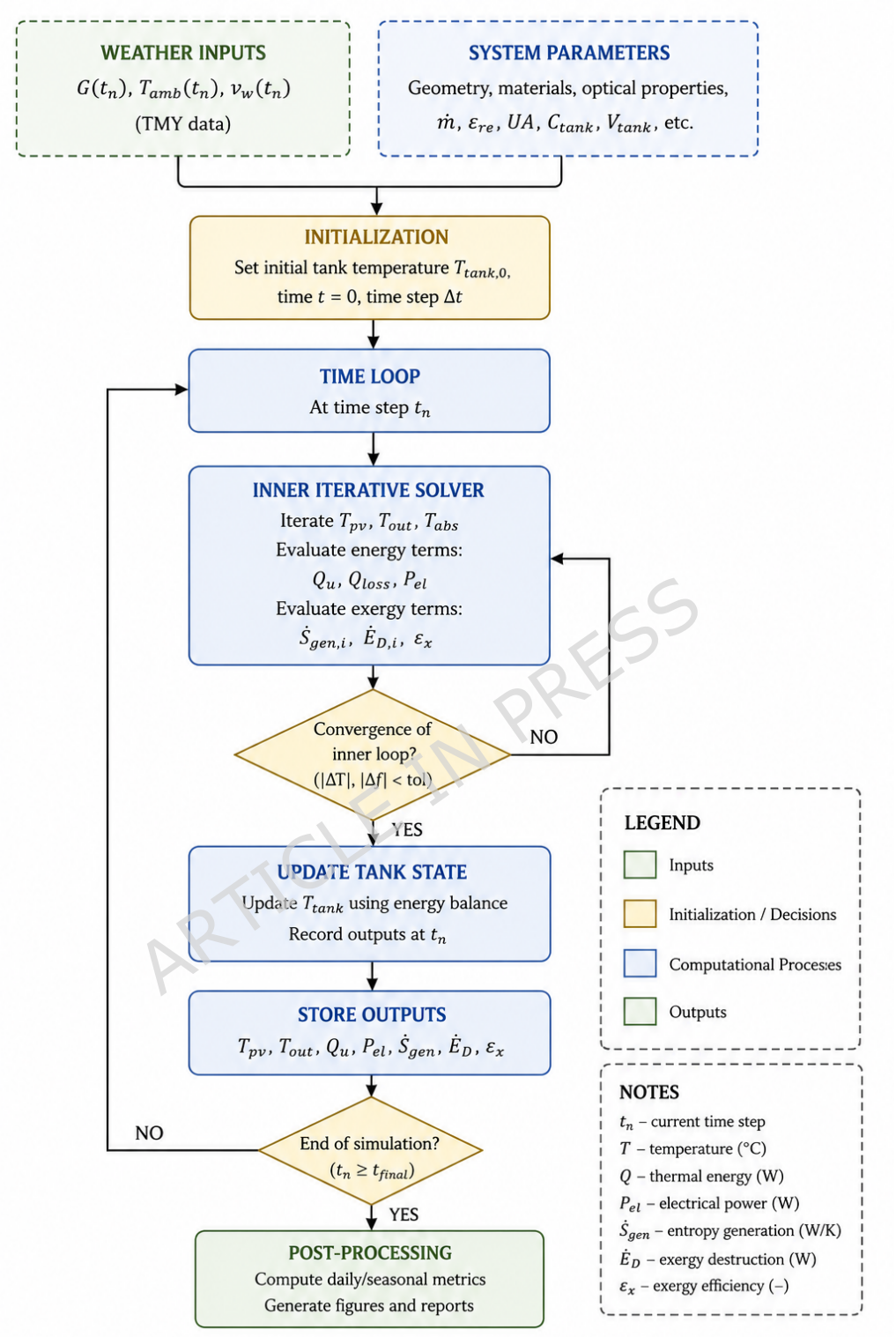

Figure 3 Workflow diagram of the numerical simulation procedure

The workflow (Figure 3) begins with the specification of time-resolved input data, including meteorological variables (G,T_{amb},v_w) and system parameters defined in Table 1. The simulation is initialized by prescribing the initial storage tank temperature $T_{tank,0}$. The solution then advances

ARTICLE IN PRESS

through a time-marching loop, within which an inner iterative solver is employed at each time step to resolve the coupled collector temperatures T_{pv} and T_{out}. Upon convergence, the instantaneous energy and exergy terms are evaluated, followed by a convergence check on the state variables. The storage tank temperature is subsequently updated, and all relevant outputs are recorded before proceeding to the next time step.

4.6 Numerical Uncertainty and Modeling Limitations

The present study is based on a transient numerical thermodynamic framework and therefore does not involve direct experimental measurement uncertainty associated with sensors or instrumentation. Nevertheless, several sources of modeling uncertainty may influence the obtained results. These include assumptions associated with thermophysical property correlations, convective heat-transfer coefficients, meteorological boundary conditions, uniform flow distribution within the absorber tubes, neglect of localized thermal contact resistances, and the use of a well-mixed storage-tank approximation. In addition, uncertainty may arise from temporal discretization and numerical convergence behavior during transient simulation. To improve robustness, parametric analyses were conducted over a range of operating conditions, including variations in solar irradiance, ambient temperature, and mass flow rate. Accordingly, the presented results should be interpreted within the assumptions and operating conditions adopted in the developed thermodynamic model.

5.0 Performance Indicators and Evaluation Metrics

To evaluate the thermodynamic performance of the PVT system shown in Figure 2, a set of energy- and exergy-based performance indicators is defined. These indicators are derived directly from the energy balances (Section 3.1), the electrical model (Section 3.2), the heat transfer sub-models (Section 3.3), and the entropy–exergy framework (Sections 3.4 and 3.5).

To ensure fair comparison with conventional PV and published PVT systems, all energy, exergy, and efficiency indicators in this study are evaluated with respect to the total solar receiving area of the collector, represented by the aperture area A_c, rather than the PV cell area alone. This normalization is essential because the PVT collector receives solar radiation over the entire collector aperture and simultaneously produces electrical and thermal outputs from the same receiving area.

5.1 Thermal Performance Metrics

(a) Useful thermal power

The useful thermal power transferred to the working fluid is given by Equation (5), repeated here for clarity (Equation (74)):

$$\dot{Q}_u = \dot{m} c_p (T_{out} - T_{in}) \tag{74}$$

(b) Thermal efficiency

The instantaneous thermal efficiency of the PVT collector is defined as the ratio of useful thermal power to the incident solar power (Equation (75)):

$$\eta_{th} = \frac{\dot{Q}_u}{A_c G} \tag{75}$$

ARTICLE IN PRESS

This indicator measures the capability of the system to recover the thermal part of the solar energy.

5.2 Electrical Performance Metrics

(a) Electrical power output

The electrical power output of the PVT collector is computed from Equation (28):

$$P_{el} = \eta_{ref}\left[1 - \beta(T_{pv} - T_{ref})\right]A_c G \tag{76}$$

The area-normalized useful thermal and electrical energy outputs are evaluated as: $E_{th,A} = \frac{E_{th}}{A_c}$ and $E_{el,A} = \frac{E_{el}}{A_c}$, where $E_{th,A}$ and $E_{el,A}$ represent the daily useful thermal and electrical energy outputs per unit solar receiving area, respectively.

(b) Electrical efficiency

The instantaneous electrical efficiency is defined as in Equation (77):

$$\eta_{el} = \frac{P_{el}}{A_c G} \tag{77}$$

This indicator reflects the effect of PV cell temperature on the electrical performance.

5.3 Overall Energy Efficiency

Since the PVT system delivers two useful energy products (electricity and heat), the overall energy efficiency is defined as the sum of thermal and electrical contributions (Equation (78)):

$$\eta_{en} = \frac{P_{el} + \dot{Q}_u}{A_c G} \tag{78}$$

Equivalently (Equation (79)):

$$\eta_{en} = \eta_{el} + \eta_{th} \tag{79}$$

In applications where a weighting factor is needed to reflect different energy values, a generalized form may be used (Equation (80)):

$$\eta_{en,w} = \frac{w_{el}P_{el} + w_{th}\dot{Q}_u}{A_c G} \tag{80}$$

where w_{el} and w_{th} are application-dependent weighting coefficients.

5.4 Exergy Performance Metrics

(a) Thermal exergy rate

From Equation (66):

ARTICLE IN PRESS

$$\dot{E}x_{th} = \dot{m}c_p\left[(T_{out} - T_{in}) - T_0 \ln\left(\frac{T_{out}}{T_{in}}\right)\right] \quad (81)$$

(b) Electrical exergy rate
Since electricity is high-grade energy (Equation (82)):

$$\dot{E}x_{el} = P_{el} \quad (82)$$

(c) Exergy destruction rate
From the Gouy–Stodola theorem (Equation 68):

$$\dot{E}x_{dest} = T_0 \dot{S}_{gen,tot} \quad (83)$$

(d) Exergy efficiencies
Thermal exergy efficiency (Equation (84)):

$$\eta_{ex,th} = \frac{\dot{E}x_{th}}{\dot{E}x_{solar}} \quad (84)$$

Electrical exergy efficiency (Equation (85)):

$$\eta_{ex,el} = \frac{P_{el}}{\dot{E}x_{solar}} \quad (85)$$

Overall exergy efficiency (Equation (86)):

$$\eta_{ex,tot} = \frac{P_{el} + \dot{E}x_{th}}{\dot{E}x_{solar}} \quad (86)$$

ARTICLE IN PRESS

5.5 Thermodynamic Optimization Criteria

The thermodynamic optimization of the PVT system is formulated based on the following competing objectives:

(a) Minimization of entropy generation

$$\min\left(\dot{S}_{gen,tot}\right) \quad (87)$$

or equivalently (Equation (88)):

$$\min\left(\dot{E}x_{dest}\right) \quad (88)$$

(b) Maximization of overall exergy efficiency

$$\max\left(\eta_{ex,tot}\right) \quad (89)$$

ARTICLE IN PRESS

(c) Trade-off criterion

Because increasing mass flow rate or heat extraction may improve electrical efficiency but reduce thermal quality (or vice versa), the optimal operating point is identified from a multi-objective compromise between: maximizing $\eta_{ex,tot}$, minimizing $\dot{S}_{gen,tot}$ and maintaining high η_{en}.
Thus, the optimal operating region is determined from parametric studies rather than a single-variable extremum.

Table 3. Performance indicators used for the thermodynamic evaluation of the PVT system

Indicator	Symbol	Definition	Unit	Physical Meaning
Useful thermal power	$\dot{Q}_u$	Eq. (74)	W	Recovered heat
Thermal efficiency	η_{th}	Eq. (75)	–	Fraction of solar energy converted to heat
Electrical power	P_{el}	Eq. (76)	W	Electrical output
Electrical efficiency	η_{el}	Eq. (77)	–	Fraction of solar energy converted to electricity
Overall energy efficiency	η_{en}	Eq. (78)	–	Total first-law performance
Thermal exergy rate	$\dot{E}x_{th}$	Eq. (81)	W	Useful thermal work potential
Solar exergy input	$\dot{E}x_{solar}$	Eq. (67)	W	Maximum theoretical work from sun
Exergy destruction	$\dot{E}x_{dest}$	Eq. (83)	W	Lost work due to irreversibility
Overall exergy efficiency	$\eta_{ex,tot}$	Eq. (86)	–	Second-law performance indicator
Entropy generation	$\dot{S}_{gen,tot}$	Eq. (60)	W/K	Measure of irreversibility

The performance indicators defined in Equations (74) – (89) and summarized in Table 3 are used in the next section to analyze the baseline performance, parametric sensitivity, and thermodynamic optimization of the PVT system.

6.0 Results and Discussion

This section presents the thermal, electrical, and thermodynamic performance characteristics of the proposed water-cooled photovoltaic–thermal system under tropical operating conditions. The analysis focuses on the coupled behavior of heat transfer, electrical generation, entropy generation, and exergy destruction within the collector and storage subsystems.

Parametric simulations were performed by systematically varying key operating parameters, including mass flow rate, solar irradiance, and ambient temperature, while monitoring their effects on thermal performance, electrical output, entropy generation, exergy destruction, and overall second-law efficiency. This approach enabled identification of the dominant thermodynamic mechanisms and operating conditions governing system optimization under tropical climatic environments. The adopted parametric framework further enabled comparative assessment of competing thermodynamic behaviors under varying operating conditions rather than merely demonstrating functional operation of the integrated PVT configuration.

6.1 Baseline Case Performance

The baseline performance of the single-module PVT system is evaluated using the fixed design and operating parameters summarized in Table 1 and a representative day extracted from the Kampala Typical Meteorological Year (TMY) dataset. The system consists of a $1.66\ m^2$ PVT

ARTICLE IN PRESS

collector coupled to a 100 L well-mixed storage tank operating in a closed loop without draw-off during the simulated day. The numerical results presented in this section are obtained from the two-node transient model described in Section 3, which explicitly resolves the PV layer and absorber temperatures and their thermal coupling to the working fluid.

Based on the total collector aperture area of 1.66 m^2, the baseline daily useful thermal and electrical outputs correspond to approximately 1.14 $kWh_{th}m^{-2}day^{-1}$and 1.17 $kWh_{el}m^{-2}day^{-1}$, respectively. These area-normalized values provide a more appropriate basis for comparison with conventional PV and other PVT systems because they refer to the same total solar receiving area.

6.1.1 Temperature Profiles

The diurnal evolution of the PV cell temperature T_{pv} and the fluid outlet temperature T_{out} is shown in Figure 4 for the baseline case.

Both temperatures increase from their early-morning values as solar irradiance rises, reach a maximum around solar noon, and decrease in the afternoon following the irradiance profile. Owing to the two-node thermal formulation, the PV temperature remains consistently higher than the fluid outlet temperature, reflecting the finite thermal resistance between the PV layer and the absorber–fluid interface.

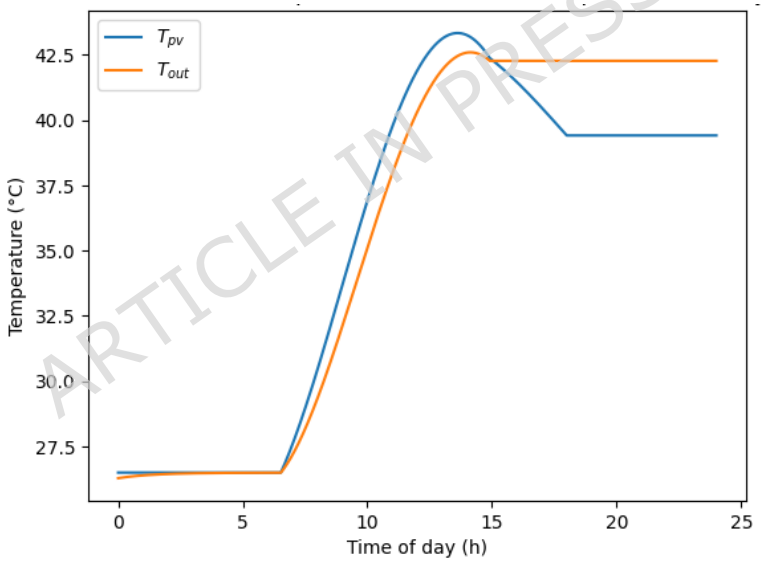

Figure 4. PV cell and outlet fluid temperatures vs time (TMY representative day, baseline case)

For the present baseline configuration, the PV temperature reaches a peak value of approximately 43.3°C, while the outlet fluid temperature peaks at about 42.6°C. These relatively moderate temperatures demonstrate the effectiveness of the active water cooling in limiting the thermal loading of the PV cells, which would otherwise operate at significantly higher temperatures in a standalone PV module under the same climatic conditions.

The gradual convergence of T_{out} and the storage tank temperature in the late afternoon reflects the absence of hot water draw-off in the present simulation and indicates that the system approaches a quasi-steady charged state. This behavior is representative of a domestic hot water system during periods of low demand and is consistent with the governing tank energy balance in Equation (58).

ARTICLE IN PRESS

6.1.2 Energy Outputs

The corresponding useful thermal power $\dot{Q}_u$ delivered to the fluid and the electrical power output P_{el} are shown in Figure 5 for the same representative day.

Both outputs follow the characteristic diurnal pattern of solar irradiance, increasing in the morning, peaking around solar noon, and decreasing thereafter. The useful thermal power, computed from Equation (74), attains significantly higher instantaneous values than the electrical power because a large fraction of the absorbed solar radiation is recovered in the form of low-grade heat in addition to electricity.

The electrical power output, evaluated using Equation (76), is slightly moderated around peak solar hours by the increase in PV operating temperature, illustrating the thermal–electrical coupling inherent to PVT systems. Nevertheless, the combined production of heat and electricity results in a substantially higher overall energy utilization compared to a standalone PV module of the same area.

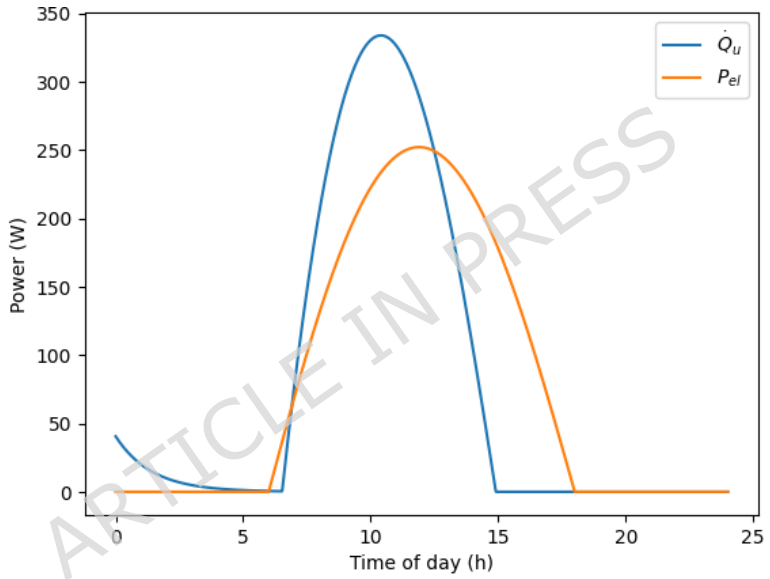

Figure 5. Useful thermal power and electrical power vs time (TMY representative day, baseline case)

When integrated over the day, the baseline system delivers approximately 1.88 kWh of thermal energy to the storage tank and about 1.95 kWh of electrical energy, confirming the suitability of the system for small-scale domestic hot water and on-site electricity supply in tropical climates.

6.1.3 Loss Breakdown

To clarify the physical origin of the performance limitations, the main heat loss components at peak operating conditions are decomposed in Figure 6.

ARTICLE IN PRESS

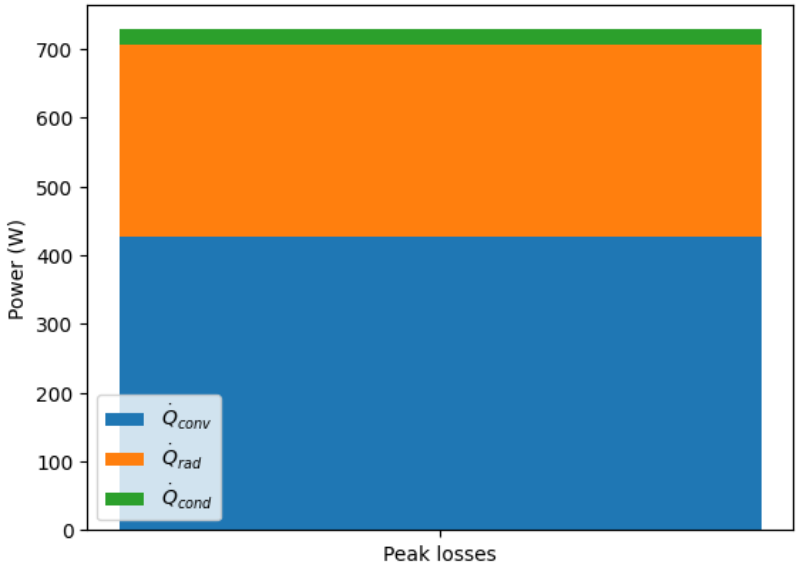

Figure 6. Breakdown of thermal losses at peak operating conditions (baseline case)

The total thermal losses are dominated by top losses, namely convective heat transfer to the ambient air and radiative heat exchange with the sky. Among these, convective losses represent the largest single contribution under the baseline wind speed of 2.4 ms^{-1}, while radiative losses constitute a comparable fraction due to the elevated surface temperature around solar noon. In contrast, conductive losses through the back insulation are relatively small, confirming the adequacy of the selected insulation thickness in Table 1.

This loss structure explains why, despite effective fluid cooling, the PV and absorber temperatures cannot be reduced indefinitely: as the surface temperature rises, an increasing fraction of the absorbed solar energy is irreversibly rejected to the environment rather than being converted into useful heat or electricity. This observation motivates the second-law analysis presented in the next section, where the same processes are examined in terms of entropy generation and exergy destruction.

ARTICLE IN PRESS

6.2 Second-Law (Entropy and Exergy) Results

While the first-law analysis in Section 6.1 quantifies how much energy is produced and lost, it does not reveal the thermodynamic quality of these energy flows or identify the true sources of performance degradation. The second-law analysis presented in this section addresses this limitation by examining the system in terms of entropy generation and exergy destruction, using the formulations introduced in Sections 3.4 and 3.5.

All results in this section correspond to the same baseline case and two-node transient simulation used to generate Figures 3–5.

6.2.1 Entropy Generation Breakdown by Mechanism

The total entropy generation rate of the system, $\dot{S}_{gen}$, is decomposed into contributions associated with the main irreversible processes, namely: (1) heat transfer between the collector surface and the ambient across a finite temperature difference, (2) heat transfer between the absorber and the working fluid, and (3) internal entropy production within the fluid due to temperature rise.

For the baseline case, the results show that heat rejection to the ambient environment constitutes the dominant source of entropy generation. This is primarily due to the relatively large temperature

ARTICLE IN PRESS

difference between the collector surface and the ambient air/sky during peak solar hours, which leads to strong irreversibility according to Equation (64).

The second most important contribution arises from heat transfer from the absorber to the fluid, which, although beneficial from an energy recovery perspective, still occurs across a finite temperature difference and therefore produces entropy internally. In contrast, the entropy generation associated with the temperature increase of the fluid itself is comparatively small.

The diurnal evolution of $\dot{S}_{gen}$ closely follows the solar irradiance profile, with negligible values during early morning and evening hours and a pronounced peak around solar noon. This behavior confirms that irreversibility is driven primarily by high-temperature operation under strong solar input, rather than by low-load operating periods. The diurnal evolution of the total entropy generation rate and its main components is shown in Figure 7.

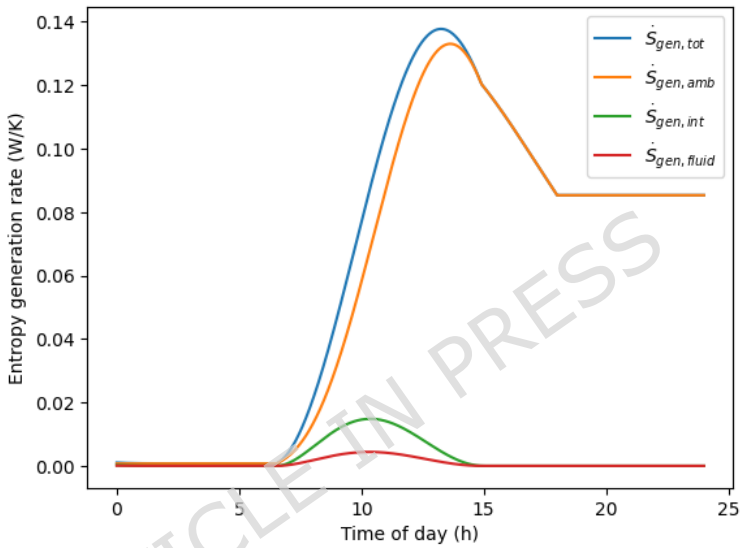

Figure 7. Diurnal evolution of entropy generation and its main components (baseline case)

ARTICLE IN PRESS

6.2.2 Exergy Destruction by Component

Using the Gouy–Stodola relation, Equation (85), the local entropy generation rates are mapped into exergy destruction rates for the main components of the system, namely: the collector (including PV surface, absorber, and top losses), the heat transfer process to the working fluid, and the thermal rejection to the environment.

ARTICLE IN PRESS

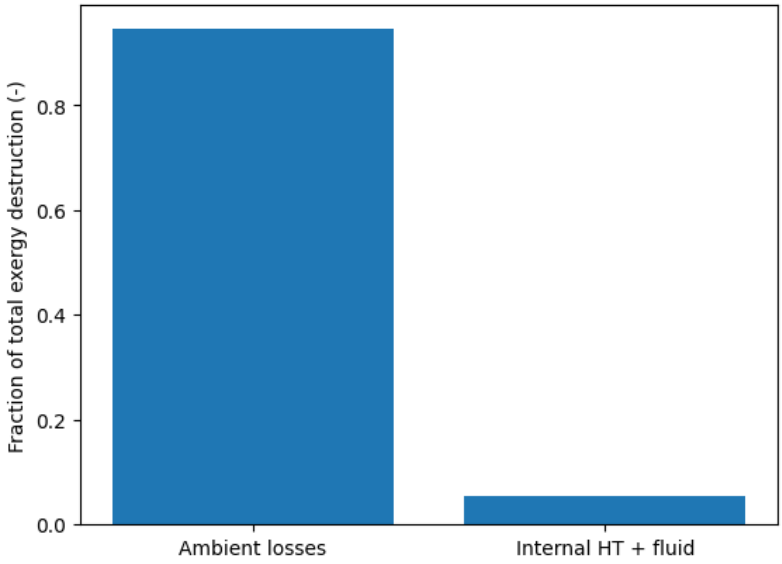

Figure 8. Distribution of exergy destruction by main components (baseline case)

Daily-integrated exergy destruction results (Figure 8) show that approximately 95% of the total destroyed exergy is associated with ambient heat losses, while only about 5% originates from internal heat transfer processes and fluid heating.

The results indicate that the collector–environment interface (i.e., combined convective and radiative top losses) accounts for the largest fraction of total exergy destruction in the system. This is expected, since rejecting heat to the ambient at a temperature close to the dead-state temperature T_0 destroys almost all of the work potential associated with that heat.

The second largest share of exergy destruction occurs within the collector heat transfer chain (PV → absorber → fluid), where finite temperature differences are required to drive heat into the fluid. Although this process produces useful thermal energy, it still degrades part of the available work potential.

In contrast, the storage tank contributes only marginally to the total exergy destruction in the present baseline case, owing to the assumption of a well-mixed tank and the absence of strong internal temperature gradients.

6.2.3 Major Irreversibility Drivers

The combined entropy-generation and exergy analyses reveal that the dominant irreversibility mechanisms in the baseline PVT system arise primarily from ambient thermal rejection and finite-temperature-difference heat transfer within the collector. Quantitatively, ambient heat rejection contributes approximately 95% of the total exergy destruction, clearly identifying external thermal losses as the principal thermodynamic limitation under tropical operating conditions. The underlying mechanism is that heat rejected from the collector to the ambient occurs across finite temperature differences, causing irreversible degradation of useful energy quality. Under high irradiance conditions, elevated absorber and PV temperatures intensify thermal gradients between the collector, working fluid, and surroundings, thereby increasing entropy generation and exergy destruction. Consequently, improvements in thermal insulation, selective coatings, reduced external heat-transfer coefficients, and enhanced PV–absorber thermal coupling may provide greater thermodynamic benefits than simply increasing heat extraction rates.

ARTICLE IN PRESS

Although higher coolant flow rates improve PV cooling and electrical performance through enhanced convective heat removal, the reduced fluid residence time lowers the outlet temperature rise and consequently decreases the thermodynamic quality of the recovered heat. Therefore, operating conditions associated with improved first-law cooling performance do not necessarily correspond to thermodynamically optimal second-law performance. Similarly, increasing solar irradiance enhances both electrical generation and thermal energy recovery, but simultaneously intensifies irreversible heat transfer due to larger collector temperature gradients. These findings confirm that energy-optimal and exergy-optimal operating conditions may diverge significantly in tropical PVT systems.

The significance of the proposed cooling strategy should therefore not be interpreted solely in terms of electrical efficiency enhancement relative to conventional PV modules. Rather, the principal thermodynamic advantage of the investigated configuration lies in simultaneous recovery of useful low-temperature thermal energy while maintaining improved PV electrical performance through temperature regulation. Consequently, the proposed system functions not only as a PV cooling mechanism but also as an integrated solar-energy recovery framework suitable for applications such as domestic hot water production and other low-temperature thermal uses under tropical climatic conditions.

Comparison with previous thermodynamic PVT investigations indicates that the present findings are consistent with reported trends in water-cooled PVT systems, where enhanced cooling improves electrical performance while simultaneously enabling useful thermal energy recovery (Rashidi et al., 2020; Rao et al., 2024; Wang et al., 2024). Similar studies also reported that entropy generation and exergy destruction are strongly influenced by thermal losses and finite-temperature-difference heat transfer processes within the collector (Ramírez-Minguela et al., 2023; Al-Najjar et al., 2024). However, unlike many existing investigations that primarily report global energy or exergy efficiencies, the present work provides a mechanism-resolved second-law interpretation by explicitly linking subsystem-level entropy generation and exergy destruction to Gibbs Tds-based thermodynamic relations under tropical operating conditions. For consistency, literature comparisons were based on aperture-area-normalized outputs or efficiency indicators where sufficient collector-area information was available.

Fluid friction and pumping losses were intentionally excluded; therefore, the identified irreversibility structure reflects predominantly thermal and thermoelectric effects. Overall, the results demonstrate that system performance is constrained less by solar absorption itself than by irreversible energy degradation associated with ambient heat rejection and finite-temperature heat transfer processes. This second-law insight, which cannot be fully inferred from first-law efficiency analysis alone, provides a rigorous thermodynamic basis for optimization of PVT systems operating in tropical environments.

6.3 Parametric and Sensitivity Analysis

To assess the robustness of the baseline conclusions and identify thermodynamically meaningful improvement directions, a parametric study was conducted by varying a limited set of key operational, environmental, and design parameters while keeping all others fixed at the baseline values (Table 1). For each case, the system was simulated over the same representative day, and the daily integrated entropy generation $S_{gen,day}$ and exergy efficiency $\eta_{ex,day}$ were evaluated.

The main trends and resulting thermodynamic design recommendations based on daily-integrated entropy generation and exergy efficiency for the baseline PVT system are summarized in Table 4.

ARTICLE IN PRESS

Table 4. Summary of parametric sensitivity results and thermodynamic optimization recommendations

Parameter	Tested range	Effect on S_{gen}	Effect on η_{ex}	Recommended baseline / optimal setting
Mass flow rate, $\dot{m}$(kg/s)	0.01 – 0.10	Increases with $\dot{m}$ (minimum at lowest $\dot{m}$)	Decreases with $\dot{m}$; maximum at lowest $\dot{m}$	$\dot{m} = 0.01$ kg/s (thermodynamically optimal in this configuration)
Wind speed, v_w(m/s)	0.5 – 5.0	Decreases strongly with v_w	Weak, shallow minimum around 3–4 m/s	Not a design variable; mitigate via wind shielding or glazing
Ambient temperature, T_{amb}(°C)	22 – 30	Increases strongly with T_{amb}	Decreases with T_{amb}	Not controllable; emphasizes need for thermal loss reduction
Peak irradiance, G_{max}(W/m²)	600 – 1050	Increases with G_{max}	Decreases with G_{max}	Not controllable; requires improved thermal management at high G
Insulation thickness, δ_{ins} (mm)	20 – 100	Slight increase with δ_{ins}	Slight increase with δ_{ins}	$\delta_{ins} \gtrsim 50$ mm (diminishing returns beyond this)
PV–absorber coupling, $U A_{pa}$(W/K)	Low → High (= 100–500 W/K)	Increases moderately with coupling	Increases clearly with coupling	As high as practically achievable (good thermal contact, soldering/bonding)

Physically, the observed reduction in exergy efficiency at higher flow rates arises because the coolant extracts heat more rapidly while simultaneously reducing the useful temperature lift across the collector. Although enhanced cooling improves PV electrical behavior, the corresponding reduction in fluid temperature gain limits the quality of the recovered thermal energy from a second-law perspective. This demonstrates the competing interaction between thermal extraction and thermodynamic usefulness within the PVT system.

6.3.1 Effect of Mass Flow Rate

The influence of the mass flow rate $\dot{m}$on the thermodynamic performance is summarized in Figure 8, which shows the variation of the daily exergy efficiency $\eta_{ex,day}$ with $\dot{m}$.

As seen in Figure 9, the exergy efficiency decreases gradually as the mass flow rate is increased over the investigated range. The best exergy performance is obtained at the lowest tested flow rate, around $\dot{m} = 0.01\ kgs^{-1}$. This behavior can be explained by the irreversibility structure identified in Section 6.2: since ambient heat losses dominate exergy destruction, increasing the flow rate does not significantly mitigate the main loss mechanism, while it redistributes irreversibility within the internal heat transfer chain.

The corresponding variation of the daily entropy generation with $\dot{m}$ exhibits the same trend, confirming that, for the present configuration, operating the system at unnecessarily high flow rates is thermodynamically suboptimal.

ARTICLE IN PRESS

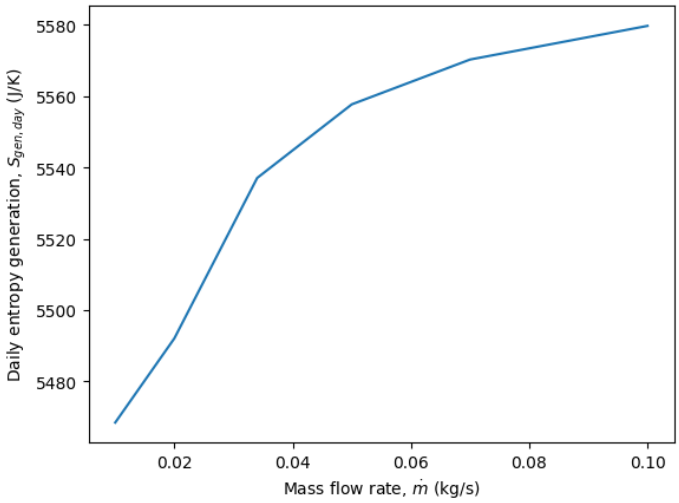

Figure 9. Effect of mass flow rate on daily entropy generation (baseline day)

6.3.2 Effect of Wind Speed and Ambient Temperature

The effect of wind speed on system irreversibility is shown in Figure 10, which presents the daily entropy generation $S_{gen,day}$ as a function of the wind speed v_w.

As illustrated in Figure 10, increasing the wind speed leads to a marked reduction in total entropy generation. This occurs because stronger convective cooling reduces the collector surface temperature and, consequently, the magnitude of finite-temperature-difference heat transfer to the environment. However, the corresponding change in exergy efficiency is comparatively modest, indicating that the beneficial effect of lower surface temperatures is partly offset by enhanced convective heat losses.

A similar sensitivity was observed for ambient temperature: higher ambient temperatures systematically increase entropy generation and reduce exergy efficiency by shifting the entire system to higher operating temperatures and degrading PV electrical performance.

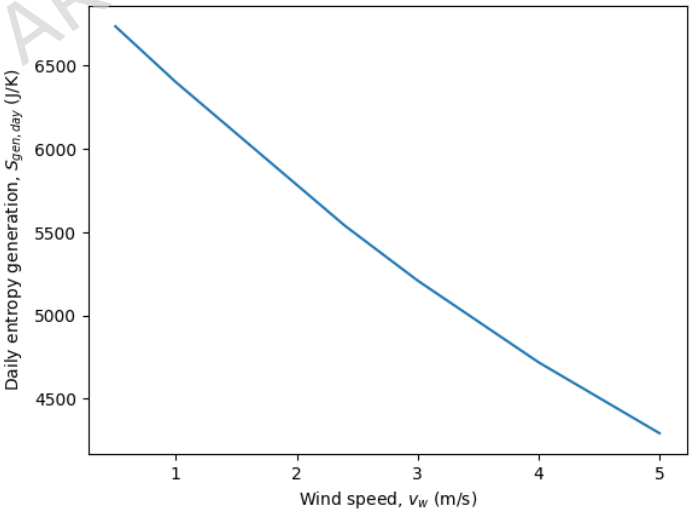

Figure 10. Effect of wind speed on daily entropy generation (baseline day)

ARTICLE IN PRESS

The results further indicate that elevated ambient temperatures reduce the thermodynamic potential for useful heat transfer to the surroundings, thereby influencing both collector cooling behavior and exergy recovery characteristics. This highlights the strong sensitivity of PVT thermodynamic performance to climatic operating conditions in tropical environments.

6.3.3 Effect of Irradiance Level

The impact of solar resource intensity on the thermodynamic performance is illustrated in Figure 10, which shows the variation of the daily exergy efficiency $\eta_{ex,day}$ with the peak irradiance level G_{max}.

As shown in Figure 11, the exergy efficiency decreases monotonically as the irradiance level increases. Although higher irradiance naturally increases absolute energy production, it also leads to higher operating temperatures and, consequently, to a disproportionate increase in ambient-loss irreversibility. As a result, a larger fraction of the available solar exergy is destroyed rather than converted into useful outputs.

The corresponding increase in total entropy generation with irradiance level confirms that stronger solar forcing amplifies irreversibility unless accompanied by improved thermal management.

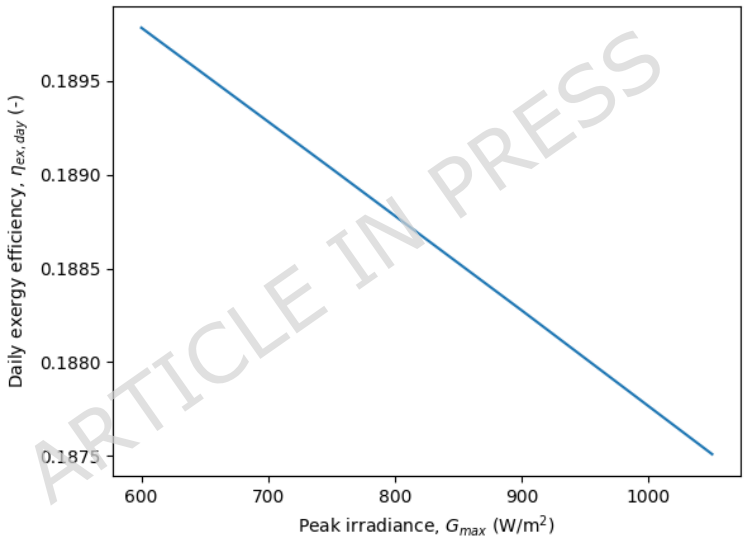

Figure 11. Effect of irradiance level on daily exergy efficiency (baseline day)

6.3.4 Effect of Design Parameters

Among the design parameters, the effects of insulation thickness and PV–absorber thermal coupling were examined. The influence of insulation thickness on the daily exergy efficiency is presented in Figure 12. Increasing the insulation thickness produces a small but systematic improvement in $\eta_{ex,day}$. This reflects the reduction of back-side heat losses and their associated exergy destruction. However, the improvement is modest, indicating that top losses remain the dominant limitation, in agreement with the second-law analysis in Section 6.2.

The effect of PV–absorber coupling strength shows that improving the thermal contact between the PV layer and the absorber enhances exergy efficiency by facilitating heat extraction and limiting PV temperature penalties, even though it redistributes entropy generation within the collector.

ARTICLE IN PRESS

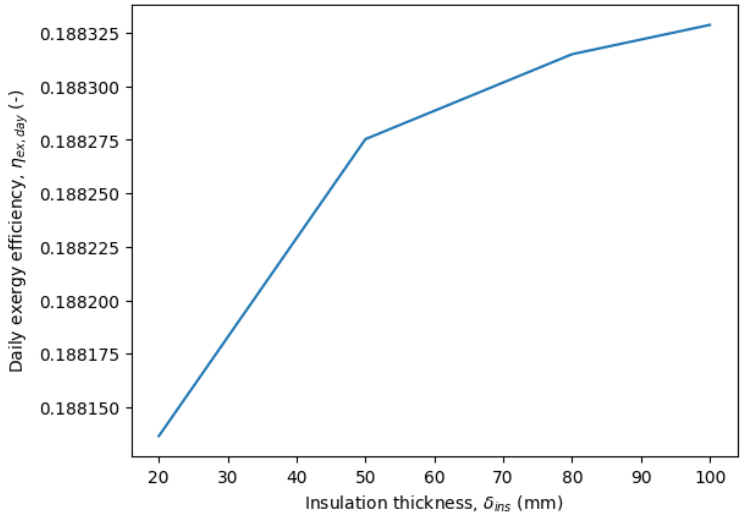

Figure 12. Effect of insulation thickness on daily exergy efficiency (baseline day)

6.4 Optimization and Recommended Operating Region

Based on the parametric results presented in Section 6.3, an optimization-oriented analysis is now performed to identify a rational operating region and extract practical design guidance for tropical PVT deployment. Since the second-law analysis has shown that the system is fundamentally limited by ambient-loss irreversibility, the optimization is formulated in terms of exergy efficiency maximization and entropy generation minimization, rather than energy efficiency alone.

6.4.1 Optimal Flow Rate and Operating Temperature

The effect of mass flow rate on the peak PV operating temperature is shown in Figure 13. It is observed that, within the investigated range, increasing $\dot{m}$produces only a modest reduction in the PV temperature. This indicates that the present system is not primarily constrained by internal heat removal capability, but rather by heat rejection to the environment.

The corresponding influence of $\dot{m}$ on the thermal, electrical, and exergy efficiencies is summarized in Figure 14. While the thermal and electrical efficiencies remain almost constant over the tested range, the exergy efficiency exhibits a slight but systematic decrease as $\dot{m}$i increases. Consequently, the best thermodynamic performance is achieved at the lowest tested mass flow rate, around: $\dot{m} = 0.01\ kg\ s^{-1}$.

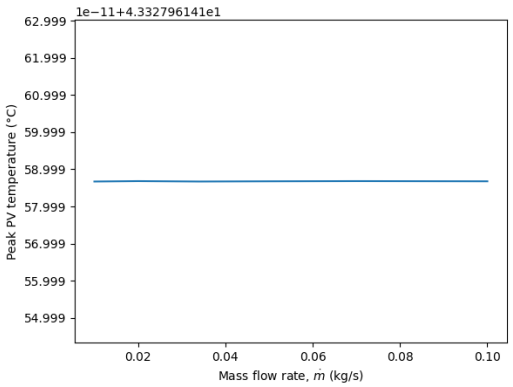

Figure 13. Effect of mass flow rate on peak PV temperature (baseline day)

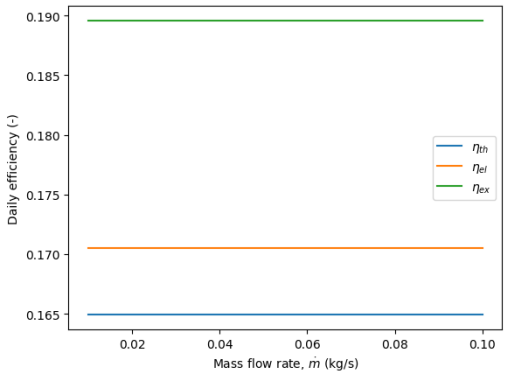

Figure 14. Effect of mass flow rate on thermal, electrical and exergy efficiencies

ARTICLE IN PRESS

This operating point also corresponds to a moderate PV temperature (Figure 13), confirming that aggressive over-cooling is neither necessary nor thermodynamically beneficial in the present configuration.

6.4.2 Energy–Exergy Trade-Off

Figure 14 provides a clear illustration of a central result of this study: the energy-optimal and exergy-optimal operating points do not necessarily coincide. From a first-law perspective, increasing the flow rate does not penalize thermal or electrical efficiency. However, from a second-law perspective, higher flow rates slightly increase the total irreversibility of the system and reduce the fraction of useful work that can be extracted from the same solar input.

This difference arises because energy metrics do not account for where and how irreversibility is produced, whereas the exergy efficiency explicitly penalizes entropy generation, particularly that associated with ambient heat losses. The present results therefore demonstrate that optimizing a PVT system solely on energy efficiency grounds can be thermodynamically misleading.

6.4.3 Design Recommendations for Tropical Deployment

Even under optimized operating conditions, the dominant share of exergy destruction in the system remains associated with heat losses to the ambient environment, while internal heat transfer processes contribute only a minor fraction. This thermodynamic structure leads to three clear and robust design recommendations for PVT systems intended for tropical deployment. First, priority should be given to minimizing top losses through improved glazing, selective coatings, and wind shielding, since these mechanisms dominate exergy destruction. Second, excellent thermal contact between the PV module and the absorber should be ensured, as this enhances heat extraction and limits PV temperature penalties without introducing significant additional irreversibility. Third, moderate mass flow rates are sufficient; oversizing pumps or operating at excessively high flow rates provides little thermodynamic benefit and may even reduce exergy efficiency.

In summary, the optimal design strategy is not to maximize heat removal, but rather to minimize irreversible heat rejection to the environment, in full agreement with the second-law analysis presented in Section 6.2.

ARTICLE IN PRESS

7.0 Conclusions and Practical Recommendations

This study developed a coupled transient thermal–electrical framework for second-law analysis of a water-cooled photovoltaic–thermal (PVT) system operating under tropical climatic conditions. Unlike conventional PVT investigations that primarily emphasize overall thermal or exergy efficiencies, the proposed framework explicitly incorporated Gibbs Tds-based thermodynamic relations to resolve subsystem-level entropy generation and exergy destruction mechanisms governing useful energy degradation. The analysis demonstrated that the baseline system (1.66 m² collector integrated with a 100 L storage tank under Kampala TMY conditions) maintained PV temperatures below approximately 43 °C while delivering about 1.9 kWh of useful thermal energy and 1.95 kWh of electrical energy over a representative operating day.

The second-law analysis revealed that ambient heat rejection constituted the dominant thermodynamic irreversibility mechanism, accounting for approximately 95% of the total exergy destruction, whereas internal heat-transfer processes contributed only a comparatively minor fraction. The results further demonstrated that operating conditions associated with maximum thermal extraction or improved first-law efficiency do not necessarily correspond to

ARTICLE IN PRESS

thermodynamically optimal conditions when entropy generation and exergy destruction are considered simultaneously. In particular, increasing mass flow rate, irradiance level, and ambient temperature reduced exergy efficiency despite relatively small changes in energy efficiency, indicating that energy-based optimization alone may provide misleading design guidance. The thermodynamically favorable operating region for the investigated configuration occurred at low-to-moderate flow rates near $\dot{m} = 0.01\ kg\ s^{-1}$.

From a practical perspective, the findings indicate that thermodynamic optimization of tropical PVT systems should prioritize reduction of irreversible ambient thermal losses through improved insulation, enhanced PV–absorber thermal coupling, selective surface treatment, and reduction of external convection losses rather than simply increasing coolant circulation rates. The study further demonstrates that the principal thermodynamic significance of the proposed configuration lies not merely in incremental electrical enhancement, but in integrated recovery of useful low-temperature thermal energy together with simultaneous PV temperature regulation. Consequently, the proposed framework provides physically diagnostic second-law design guidance for tropical solar-energy applications including domestic hot water production, building-integrated systems, and decentralized renewable-energy deployment.

Declarations

Authors contribution: **Conceptualization, MMM, JIS, SNN, DEU, writing – original draft:** MMM, **Writing – review & editing: All authors**

Competing interests: None

Consent to participate: NA

Consent to publish: NA

Ethical Approval: NA

Funding: No funding received

Data availabity: Data will be made available on request from the authors

ARTICLE IN PRESS

References

Abdulameer, L., Dzhumagulova, N., Algretawee, H., Zhuravleva, L., & Alshammari, M. (2022). Comparison between Hazen-Williams and Darcy-Weisbach equations to calculate head loss through conveyancing treated wastewater in Kerbala city, Iraq. *Eastern-European Journal of Enterprise Technologies*. https://doi.org/10.15587/1729-4061.2022.251385

Abdul-Ganiyu, S., Quansah, D., Ramde, E., Seidu, R., & Adaramola, M. (2021). Study effect of flow rate on flat-plate water-based photovoltaic-thermal (PVT) system performance by analytical technique. *Journal of Cleaner Production*. https://doi.org/10.1016/j.jclepro.2021.128985

Abdullah, A., Misha, S., Tamaldin, N., Rosli, M., & Sachit, F. (2020). Theoretical study and indoor experimental validation of performance of the new photovoltaic thermal solar collector (PVT) based water system. *Case Studies in Thermal Engineering*, 18, 100595. https://doi.org/10.1016/j.csite.2020.100595

Abimanyu, R., Yanuar, Y., Waskito, K., Sari, W., & Ogata, S. (2025). Impact of Reynolds Number on Flow Behavior in Spiral Pipe Profiles: A Review. *Journal of Advanced Research in Fluid Mechanics and Thermal Sciences*. https://doi.org/10.37934/arfmts.129.2.216243

Alami, Y., Baghaz, E., Nasrin, R., Al-Damook, M., Bendaoud, R., Bouragba, T., Melhaoui, M., & Benhmida, M. (2025). Up-to-Date Review on Flat-Plate Solar Hybrid Photovoltaic

ARTICLE IN PRESS

Thermal Systems: Absorber Designs and Fabrication Materials. *International Journal of Energy Research*. https://doi.org/10.1155/er/5547555

Alessandro, M., Aste, N., Claudio, D., & Fabrizio, L. (2021). Photovoltaic-thermal solar-assisted heat pump systems for building applications: Integration and design methods. *Energy and Built Environment*. https://doi.org/10.1016/j.enbenv.2021.07.002

Al-Najjar, H., Mahdi, J., Alsharifi, T., Homod, R., Talebizadehsardari, P., & Keshmiri, A. (2024). Thermodynamic Modeling and Performance Analysis of Photovoltaic-Thermal Collectors Integrated with Phase Change Materials: Comprehensive Energy and Exergy Analysis. *Results in Engineering*. https://doi.org/10.1016/j.rineng.2024.102277

Al-Najjar, H., Mahdi, J., Alsharifi, T., Homod, R., Talebizadehsardari, P., & Keshmiri, A. (2024). Thermodynamic modeling and performance analysis of photovoltaic–thermal collectors integrated with phase change materials: Comprehensive energy and exergy analysis. *Results in Engineering, 22*, 102277. https://doi.org/10.1016/j.rineng.2024.102277

Al-Waeli, A., Kazem, H., Chaichan, M., & Sopian, K. (2020). A review of photovoltaic thermal systems: Achievements and applications. *International Journal of Energy Research*, 45, 1269 - 1308. https://doi.org/10.1002/er.5872

Arenandan, V., Wong, J., Ahmed, A., & Chow, M. (2022). Efficiency enhancement in energy production of photovoltaic modules through green roof installation under tropical climates. *Ain Shams Engineering Journal*. https://doi.org/10.1016/j.asej.2022.101741

Asefi, G., Ma, T., & Wang, R. (2022). Parametric investigation of photovoltaic–thermal systems integrated with porous phase change material. *Applied Thermal Engineering, 201*, 117727. https://doi.org/10.1016/j.applthermaleng.2021.117727

Attia, M. E. H., Kabeel, A. E., Khelifa, A., Abdelgaied, M., Arıcı, M., & Abdel-Aziz, M. M. (2025). Performance enhancement of PVT modules using bi-fluid air/CuO–water-based nanofluid and fins: Energy and exergy analysis. *Clean Technologies and Environmental Policy, 27*, 4541–4559. https://doi.org/10.1007/s10098-025-03149-1

Bakari, R., Minja, R., & Njau, K. (2014). Effect of Glass Thickness on Performance of Flat Plate Solar Collectors for Fruits Drying. *Journal of Energy*, 2014, 1-8. https://doi.org/10.1155/2014/247287

Ballina, J., & Go, Y. (2025). Quantification and Comparative Analysis of Environmental Factors to Large-Scale Solar Plant's Energy Performance via Regression and Linear Correlation Models. *Journal of Energy and Power Technology*. https://doi.org/10.21926/jept.2501001

Bandaru, S., Becerra, V., Khanna, S., Radulovic, J., Hutchinson, D., & Khusainov, R. (2021). A Review of Photovoltaic Thermal (PVT) Technology for Residential Applications: Performance Indicators, Progress, and Opportunities. *Energies*. https://doi.org/10.3390/en14133853

Basuhaib, A., Selvaraj, J., Hasanuzzaman, M., Anjum, T., & Kumar, L. (2024). Experimental investigation the effect of different operating parameters and optimized the water-based PVT system for domestic applications. *Solar Energy*. https://doi.org/10.1016/j.solener.2023.112278

Bejan, A. (2002). Fundamentals of exergy analysis, entropy generation minimization, and the generation of flow architecture. *International Journal of Energy Research*, 26. https://doi.org/10.1002/er.804

Bejan, A. (2013). *Entropy generation minimization: the method of thermodynamic optimization of finite-size systems and finite-time processes*. CRC press.

ARTICLE IN PRESS

Bian, C., Song, J., Jin, X., Jiang, W., Jie, X., & Yang, L. (2025). Thermal management in photovoltaic–thermal systems: Advances, challenges, and cross-domain applications. *Applied Thermal Engineering, 279*, 127791. https://doi.org/10.1016/j.applthermaleng.2025.127791

Bigorajski, J., & Chwieduk, D. (2018). Analysis of a micro photovoltaic/thermal – PV/T system operation in moderate climate. *Renewable Energy*. https://doi.org/10.1016/j.renene.2018.01.116

Cengel, Y. A., & Boles, M. A. (2002). Thermodynamics: an engineering approach. *Sea*, *1000*(8862), 287-93.

Chander, S., Purohit, A., Sharma, A., , A., Nehra, S., & Dhaka, M. (2015). A study on photovoltaic parameters of mono-crystalline silicon solar cell with cell temperature. *Energy Reports*, 1, 104-109. https://doi.org/10.1016/j.egyr.2015.03.004

Chyngyzbekkyzy, Z., & Satybaldyev, A. (2025). Comparative Multicriteria Analysis of Thermophysical and Corrosion Properties of main Types of Heat Transfer fluids for Solar Water Heating Collectors. *Bulletin of Science and Practice*. https://doi.org/10.33619/2414-2948/118/17

Ciprian, B. (2019). The Quest for the Ideal Darcy-Weisbach Friction Factor Equation from the Perspective of a Building Services Engineer. *Ovidius University Annals of Constanta - Series Civil Engineering*, 21, 65 - 73. https://doi.org/10.2478/ouacsce-2019-0008

Costa, S., & Kenisarin, M. (2022). A review of metallic materials for latent heat thermal energy storage: Thermophysical properties, applications, and challenges. *Renewable and Sustainable Energy Reviews*. https://doi.org/10.1016/j.rser.2021.111812

Cotfas, D., Cotfas, P., & Machidon, O. (2018). Study of Temperature Coefficients for Parameters of Photovoltaic Cells. *International Journal of Photoenergy*, 2018, 1-12. https://doi.org/10.1155/2018/5945602

Dancker, J., & Wolter, M. (2021). Improved quasi-steady-state power flow calculation for district heating systems: A coupled Newton-Raphson approach. *Applied Energy*, 295, 116930. https://doi.org/10.1016/j.apenergy.2021.116930

David, A., Lakshya, A., Sahu, M., & Sinha, R. (2021). Stating and Deriving Bernoulli's Theorem as a Special Case of Steady Flow Energy Equation. *Lecture Notes in Mechanical Engineering*. https://doi.org/10.1007/978-981-16-4489-4_20

David, M., Toutant, A., & Bataille, F. (2021). Numerical development of heat transfer correlation in asymmetrically heated turbulent channel flow. *International Journal of Heat and Mass Transfer*, 164, 120599. https://doi.org/10.1016/j.ijheatmasstransfer.2020.120599

Design and Simulation of an Inverter Muhamad, M. M., Kibirige, D., Uzorka, A., & John, U. K. (2022). Drive System with a Display for a Renewable Energy System in the Rural Isolated Communities of Uganda. *Journal of Power and Energy Engineering*, *10*(12), 1-14. https://doi.org/10.4236/jpee.2022.1012001

Diwania, S., Agrawal, S., Siddiqui, A., & Singh, S. (2020). Photovoltaic–thermal (PV/T) technology: a comprehensive review on applications and its advancement. *International Journal of Energy and Environmental Engineering*, 11, 33-54. https://doi.org/10.1007/s40095-019-00327-y

Dubey, S., & Tay, A. (2013). Testing of two different types of photovoltaic–thermal (PVT) modules with heat flow pattern under tropical climatic conditions. *Energy for Sustainable Development*, 17, 1-12. https://doi.org/10.1016/j.esd.2012.09.001

ARTICLE IN PRESS

ARTICLE IN PRESS

Eicker, U., & Dalibard, A. (2011). Photovoltaic–thermal collectors for night radiative cooling of buildings. *Solar Energy*, 85, 1322-1335. https://doi.org/10.1016/j.solener.2011.03.015

Elsabahy, M., Emam, M., Sekiguchi, H., & Ahmed, M. (2024). Performance mapping of silicon-based solar cell for efficient power generation and thermal utilization: Effect of cell encapsulation, temperature coefficient, and reference efficiency. *Applied Energy*. https://doi.org/10.1016/j.apenergy.2023.122385

Evola, G., & Marletta, L. (2014). Exergy and thermoeconomic optimization of a water-cooled glazed hybrid photovoltaic/thermal (PVT) collector. *Solar Energy*, 107, 12-25. https://doi.org/10.1016/j.solener.2014.05.041

Fashina, A., Mundu, M., Akiyode, O., Abdullah, L., Sanni, D., & Ounyesiga, L. (2018). The drivers and barriers of renewable energy applications and development in Uganda: a review. *Clean Technologies*, *1*(1), 9-39.

Francisco, B., Nelson, S., Christoph, R., & Hatef, M. (2024). Cold solar: PVT heat exchanger designs for heat pump integration. *Applied Thermal Engineering*. https://doi.org/10.1016/j.applthermaleng.2024.125020

Giovannetti, F., Föste, S., Ehrmann, N., & Rockendorf, G. (2014). High transmittance, Low Emissivity Glass Covers for Flat Plate Collectors: Applications and Performance. *Energy Procedia*, 30, 106-115. https://doi.org/10.1016/j.egypro.2012.11.014

Guarracino, I., Freeman, J., Ramos, A., Kalogirou, S., Ekins-Daukes, N., & Markides, C. (2019). Systematic testing of hybrid PV-thermal (PVT) solar collectors in steady-state and dynamic outdoor conditions. *Applied Energy*. https://doi.org/10.1016/j.apenergy.2018.12.049

Guarracino, I., Mellor, A., Ekins-Daukes, N., & Markides, C. (2016). Dynamic coupled thermal-and-electrical modelling of sheet-and-tube hybrid photovoltaic/thermal (PVT) collectors. *Applied Thermal Engineering*, 101, 778-795. https://doi.org/10.1016/j.applthermaleng.2016.02.056

Hai, T., El-Rahman, M., Li, S., Malekshah, E., Aybar, H., & El-Shafay, A. (2023). The entropy generation analysis and optimization of a water/silver nanofluid flow inside a photovoltaic thermal collector considering plain, ribbed, and porous-ribbed absorber tubes. *Journal of the Taiwan Institute of Chemical Engineers*. https://doi.org/10.1016/j.jtice.2023.104695

Hellström, B., Adsten, M., Nostell, P., Karlsson, B., & Wäckelgård, E. (2003). The impact of optical and thermal properties on the performance of flat plate solar collectors. *Renewable Energy*, 28, 331-344. https://doi.org/10.1016/s0960-1481(02)00040-x

Herrando, M., Ramos, A., Zabalza, I., & Markides, C. (2019). A comprehensive assessment of alternative absorber-exchanger designs for hybrid PVT-water collectors. *Applied Energy*. https://doi.org/10.1016/j.apenergy.2018.11.024

Hong, W., Li, B., Li, H., Niu, X., Li, Y., & Lan, J. (2022). Recent progress in thermal energy recovery from the decoupled photovoltaic/thermal system equipped with spectral splitters. *Renewable and Sustainable Energy Reviews*. https://doi.org/10.1016/j.rser.2022.112824

Hu, M., Zhao, B., , S., Ao, X., Cao, J., Wang, Q., Riffat, S., Su, Y., & Pei, G. (2022). Applications of radiative sky cooling in solar energy systems: Progress, challenges, and prospects. *Renewable and Sustainable Energy Reviews*. https://doi.org/10.1016/j.rser.2022.112304

Huang, Y., Sun, Q., Li, Y., Sun, C., & Chen, Z. (2023). Damping technique empowered robust energy flow calculation for integrated energy systems. *Applied Energy*. https://doi.org/10.1016/j.apenergy.2023.121168

Incropera, F. P., DeWitt, D. P., Bergman, T. L., & Lavine, A. S. (1996). *Fundamentals of heat and mass transfer* (Vol. 6, p. 116). New York: Wiley.

ARTICLE IN PRESS

Jamshed, W., Eid, M., Aissa, A., Mourad, A., Nisar, K., Shahzad, F., Saleel, C., & Vijayakumar, V. (2021). Partial velocity slip effect on working magneto non-Newtonian nanofluids flow in solar collectors subject to change viscosity and thermal conductivity with temperature. *PLoS ONE*, 16. https://doi.org/10.1371/journal.pone.0259881

Jia, L., Lu, L., Chen, J., & Han, J. (2022). A novel radiative sky cooling-assisted ground-coupled heat exchanger system to improve thermal and energy efficiency for buildings in hot and humid regions. *Applied Energy*. https://doi.org/10.1016/j.apenergy.2022.119422

Jia, Y., Alva, G., & Fang, G. (2019). Development and applications of photovoltaic–thermal systems: A review. *Renewable and Sustainable Energy Reviews*. https://doi.org/10.1016/j.rser.2018.12.030

Joshi, A., Dincer, I., & Reddy, B. (2009). Thermodynamic assessment of photovoltaic systems. *Solar Energy*, 83, 1139-1149. https://doi.org/10.1016/j.solener.2009.01.011

Kalateh, M. R., Kianifar, A., & Sardarabadi, M. (2022). Energy, exergy, and entropy generation analyses of a water-based photovoltaic thermal system equipped with clockwise–counter-clockwise twisted tapes: An indoor experimental study. *Applied Thermal Engineering, 215*, 118906. https://doi.org/10.1016/j.applthermaleng.2022.118906

Kallio, S., & Siroux, M. (2020). Energy Analysis and Exergy Optimization of Photovoltaic-Thermal Collector. *Energies*. https://doi.org/10.20944/preprints202009.0219.v1

Kenfack, A., Nematchoua, M., Simo, E., Mfoundikou, M., Fosso, J., Babikir, M., & Chara-Dackou, V. (2023). Exergetic optimization of some design parameters of the hybrid photovoltaic/thermal collector with bi-fluid air/ternary nanofluid (CuO/MgO/TiO2). *SN Applied Sciences*, 5. https://doi.org/10.1007/s42452-023-05455-z

Khoukhi, M., & Maruyama, S. (2005). Theoretical approach of a flat plate solar collector with clear and low-iron glass covers taking into account the spectral absorption and emission within glass covers layer. *Renewable Energy*, 30, 1177-1194. https://doi.org/10.1016/j.renene.2004.09.014

Khoukhi, M., & Maruyama, S. (2006). Theoretical approach of a flat-plate solar collector taking into account the absorption and emission within glass cover layer. *Solar Energy*, 80, 787-794. https://doi.org/10.1016/j.solener.2005.06.002

Kim, J., & Kim, J. (2012). The Experimental Performance of an Unglazed PVT Collector with Two Different Absorber Types. *International Journal of Photoenergy*, 2012, 1-6. https://doi.org/10.1155/2012/312168

Kotas, T. J. (2012). *The exergy method of thermal plant analysis*. Paragon Publishing.

Kramer, K., Mehnert, S., Munz, G., Helmling, S., & Lämmle, M. (2023). Photovoltaic-Thermal Technology – PVT Collectors, Systems and Applications. *Energy Technology*. https://doi.org/10.1002/ente.202300378

Krishna, Y., Faizal, M., Saidur, R., Ng, K., & Aslfattahi, N. (2020). State-of-the-art heat transfer fluids for parabolic trough collector. *International Journal of Heat and Mass Transfer*. https://doi.org/10.1016/j.ijheatmasstransfer.2020.119541

Kumar, S. (2022). Application of First Law of Thermodynamics to Flow Processes Thermodynamics. *Thermal Engineering Volume 1*. https://doi.org/10.1007/978-3-030-67274-4_4

Lima, G., Flores, J., Faria, L., Da Silva Martins Pitana, K., Saretta, E., Massey, J., & De Oliveira, H. (2025). Darcy Friction Factor Equations for Small-Diameter Pipes in Lateral Irrigation Systems: An Experimental Study. *Journal of the ASABE*. https://doi.org/10.13031/ja.16338

ARTICLE IN PRESS

Liu, L., Shalwan, A., Teng, J., Liu, C., & Li, Z. (2023). The entropy generation analysis of a PVT solar collector with internally needle finned serpentine absorber tube. *Engineering Analysis with Boundary Elements*. https://doi.org/10.1016/j.enganabound.2023.07.018

Maadi, S., Kolahan, A., Passandideh-Fard, M., Sardarabadi, M., & Moloudi, R. (2017). Characterization of PVT systems equipped with nanofluids-based collector from entropy generation. *Energy Conversion and Management*, 150, 515-531. https://doi.org/10.1016/j.enconman.2017.08.039

Malekan, M., Khosravi, A., & Syri, S. (2019). Heat transfer modeling of a parabolic trough solar collector with working fluid of Fe3O4 and CuO/Therminol 66 nanofluids under magnetic field. *Applied Thermal Engineering*. https://doi.org/10.1016/j.applthermaleng.2019.114435

Maoulida, F., Djedjig, R., Kassim, M., & Ganaoui, M. (2022). Numerical Study for the Evaluation of the Effectiveness and Benefits of Using Photovoltaic-Thermal (PV/T) System for Hot Water and Electricity Production under a Tropical African Climate: Case of Comoros. *Energies*. https://doi.org/10.3390/en16010240

Misha, S., Abdullah, A., Tamaldin, N., Rosli, M., & Sachit, F. (2019). Simulation CFD and experimental investigation of PVT water system under natural Malaysian weather conditions. *Energy Reports*. https://doi.org/10.1016/j.egyr.2019.11.162

Mohammad, A., & Al-Shohani, W. (2022). Numerical and experimental investigation for analyzing the temperature influence on the performance of photovoltaic module. *AIMS Energy*. https://doi.org/10.3934/energy.2022047

Moran, M. J., Shapiro, H. N., Boettner, D. D., & Bailey, M. B. (2010). *Fundamentals of engineering thermodynamics*. John Wiley & Sons.

Mundu, M. M., Nnamchi, S. N., & Muhaise, H. (2024). Sustainable Energy transitions in Uganda: Influential determinants of the renewable energy landscape. *IAA Journal of Applied Sciences*, *11*(1), 57–72. https://doi.org/10.59298/iaajas/2024/6.68.40.35

Mundu, M. M., Nnamchi, S. N., & Ukagwu, K. J. (2020). Algorithmized modelling, simulation and validation of clearness index in four regions of Uganda. *Journal of Solar Energy Research*, *5*(2), 432–452. https://doi.org/10.22059/jser.2020.300924.1150

Mundu, M. M., Nnamchi, S. N., Ukagwu, K. J., Peter, B. A., Nnamchi, O. A., & Ssempewo, J. I. (2022). Numerical modelling of wind flow for solar power generation in a case study of the tropical zones. *Modeling Earth Systems and Environment*, *8*(3), 4123–4134. https://doi.org/10.1007/s40808-021-01343-w

Mundu, M. M., Sempewo, J. I., Nnamchi, S. N., & Uti, D. E. (2025a). Solar-Powered desalination technologies for sustainable water security solutions. *International Journal of Energy Research*, *2025*(1). https://doi.org/10.1155/er/3482306

Mundu, M. M., Sempewo, J. I., Nnamchi, S. N., Mahoro, G. B., & Uti, D. E. (2025b). Integration of wind flow effects in theoretical and experimental models for solar power generation. *Scientific Reports*, *15*(1). https://doi.org/10.1038/s41598-025-90680-2

Mundu, M., Nnamchi, S., Sempewo, J., & Uti, D. E. (2024). Simulation modeling for energy systems analysis: A critical review. *Energy Informatics*, *7*(1), 75. https://doi.org/10.1186/s42162-024-00374-8

Mwesigye, A., Yılmaz, İ., & Meyer, J. (2018). Numerical analysis of the thermal and thermodynamic performance of a parabolic trough solar collector using SWCNTs-Therminol®VP-1 nanofluid. *Renewable Energy*, 119, 844-862. https://doi.org/10.1016/j.renene.2017.10.047

ARTICLE IN PRESS

Narkwatchara, P., Ratanatamskul, C., & Chandrachai, A. (2020). Effects of particulate matters and climate condition on photovoltaic system efficiency in tropical climate region. *Energy Reports*, 6, 2577-2586. https://doi.org/10.1016/j.egyr.2020.09.016

Nasrin, R., Alim, M., & Hasanuzzzaman, M. (2016). Assisted convective heat transfer and entropy generation in a solar collector filled with nanofluid. *Journal of Naval Architecture and Marine Engineering*, 13, 135-150. https://doi.org/10.3329/jname.v13i2.27774

Nnamchi, S. N., & Mundu, M. M. (2022a). Development of solar isodose lines: Mercatorian and spatial guides for mapping solar installation areas. *Heliyon*, *8*(10), e11045. https://doi.org/10.1016/j.heliyon.2022.e11045

Nnamchi, S. N., Mundu, M. M., Nnamchi, O. A., Onochie, U., & Jagun, Z. O. (2021). Differential modelling and simulation of solar power potential: a helio-application of biharmonic model. *Modeling Earth Systems and Environment*, *8*(2), 2383–2400. https://doi.org/10.1007/s40808-021-01232-2

Nnamchi, S. N., Mundu, M. M., Ukagwu, K. J., & Oyagbola, I. A. (2022b). Development and adaptation of relative sunshine hours models for the equatorial latitudes: a case study. *Modeling Earth Systems and Environment*, *8*(1), 1191-1201. https://doi.org/10.1007/s40808-021-01147-y

Nnamchi, S. N., Nnamchi, O. A., Sanya, O. D., Mundu, M. M., & Gabriel, V. (2020). Dynamic analysis of performance of photovoltaic generators under moving cloud conditions. *Journal of Solar Energy Research*, *5*(2), 453-468. https://doi.org/10.22059/jser.2020.304561.1158

Omara, A., Mohamed, O., Mohammedali, A., & Ahmed, M. (2024). Effect of ten different physical parameters on solar still productivity: Theoretical modeling. *Environmental Progress & Sustainable Energy*, 43. https://doi.org/10.1002/ep.14416

Osara, J., & Bryant, M. (2024). Methods to Calculate Entropy Generation. *Entropy*, 26. https://doi.org/10.3390/e26030237

Osorio, L., Moreno, M., Rivera, M., Tuninetti, V., Chavarria, G., Duchêne, L., & Wheeler, P. (2024). A metaheuristic-based method for photovoltaic temperature computation under tropical conditions. *Solar Energy*. https://doi.org/10.1016/j.solener.2024.112414

Ozcan, B., & Seval, M. (2022). Temperature-Irradiance Matrix and Determination of Temperature Coefficients of a Monocrystalline PV Module. *Open Journal of Energy Efficiency*. https://doi.org/10.4236/ojee.2022.113008

Pal, R. (2017). Demystification of the Gouy-Stodola theorem of thermodynamics for closed systems. *International Journal of Mechanical Engineering Education*, 45, 142 - 153. https://doi.org/10.1177/0306419016689501

Pal, R. (2018). Entropy Generation and Exergy Destruction in Flow of Multiphase Dispersions of Droplets and Particles in a Polymeric Liquid. *Fluids*, 3, 19. https://doi.org/10.3390/fluids3010019

Pal, R. (2019). Comparison of entropic and exergetic methods of quantification of loss of power due to irreversibilities in real processes using the Gouy–Stodola theorem. *International Journal of Mechanical Engineering Education*, 47, 73 - 96. https://doi.org/10.1177/0306419017749801

Poongavanam, P., Chand, A., Tai, V., Gupta, Y., Kuppusamy, M., Dhanraj, J., Velmurugan, K., Rajagopal, R., Ramachandran, T., Prasad, K., Chand, S., Raj, S., & Mamun, K. (2023). Annual Thermal Management of the Photovoltaic Module to Enhance Electrical Power and Efficiency Using Heat Batteries. *Energies*. https://doi.org/10.3390/en16104049

ARTICLE IN PRESS

Ramírez-Minguela, J., Rangel-Hernandez, V., Alfaro-Ayala, J., Elizalde-Blancas, F., Ruíz-Camacho, B., López-Núñez, O., & Alvarado-Rodríguez, C. (2023). Performance Comparison of Different Flat Plate Solar Collectors by Means of the Entropy Generation Rate Using Computational Fluid Dynamics. *Entropy*, 25. https://doi.org/10.3390/e25040621

Rao, T., Sekhar, R., Arıcı, M., Pochont, N., & Prasad, D. (2024). Experimental investigations on bi-symmetrical web flow water based photovoltaic-thermal (PVT) system: Energy, exergy, and entropy (3-E) analysis. *Solar Energy*. https://doi.org/10.1016/j.solener.2024.112445

Rashidi, S., Yang, L., Khoosh-Ahang, A., Jing, D., & Mahian, O. (2020). Entropy generation analysis of different solar thermal systems. *Environmental Science and Pollution Research*, 27, 20699-20724. https://doi.org/10.1007/s11356-020-08472-2

Saldaña, M., Gallegos, S., Gálvez, E., Castillo, J., Salinas-Rodríguez, E., Cerecedo-Sáenz, E., Hernández-Ávila, J., Navarra, A., & Toro, N. (2024). The Reynolds Number: A Journey from Its Origin to Modern Applications. *Fluids*. https://doi.org/10.3390/fluids9120299

Samykano, M. (2023). Hybrid Photovoltaic Thermal Systems: Present and Future Feasibilities for Industrial and Building Applications. *Buildings*. https://doi.org/10.3390/buildings13081950

Satpute, J., Deshmukh, S., Kale, P., & Patil, R. (2025). Computational study on water-based hybrid photovoltaic thermal absorber configurations. *Scientific Reports, 15*, 82690. https://doi.org/10.1038/s41598-024-82690-3

Shaik, S., Bhardwaj, M., Agarwal, S., Yendaluru, R., , H., & Sharma, K. (2021). Evaluation of Optical Transmissivity of Transparent Materials on the Performance of Solar Flat Plate Collectors. *Journal of Solar Energy Engineering-transactions of The Asme*, 143. https://doi.org/10.1115/1.4050214

Shao, N., , L., Zhou, C., & Zhang, D. (2022). Experimental study on the heat transfer performance of the PVT ventilated roof as heat exchanger for heat pump system. *Renewable Energy*. https://doi.org/10.1016/j.renene.2022.01.084

Skoplaki, E., & Palyvos, J. (2009). On the temperature dependence of photovoltaic module electrical performance: a review of efficiency/ power correlations. *Solar Energy*, 83, 614-624. https://doi.org/10.1016/j.solener.2008.10.008

Soliman, A. (2023). A Numerical Investigation of PVT System Performance with Various Cooling Configurations. *Energies*. https://doi.org/10.3390/en16073052

Sun, V., Asanakham, A., Deethayat, T., & Kiatsiriroat, T. (2021). Evaluation of nominal operating cell temperature (NOCT) of glazed photovoltaic thermal module. *Case Studies in Thermal Engineering*, 28, 101361. https://doi.org/10.1016/j.csite.2021.101361

Takyi, G., & Nyarko, F. (2020). Investigation of the Effect of Temperature Coefficients on Mono-Crystalline Silicon PV Module Installed in Kumasi, Ghana. *Journal of Power and Energy Engineering*. https://doi.org/10.4236/jpee.2020.89003

Tamburrino, A., & Niño, Y. (2025). The Universal Presence of the Reynolds Number. *Fluids*. https://doi.org/10.3390/fluids10050117

Torabi, M., Karimi, N., Torabi, M., Peterson, G., & Simonson, C. (2020). Generation of entropy in micro thermofluidic and thermochemical energy systems-A critical review. *International Journal of Heat and Mass Transfer*. https://doi.org/10.1016/j.ijheatmasstransfer.2020.120471

ARTICLE IN PRESS

Unar, I., Maitlo, G., Ahmed, S., Ali, S., Memon, A., Kandhro, G., & Jatoi, A. (2020). Performance evaluation of solar flat plate collector using different working fluids through computational fluid dynamics. *SN Applied Sciences*, 2. https://doi.org/10.1007/s42452-020-2005-z

Van Zyl, W., Dirker, J., & Meyer, J. (2013). Single-Phase Convective Heat Transfer and Pressure Drop Coefficients in Concentric Annuli. *Heat Transfer Engineering*, 34, 1112 - 1123. https://doi.org/10.1080/01457632.2013.763550

Wang, Y., & Wang, P. (2020). Application of stable flow energy equation in steam turbine and other power machines. *IOP Conference Series: Earth and Environmental Science*, 474. https://doi.org/10.1088/1755-1315/474/5/052087

Wang, Z., Hou, G., Taherian, H., & Song, Y. (2024). Numerical Investigation of Innovative Photovoltaic–Thermal (PVT) Collector Designs for Electrical and Thermal Enhancement. *Energies*. https://doi.org/10.3390/en17102429

Wang, Z., Li, H., Chen, Y., & Zhang, X. (2024). Numerical investigation of innovative photovoltaic–thermal structures. *Energies, 17*(10), 2429. https://doi.org/10.3390/en17102429

Yan, B., Wu, Q., Chi, X., Wu, C., Luo, P., Luo, Y., & Zeng, P. (2022). Numerical and Experimental Investigation of Photovoltaic/Thermal Systems: Parameter Analysis and Determination of Optimum Flow. *Sustainability*. https://doi.org/10.3390/su141610156

Zhao, B., Ao, X., Chen, N., Xuan, Q., Hu, M., & Pei, G. (2020). A spectrally selective surface structure for combined photothermic conversion and radiative sky cooling. *Frontiers in Energy*, 14, 882 - 888. https://doi.org/10.1007/s11708-020-0694-z

Zm, A., Sinuraya, E., & Winardi, B. (2025). The Effect of Temperature and Weather Conditions on the Performance of Photovoltaic Modules in Tropical Indonesia. *West Science Information System and Technology*. https://doi.org/10.58812/wsist.v3i01.1870

ARTICLE IN PRESS